

VLRS-Bench: A Vision-Language Reasoning Benchmark for Remote Sensing

Zhiming Luo^{1,2}, Di Wang^{1,2†}, Haonan Guo^{1,2}, Jing Zhang^{1,2†}, Bo Du^{1,2†}

¹School of Computer Science, Wuhan University, ²Zhongguancun Academy

[thislzm@whu.edu.cn](mailto>thislzm@whu.edu.cn); d_wang@whu.edu.cn; jingzhang.cv@gmail.com; dubo@whu.edu.cn

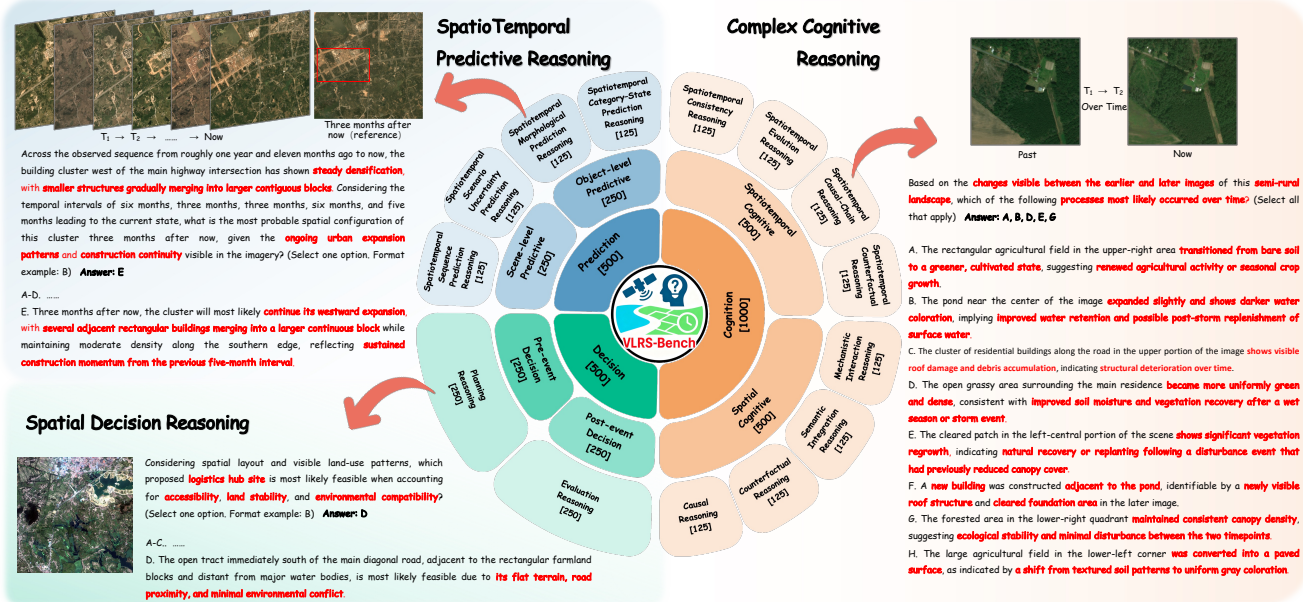


Figure 1. Sample cases from VLRS-Bench. It comprises three core reasoning dimensions (Cognition Reasoning: *Why is this*; Decision Reasoning: *How to do*; Prediction Reasoning: *What will happen*), further decomposed into a structured hierarchy of six specific abilities and fourteen fine-grained tasks for comprehensive evaluation of MLLMs reasoning.

Abstract

Recent advancements in Multimodal Large Language Models (MLLMs) have enabled complex reasoning. However, existing remote sensing (RS) benchmarks remain heavily biased toward perception tasks, such as object recognition and scene classification. This limitation hinders the development of MLLMs for cognitively demanding RS applications. To address this, we propose a *Vision Language ReaSoning Benchmark (VLRS-Bench)*, which is the first benchmark exclusively dedicated to complex RS reasoning. Structured across the three core dimensions of Cognition, Decision, and Prediction, VLRS-Bench comprises 2,000 question-answer pairs with an average length of 71 words, spanning 14 tasks and up to eight temporal phases. VLRS-Bench is constructed via a specialized pipeline that integrates RS-specific priors and expert knowledge to ensure

geospatial realism and reasoning complexity. Experimental results reveal significant bottlenecks in existing state-of-the-art MLLMs, providing critical insights for advancing multimodal reasoning within the remote sensing community. The source data will be available at <https://github.com/MiliLab/VLRS-Bench>

1. Introduction

Multimodal Large Language Models (MLLMs) [15, 31, 47] have substantially advanced visual understanding and complex reasoning by integrating powerful visual encoders with large language models. There is now broad agreement in the research community that well-designed benchmarks are essential for guiding model development and advancing model capabilities. This consensus has motivated extensive benchmarking efforts across diverse domains, spanning

computer vision and medical diagnosis [4, 16], autonomous driving [8, 58], and emerging areas such as remote sensing [14, 45].

Remote sensing imagery presents a unique evaluation landscape for MLLMs, characterized by highly intricate spatial dependencies and long-term, dynamic temporal evolution. Previous benchmarks [29, 57] have predominantly focused on perception tasks, such as object recognition and basic relational understanding. However, the fundamental scientific value of remote sensing lies in deciphering causal mechanisms and evolutionary patterns. Comprehending these dynamics demands complex reasoning capabilities that transcend the scope of existing perception-oriented frameworks.

Although some recent benchmarks [1, 24] have begun to consider incorporating reasoning dimensions into their evaluation dimension, they still suffer from notable limitations in evaluating genuine reasoning ability: **(1) Reasoning tasks lack a clear classification system and hierarchical structure.** Most existing benchmarks [29, 57] define task categories according to application scenarios (*e.g.* environmental assessment or path planning) or task formats (*e.g.* attribute judgment or area counting), resulting in task-driven rather than cognition-driven designs. Such categorization lacks a coherent cognitive progression from basic to advanced abilities, making it difficult to systematically assess whether a model possesses the underlying cognitive skills required for higher-level reasoning. **(2) Reasoning forms are limited to simple relational or descriptive tasks.** Previous benchmarks [15, 32] have focused primarily on perception tasks such as object recognition and basic relational understanding, which assess only interpretative abilities. Yet remote sensing imagery, with its complex semantics and explicit spatiotemporal structure, demands complex reasoning capable of uncovering causal mechanisms and evolutionary patterns. **(3) Current benchmarks underutilize remote sensing-specific priors.** Existing benchmarks [48, 50] primarily rely on standard RGB imagery, they largely overlook remote sensing-specific priors such as elevation data (DSM), non-visible spectra (NIR), and expert annotations (Masks, bounding boxes). Derived from specialized sensors and expert analysis, these multi-modal data are crucial for designing realistic and complex reasoning tasks. Their integration would enable benchmarks to support more challenging, authentic reasoning and yield more robust evaluations of remote sensing MLLMs.

To address these limitations, we introduce VLRS-Bench, the first benchmark designed to systematically evaluate complex reasoning in remote sensing. As shown in Figure 1, inspired by neuroscientific research [19, 42], we structure VLRS-Bench around three L-1 dimensions: (1) Cognition Reasoning (*Why is this*), representing causal understanding; (2) Decision Reasoning (*How to do*), repre-

senting strategic execution; and (3) Prediction Reasoning (*What will happen*), temporal extrapolation of geospatial states. These dimensions are further organized into six L-2 specific abilities and fourteen L-3 tasks. This hierarchical framework enables a comprehensive evaluation of model reasoning capabilities. To construct VLRS-Bench, we develop a highly automated pipeline that explicitly integrates multi-modal priors, such as DSM and NIR imagery, and RS expert pixel-level annotations to generate evaluation scenarios grounded in authentic physical constraints and complex geospatial logic. Extensive experiments validate the rigor of this design, demonstrating that VLRS-Bench poses significant challenges to current MLLMs while effectively highlighting the distinctive reasoning demands of the remote sensing domain. In summary, our main contributions are as follows:

- We propose VLRS-Bench, the first benchmark tailored for remote sensing multimodal reasoning tasks. It systematically decomposes complex reasoning into three core dimensions: Cognition, Decision, and Prediction, encompassing 14 fine-grained tasks, which facilitates a comprehensive and holistic quantitative assessment of MLLMs’ reasoning capabilities.
- We introduce a highly automated pipeline for constructing VLRS-Bench. It explicitly leverages key RS specific priors such as DSM, NIR imagery, and expert-annotated pixel-level masks to generate evaluation tasks with significantly enhanced geospatial realism and reasoning complexity.
- Experimental results demonstrate that generalist MLLMs exhibit significant deficiencies in geospatial reasoning. Although RS specific MLLMs achieve superior performance, they still face critical limitations in complex decision-making and prediction tasks, highlighting the challenging nature of VLRS-Bench and the necessity for further architectural advancements.

2. Related Work

MLLMs. The significant advances in vision-language understanding are largely driven by MLLMs. vision-language models such as CLIP [36] and ALIGN [18] established scalable pretraining through contrastive alignment, paving the way for subsequent instruction-tuned architectures like LLaVA [27] and GPT-4V [51] that exhibit sophisticated open-ended reasoning capabilities. However, the performance of these general-domain models is constrained by their reliance on object-centric natural image datasets like COCO [25], which lack the high spatial resolution and complex semantic context characteristic of remote sensing imagery. To bridge this gap, a dedicated line of research has emerged to adapt MLLMs for Earth observation. GeoChat [20] pioneered versatile conversational capabilities by enabling region-level reasoning and visual ground-

Table 1. Comparison of multimodal benchmarks in general and RS domains.

Benchmark	Data Source	Avg. QA Len.	Type	Reason. Dim.	Temporals	RS Priors
General Benchmarks						
MMBench [28]	10 Public Datasets	✗	MCQ	8	✗	✗
MMStar [5]	6 Public Benchmarks	✗	MCQ	6	✗	✗
SEED-Bench-2 [21]	5 Public Datasets	✗	MCQ	7	✗	✗
Remote Sensing Benchmarks						
LEVIR-CC [26]	LEVIR-CD	7.99	FF	✗	2	✗
RSVGD [56]	DIOR Dataset	7.47	FF	✗	✗	BBox
RSVQA [29]	HR & LR Datasets	✗	FF	✗	✗	✗
RSIEval [15]	DOTA Val. Dataset	✗	FF	1	✗	BBox
LHRS-Bench [32]	Google Earth	✗	MCQ	1	✗	✗
GeoChat [20]	SAMRS, LRBEN	✗	FF	✗	✗	BBox, Mask
EarthVQA [50]	LoveDA Dataset	✗	FF	3	✗	Mask
VRSBench [24]	DOTA-v2, DIOR	52	FF	1	✗	BBox
RSVLM-QA [59]	WHU, LoveDA, iSAID	9.23	FF	2	✗	Mask
GEOBench-VLM [7]	8 Public Datasets	✗	MCQ, BBox	4	✗	BBox, Mask
XLRS-Bench [48]	6 Public Datasets	✗	MCQ, TF	6	2	BBox
CHOICE [1]	Multi-sat. (non-public)	✗	MCQ	7	4	BBox, Mask
VLRS-Bench	11 Public Datasets	70.96	MCQ, FF, TF	14	8	BBox, Mask, DSM, NIR

Note: MCQ = Multiple/Single Choice Questions; TF = True/False Questions; FF = Free-Form Questions.

ing, while LHRS-Bot [32] advanced RS image understanding through a novel multi-level vision-language alignment strategy supported by large-scale instruction datasets. Subsequently, models like VHM [35] have been developed to enhance generalization across diverse tasks. More recent work has concentrated on improving fine-grained comprehension through specialized instruction tuning, as demonstrated by SkySenseGPT [31] for region-level semantics, and GeoPixel [39], which introduced pixel-level grounding capabilities for high-resolution imagery. Furthermore, on addressing the unique challenge of ultra-high-resolution and multi-modal data, imagery with models like GeoLLaVA-8K [47] and EarthDial [40] have expanded capabilities to support multi-sensory and multi-temporal analysis. Despite advancing performance on various vision-language tasks in remote sensing, a systematic evaluation of these specialized models' complex reasoning abilities remains lacking.

Benchmarks for MLLMs. Comprehensive benchmarks in the general domain, such as MMBench [28] and SEED-Bench [21], have been established to evaluate MLLMs. However, their focus on tasks with limited spatial and temporal complexity renders them insufficient for the unique challenges of Earth observation. This gap prompted the development of domain-specific benchmarks. Early efforts like RSVQA [29] introduced visual question answering to satellite imagery but primarily assessed recognition and basic relational understanding. Subsequent benchmarks expanded this foundation by incorporating higher-

resolution imagery [23] and addressing specific technical challenges such as reference grounding [57]. Recent contributions like RSVLM-QA [59] and GEOBench-VLM [7] have further enriched the field by integrating diverse public datasets to evaluate capabilities ranging from object counting to fine-grained categorization. Although the most recent benchmarks, such as CHOICE [1] and XLRS-Bench [48], have begun to explicitly target higher-order cognition, they do not yet offer a systematic framework for evaluating reasoning. As illustrated in Table 1, these datasets remain constrained in the diversity and depth of reasoning forms they capture, typically featuring limited reasoning dimensions (e.g., only 2-4 dimensions in RSVLM-QA and GEOBench-VLM) and restricted temporal contexts, often relying on application-driven rather than cognition-driven task designs.

3. VLRS-Bench

This section outlines the hierarchical reasoning taxonomy defining VLRS-Bench, describes the automated pipeline implemented for its construction. Specific details regarding the benchmark configuration and the statistical distribution of question types are presented in Appendix 3.1.

3.1. Reasoning Dimension of VLRS-Bench

As illustrated in Figure 1, we structure VLRS-Bench around three L-1 reasoning levels: **(1) Cognition.** Interpreting a scene's current state through retrospective reasoning; **(2)**

Decision. Determining what actions should be taken based on the current observation; and **(3) Prediction.** Forecasting what will happen next. In the following subsections, we elaborate on the L-2 dimensions and briefly outline their associated L-3 capabilities, while comprehensive definitions for each L-3 capability are provided in [Appendix 3.2](#).

3.1.1. Cognition

This dimension evaluates the model’s ability to perform deep reasoning into the causality and mechanisms of geospatial phenomena. We assess this across two complementary L-2 dimensions: static spatial relationships and dynamic spatiotemporal evolutions.

Spatial Cognitive (SC). This dimension evaluates whether a model can move beyond surface-level object recognition to capture the intrinsic causal logic underlying a static scene. Its core objective is to assess whether the model can synthesize isolated visual cues into a coherent causal understanding, bridging the gap between “what is present” and “why it is present.” To this end, we incorporate four interconnected L-3 reasoning capabilities: 1) *Causal Reasoning (CR)*, which identifies latent etiological factors driving observed phenomena; 2) *Counterfactual Reasoning (CFR)*, which examines the consequences of hypothetical interventions under alternative scenarios; 3) *Mechanistic Interaction Reasoning (MIR)*, which infers implicit physical interactions and feedback mechanisms among spatial elements; and 4) *Semantic Integration Reasoning (SIR)*, which integrates low-level visual primitives into coherent high-level regional semantics.

Spatiotemporal Cognitive (ST-C). Extending reasoning into the temporal domain, this dimension evaluates a model’s ability to uncover the mechanisms governing geospatial evolution. The core objective of ST-C is to assess whether the model perceives spatiotemporal change as a structured and rule-driven process rather than a random sequence, requiring an understanding of how past events shape present states. Accordingly, we assess four interconnected L-3 reasoning capabilities: 1) *Spatiotemporal Causal-Chain Reasoning (ST-CCR)*, which infers and explains causal event chains across time; 2) *Spatiotemporal Counterfactual Reasoning (ST-CFR)*, which explores alternative evolutionary trajectories by hypothetically modifying critical past events; 3) *Spatiotemporal Evolution Reasoning (ST-ER)*, which captures functional transformations and semantic shifts of regions over time; and 4) *Spatiotemporal Consistency Reasoning (ST-CR)*, which verifies the logical coherence of temporal changes under geospatial constraints.

3.1.2. Decision

This dimension evaluates a model’s capacity for spatial decision-making. It shifts the focus from passive observation to active strategy formulation, requiring the model to

reason about how to achieve specific objectives within complex geospatial environments. This dimension is further categorized into generative planning and critical evaluation.

Pre-event Decision (PRE-D). This dimension focuses on the proactive generation of spatial strategies. Its objective is to assess whether a model can synthesize environmental constraints into actionable plans, thereby moving beyond scene understanding toward goal-driven intervention. To this end, we define *Planning Reasoning (PR)*, which examines the model’s ability to formulate spatially optimized solutions that satisfy implicit logistical constraints for achieving predefined objectives, such as site selection or route planning.

Post-event Decision (POST-D). This dimension complements proactive planning with retrospective evaluation. Its objective is to assess whether a model can critically examine proposed interventions before execution, ensuring that theoretical strategies are consistent with physical and environmental constraints. To this end, we define *Evaluation Reasoning (ER)*, which examines the model’s ability to assess the feasibility and robustness of candidate plans by analyzing their compatibility with the scene context and identifying potential risks.

3.1.3. Prediction

This dimension evaluates a model’s capacity for spatiotemporal forecasting. It requires the model to extrapolate from historical observations to infer future states, reasoning about how observed patterns and constraints evolve over time. Predictions are assessed at both the discrete object level and the holistic scene level.

Object-level Predictive (OP). This dimension focuses on forecasting the future evolution of individual entities. It assesses whether a model can reason about object-specific trajectories driven by observable pressures, rather than treating the scene as a static background. Accordingly, we evaluate two L-3 reasoning capabilities: 1) *Spatiotemporal Category-State Prediction Reasoning (ST-CS-PR)*, which predicts semantic state transitions by inferring future object identities from developmental trends; and 2) *Spatiotemporal Morphological Prediction Reasoning (ST-M-PR)*, which extrapolates geometric evolution by modeling the physical dynamics governing changes in object shape or extent.

Scene-level Predictive (SP). This dimension extends prediction to the macro-scale evolution of entire landscapes. It evaluates whether a model can reason about the inherently uncertain dynamics of complex geospatial systems, where future states are often non-deterministic. Accordingly, we assess two L-3 reasoning capabilities: 1) *Spatiotemporal Scenario Uncertainty Prediction Reasoning (ST-SU-PR)*, which performs probabilistic forecasting by modeling multiple plausible evolutionary trajectories; and 2) *Spatiotemporal Sequence Prediction Reasoning (ST-SQ-PR)*, which requires predicting scene-level spatial states by reasoning

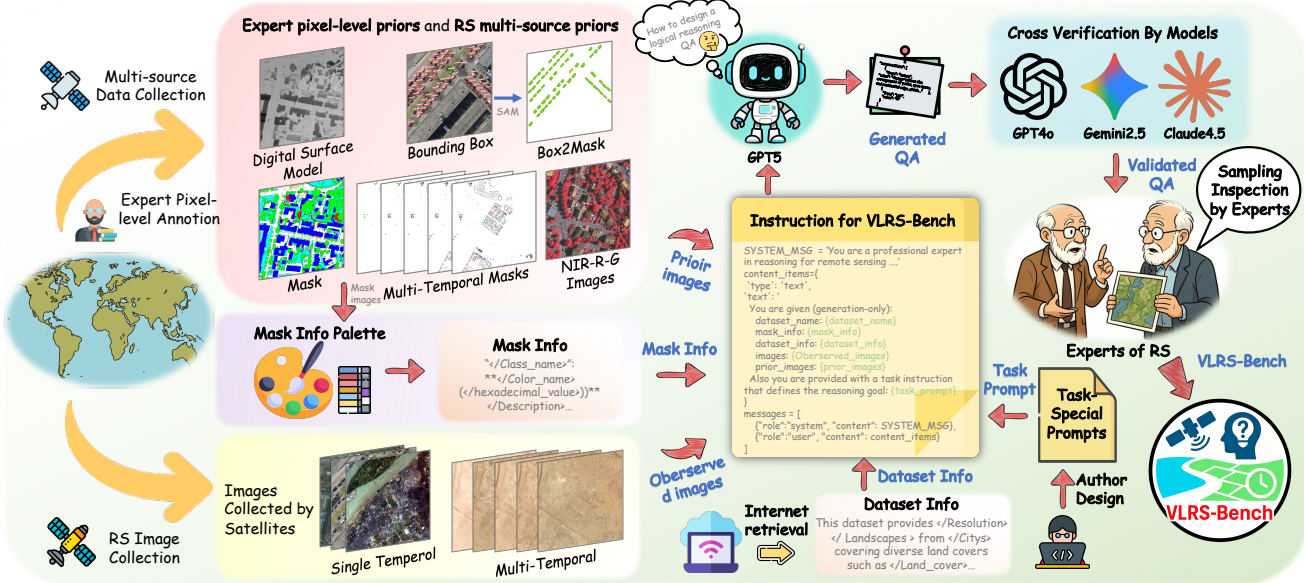


Figure 2. Pipeline for constructing VLRS-Bench. The process integrates the target RGB image with multi-source remote sensing priors (e.g., DSM and expert masks) to form a structured multimodal instruction, which guides a GPT-5-chat to produce reasoning tasks across cognitive dimensions. Each generated item is then verified through a three-stage protocol, including automated filtering, multi-MLM cross-validation, and human expert review.

over temporal dependencies across sequential observations.

3.2. Pipeline of VLRS-Bench

This section details the automated construction pipeline of VLRS-Bench, encompassing data curation, instruction synthesis, and rigorous quality verification. Further technical specifications regarding the pipeline implementation are provided in [Appendix 4](#).

3.2.1. Data preparation of VLRS-Bench

To construct a comprehensive remote sensing (RS) reasoning benchmark, we curate a diverse data foundation comprising publicly available RS imagery spanning multiple sources, time periods, and scene types.

Single-temporal datasets: We select several public semantic segmentation and object detection datasets, including LoveDA [49], Potsdam [38], Vaihingen [38], GID15 [44], DIOR [22], DOTA [3, 53], and FAIR1M [41]. These datasets span spatial resolutions from 0.3 m to 30 m and cover a wide range of land-cover categories, providing a multi-scale and semantically diverse visual foundation.

Multi-temporal datasets: We introduce typical change detection and temporal inference datasets such as Xview2 [13], SECOND [55], miniUCD [43], and SpaceNet7 [10]. These datasets provide paired multi-temporal image sequences capturing explicit temporal changes and corresponding expert pixel-level annotated masks, covering dynamic scenes such as urban expansion and land surface changes.

To further expand pixel-level annotations, we employ the SAMRS framework [46] to convert bounding-box annotations from public datasets into high-quality segmentation masks, unifying the annotation format at scale.

3.2.2. Instruction of Pipeline

As illustrated in Figure 2, VLRS-Bench is constructed via a highly automated generation pipeline. For each RS scene, the pipeline fuses the observed RGB image with auxiliary RS priors (e.g., DSM and NIR), selected multi-temporal references, and expert-provided pixel-level masks (used as conditioning priors rather than prediction targets). It then packages these inputs—together with mask definitions, dataset metadata, and a task-specific prompt—into a unified multimodal instruction. Specifically, the instruction consists of the following five complementary components:

Observed Image. The original RGB RS image provided as the primary visual input for the task.

Prior Images. This component incorporates multi dimensional cross-modal contextual information through three complementary elements: (1) *Multi-source RS Priors*, which load DSM and NIR data to provide structural and spectral cues beyond standard RGB perception; (2) *Expert Pixel-Level Priors*, which use predefined masks as conditioning inputs rather than prediction targets to constrain reasoning within expert-defined contexts; and (3) *Multi-temporal Reference Priors*, which leverage selected temporal observations as causal anchors to support logically consistent multi-temporal reasoning.

Mask Info. It defines a dedicated palette for each mask type, mapping pixel colors to corresponding land-cover categories. Each category is accompanied by a textual description that specifies its semantic meaning and functional role, providing the model with structured semantic priors.

Dataset Info. It provides metadata describing the dataset’s composition, source, and characteristics, offering high-level contextual information for task interpretation.

Task Special Prompt. This component provides a task-specific prompt tailored to each subtask (Section 3.1), defining the underlying reasoning logic and problem orientation. It guides the model toward the intended analytical objectives and multi-step reasoning processes, with illustrative task-specific examples provided as reference.

After instruction assembly, the pipeline iteratively generates aligned question–answer (QA) pairs using GPT-5-chat. These QA pairs are then organized into multiple-choice, single-choice, fill-in-the-blank, and true/false formats, covering all reasoning dimensions.

3.2.3. Verification of Pipeline

Following the automatic generation of QA pairs, we apply a three-stage verification pipeline to ensure the quality and reliability of VLRS-Bench.

First, an automated filtering stage quantitatively evaluates each item based on fundamental criteria, including clarity, image relevance, and ambiguity, removing low-quality samples. Second, to mitigate single-model bias, the remaining items undergo multi-model cross-validation: a proposer model generates a design justification for each QA pair, which is then examined for logical consistency and factual correctness by a panel of distinct models.

Finally, items that pass automated verification proceed to human expert review. A panel of remote sensing experts performs a sampling-based assessment, evaluating professional relevance, logical rigor, and ground-truth correctness. This verification pipeline ensures that only high-quality and reliable items are included in the final VLRS-Bench.

4. Experiment

We evaluate the reasoning capabilities of current MLLMs on VLRS-Bench. This section presents the experimental setup, including the evaluated models, evaluation protocols, and experimental results.

4.1. Experimental Setup

We evaluate a broad range of state-of-the-art MLLMs, grouped into three categories. The first category includes closed-source proprietary models, such as GPT-5-chat [34], the GPT-4o series [17], Claude-3.5-haiku, Gemini-2.5-flash [6], Grok-2-Vision [52], DeepSeek-VL [30], and GLM-4.5V [12]. The second category comprises open-source general-purpose models, including multiple sizes of the

Llama-3.2 series [9], as well as the Qwen2.5-VL [2] and Qwen3-VL series [54]. The third category focuses on domain-specialized models, including ScoreRS [33] under both SFT and RL training paradigms. To ensure fair comparison, all models are evaluated under a zero-shot setting using a standardized prompt.

4.2. Evaluation Strategy

To evaluate reasoning performance in VLRS-Bench, we adopt a tiered scoring scheme tailored to different question formats. For 8-select-N multiple-choice questions ($N \geq 2$), partial credit is assigned: 1.0 for perfect selections, 0.5 for incomplete but error-free answers, and 0 for any incorrect choice. Other question formats, including 5-select-1 single-choice and binary true/false questions, are scored with one point per correct response. The fill-in-the-blank questions are evaluated using a semantic similarity-based criterion rather than exact string matching. We compute embedding similarity using the all-MiniLM-L6-v2 model [37] and consider an answer correct if its similarity to the ground truth exceeds an 80% threshold. Partial credit is supported: responses receive 0.5 points when the answer is partially correct, and 1.0 point only when all blanks are filled correctly. Finally, the overall performance is reported as the mean percentage score across all benchmark questions, providing a holistic measure of high-level reasoning performance in remote sensing.

4.3. Main Results

This section presents a fine-grained, detailed analysis of L-3 capabilities to identify specific cognitive nuances and reasoning bottlenecks. A complementary macro-level analysis at the L-2 dimension level, along with qualitative visualizations for each individual L-3 task, is provided in Appendix 2 and Appendix 5, respectively.

4.3.1. Results on Cognition Ability

Table 2 reveals distinct performance patterns under the Cognition dimension, which evaluates causal, relational, and process-oriented reasoning beyond visual recognition. Two consistent trends can be observed. **(1) Degradation from single-state cognition to spatiotemporal reasoning.** General MLLMs demonstrate noticeably weaker performance when reasoning requires modeling temporal evolution and change attribution, compared with cognition dimension that can be resolved from a single observation. This suggests that their reasoning is largely anchored in static semantic cues, with limited capacity for modeling temporal dependencies. In contrast, RS MLLMs show relatively consistent behavior across both single-state and spatiotemporal cognition tasks, indicating stronger alignment with geospatial change semantics and improved ability to associate observed variations with underlying causes. **(2) Disparity between semantic integration and mechanistic inference.**

Table 2. Performance evaluation of different MLLMs on the L-3 subtasks of VLRS-Bench. The models are categorized into general MLLMs and RS MLLMs, with average scores provided for each category.

Models	Cognition								Decision		Prediction				Avg. Score.
	CR	CFR	SIR	MIR	ST-CFR	ST-CCR	ST-ER	ST-CR	PR	ER	ST-CS-PR	ST-M-PR	ST-SU-PR	ST-SQ-PR	
General MLLMs															
GPT-5-chat	0.424	0.400	0.472	0.316	0.276	0.352	0.380	0.368	0.388	0.388	0.388	0.276	0.280	0.292	0.356
GPT-4o-2024-11-20	0.376	0.432	0.420	0.332	0.360	0.352	0.400	0.364	0.286	0.334	0.416	0.352	0.284	0.340	0.361
GPT-4o-mini	0.428	0.416	0.428	0.328	0.400	0.356	0.352	0.336	0.248	0.304	0.424	0.372	0.280	0.304	0.355
Gemini-2.5-flash	0.200	0.188	0.264	0.240	0.188	0.160	0.116	0.160	0.232	0.240	0.164	0.168	0.116	0.152	0.190
Claude-3.5-haiku	0.308	0.316	0.304	0.360	0.192	0.208	0.232	0.200	0.372	0.370	0.208	0.224	0.248	0.168	0.270
Grok-2-vision	0.188	0.216	0.288	0.368	0.232	0.240	0.240	0.280	0.252	0.300	0.220	0.196	0.172	0.148	0.240
Deepseek-v12	0.372	0.392	0.452	0.344	0.144	0.216	0.200	0.148	0.416	0.446	0.096	0.128	0.064	0.080	0.250
GLM-4.5v	0.268	0.136	0.248	0.312	0.152	0.084	0.084	0.132	0.312	0.340	0.132	0.172	0.180	0.112	0.190
LLama-3.2-11B	0.232	0.228	0.244	0.264	X	X	X	X	0.292	0.286	X	X	X	X	0.110
LLama-3.2-90B	0.368	0.364	0.356	0.308	0.236	0.268	0.300	0.268	0.408	0.430	0.308	0.352	0.268	0.212	0.318
Qwen2.5-VL-7B	0.256	0.172	0.384	0.176	0.224	0.324	0.248	0.216	0.198	0.238	0.328	0.280	0.232	0.212	0.249
Qwen2.5-VL-32B	0.292	0.312	0.368	0.296	0.244	0.300	0.256	0.236	0.370	0.308	0.276	0.284	0.236	0.156	0.281
Qwen2.5-VL-72B	0.216	0.300	0.296	0.392	0.316	0.240	0.216	0.204	0.402	0.370	0.172	0.180	0.204	0.188	0.264
Qwen3-VL-2B	0.350	0.361	0.468	0.185	0.204	0.428	0.412	0.336	0.287	0.260	0.380	0.312	0.304	0.312	0.330
Qwen3-VL-8B	0.341	0.363	0.472	0.211	0.388	0.405	0.398	0.371	0.233	0.275	0.381	0.401	0.401	0.384	0.359
Qwen3-VL-32B	0.372	0.416	0.476	0.316	0.408	0.428	0.388	0.392	0.416	0.364	0.388	0.456	0.336	0.372	0.395
Gen. MLLMs Avg.	0.312	0.313	0.371	0.297	0.248	0.273	0.264	0.251	0.320	0.328	0.268	0.260	0.225	0.215	0.282
Remote Sensing MLLMs															
GeoChat	0.280	0.332	0.360	0.308	X	X	X	X	0.352	0.356	X	X	X	X	0.331
VHM	0.302	0.297	0.308	0.210	X	X	X	X	0.324	0.332	X	X	X	X	0.296
ScoreRS w/ SFT	0.403	0.367	0.421	0.345	0.294	0.310	0.288	0.284	0.382	0.419	0.341	0.320	0.313	0.295	0.347
ScoreRS w/ RL	0.313	0.338	0.382	0.295	0.399	0.335	0.367	0.392	0.409	0.371	0.338	0.313	0.382	0.342	0.355
RS MLLMs Avg.	0.325	0.334	0.368	0.290	0.347	0.323	0.328	0.338	0.367	0.370	0.340	0.317	0.348	0.319	0.332

Across all evaluated models, Semantic Integration Reasoning consistently outperforms Mechanistic Interaction Reasoning, revealing that current MLLMs are more proficient at organizing observable semantic elements than at inferring latent interaction mechanisms. Mechanistic reasoning requires abstraction over indirect, non-visual dependencies, which remains a formidable challenge even for specialized domain-adapted models. Collectively, these results suggest that cognition in remote sensing extends well beyond simple semantic recognition and that VLRS-Bench provides a structured evaluation setting that exposes such complex reasoning limitations in a systematic manner.

4.3.2. Results on Decision Ability

The Decision dimension assesses a model’s capability to perform spatial planning and outcome assessment under explicit constraints. Analysis of the results in Table 2 reveals two consistent patterns. **(1) Scale-dependent performance under decision complexity.** Model performance on Decision dimension improves with increasing model scale, indicating that planning and evaluation reasoning impose higher logical and comparative demands than Cognition dimension. Larger models demonstrate stronger ability to generate feasible plans and assess alternatives under competing spatial constraints, suggesting that Decision reasoning requires the coordination of multiple conditions and trade-offs rather than isolated judgments. **(2) Non-equivalence between PR and ER.** PR and ER do not form a single, monotonic decision capability. Across both General and

RS MLLMs, the relative performance between PR and ER varies substantially, indicating that success in one subtask does not guarantee robust competence in the other. Some models achieve comparable scores on PR and ER, while others exhibit clear asymmetry, regardless of model scale or domain specialization. This variability suggests that decision-making in VLRS-Bench involves at least two decoupled processes: generating plausible candidate actions under spatial constraints and assessing their potential outcomes. By explicitly separating PR and ER, VLRS-Bench avoids collapsing decision reasoning into a single aggregate score and instead reveals meaningful structural differences in how models plan actions and judge their consequences.

4.3.3. Results on Prediction Ability

The Prediction dimension evaluates a model’s ability to anticipate future geospatial states under varying degrees of temporal dependency and uncertainty. Results in Table 2 also reveal two notable patterns. **(1) Increasing difficulty from local state prediction to global system evolution.** Model performance tends to decline as prediction tasks shift from localized object changes to integrated scene-level evolution. General MLLMs perform relatively better when future states can be inferred from limited and localized cues, but struggle when predictions depend on the coordinated evolution of multiple entities over time, highlighting limitations in modeling long-range temporal and structural dependencies. **(2) Sensitivity to uncertainty and temporal complexity.** RS MLLMs demonstrate more differentiated

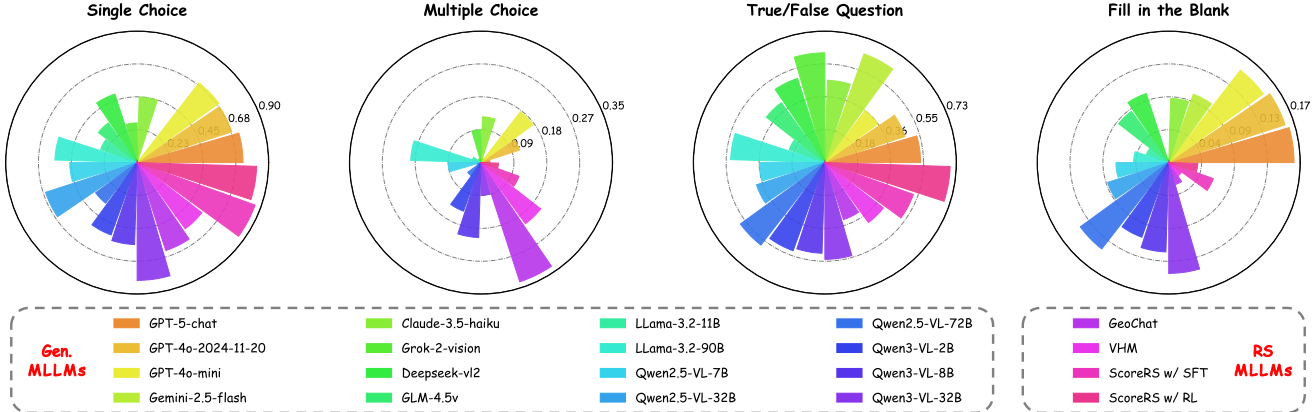


Figure 3. Avg. Score of various MLLMs across four QA-types. The distinct color coding (e.g. Qwen2.5-VL-32B in Blue, GPT-4o-mini in Yellow) highlights a critical phenomenon: a sharp performance drop from Single-Choice to Multi-Choice and Fill in Blank tasks. This trend, consistent across model sizes, validates the high reasoning ceiling of VLRS-Bench.

behavior across prediction settings, showing stronger performance when future outcomes follow clearer physical or semantic regularities, while exhibiting increased variability under prediction scenarios with higher uncertainty and longer temporal horizons. This contrast indicates that prediction in remote sensing is not a uniform capability, but depends critically on how well models internalize domain-specific evolution patterns and uncertainty structures. Overall, these results indicate that Prediction dimension impose distinct challenges beyond cognition and decision-making, and they illustrate how VLRS-Bench systematically exposes differences in models’ ability to reason about future geospatial dynamics rather than static observations.

4.3.4. Results on different QA-type tasks

Figure 3 summarizes the average performance of all evaluated MLLMs across four QA-types, revealing clear disparities in how models respond to different answer spaces and scoring mechanisms. Two consistent patterns can be observed. **(1) Sensitivity to output space complexity.** Most general MLLMs achieve their highest scores on Single-Choice and True/False questions, where the decision space is tightly constrained, but exhibit a sharp performance drop on Multi-Choice and Fill-in-the-Blank tasks, which require selecting or generating multiple correct elements. This indicates that their reasoning is more reliable when the output space is limited, while uncertainty grows rapidly as answer complexity increases. **(2) Strategy-driven behavior under partial-credit evaluation.** Under partial-credit evaluation, a non-linear relationship emerges between reasoning strength and final score. Models with very limited reasoning capacity may rely on conservative guessing and still accumulate partial scores, while models with stronger reasoning attempt more comprehensive predictions and risk zero scores when even a single element is incor-

rect. For example, RS MLLMs exhibit more diverse behaviors across QA-types. Models such as GeoChat and VHM, which are primarily trained on single-choice supervision, tend to select only one option in Multi-Choice questions. As a result, they obtain non-trivial average scores despite achieving zero fully correct answers, reflecting a strategy that prioritizes partial correctness over exhaustive reasoning. In contrast, some general MLLMs attempt broader option coverage but incur higher penalties due to incorrect selections. These observations indicate that QA-type performance reflects not only reasoning ability but also implicit decision strategies under uncertainty. Overall, these results show that QA-type variation provides a complementary perspective for analyzing model behavior, demonstrating how VLRS-Bench differentiates reasoning robustness and decision strategies under different output constraints, rather than relying solely on accuracy.

5. Conclusion

This study introduces VLRS-Bench, the first benchmark to systematically evaluate complex reasoning capabilities of Multimodal Large Language Models (MLLMs) in remote sensing across the dimensions of Cognition, Decision, and Prediction. Our evaluation reveals fundamental limitations of current MLLMs, including insufficient causal and counterfactual reasoning, weak generative spatial planning, and limited scalability in modeling long-term geospatial dynamics. We further show that domain-specialized RS models often outperform substantially larger general-purpose models, suggesting that genuine geospatial intelligence depends less on parameter scale than on RS-specific reasoning design. We anticipate that VLRS-Bench will foster future research toward MLLMs capable of principled reasoning and decision-making in complex Earth systems.

References

- [1] Xiao An, Jiaxing Sun, Zihan Gui, and Wei He. Choice: Benchmarking the remote sensing capabilities of large vision-language models. In *The Thirty-ninth Annual Conference on Neural Information Processing Systems Datasets and Benchmarks Track*, 2025. 2, 3
- [2] Shuai Bai, Kejin Chen, Xuejing Liu, Jialin Wang, Wenbin Ge, Sibo Song, Kai Dang, Peng Wang, Shijie Wang, Jun Tang, et al. Qwen2. 5-vl technical report. *arXiv preprint arXiv:2502.13923*, 2025. 6
- [3] Christopher Berner, Greg Brockman, Brooke Chan, Vicki Cheung, Przemysław Dębiak, Christy Dennison, David Farhi, Quirin Fischer, Shariq Hashme, Chris Hesse, et al. Dota 2 with large scale deep reinforcement learning. *arXiv preprint arXiv:1912.06680*, 2019. 5
- [4] Junying Chen, Chi Gui, Ruyi Ouyang, Anningzhe Gao, Shunian Chen, Guiming Hardy Chen, Xidong Wang, Zhenyang Cai, Ke Ji, Xiang Wan, et al. Towards injecting medical visual knowledge into multimodal llms at scale. In *Proceedings of the 2024 conference on empirical methods in natural language processing*, pages 7346–7370, 2024. 2
- [5] Lin Chen, Jinsong Li, Xiaoyi Dong, Pan Zhang, Yuhang Zang, Zehui Chen, Haodong Duan, Jiaqi Wang, Yu Qiao, Dahua Lin, et al. Are we on the right way for evaluating large vision-language models? *arXiv preprint arXiv:2403.20330*, 2024. 3
- [6] Gheorghe Comanici, Eric Bieber, Mike Schaeckermann, Ice Pasupat, Noveen Sachdeva, Inderjit Dhillon, Marcel Blissein, Ori Ram, Dan Zhang, Evan Rosen, et al. Gemini 2.5: Pushing the frontier with advanced reasoning, multimodality, long context, and next generation agentic capabilities. *arXiv preprint arXiv:2507.06261*, 2025. 6
- [7] Muhammad Danish, Muhammad Akhtar Munir, Syed Roshaan Ali Shah, Kartik Kuckreja, Fahad Shahbaz Khan, Paolo Fraccaro, Alexandre Lacoste, and Salman Khan. Geobench-vlm: Benchmarking vision-language models for geospatial tasks. In *Proceedings of the IEEE/CVF International Conference on Computer Vision*, pages 7132–7142, 2025. 3
- [8] Xinpeng Ding, Jianhua Han, Hang Xu, Wei Zhang, and Xiaomeng Li. Hilm-d: Enhancing mllms with multi-scale high-resolution details for autonomous driving. *International Journal of Computer Vision*, pages 1–17, 2025. 2
- [9] Abhimanyu Dubey, Abhinav Jauhri, Abhinav Pandey, Abhishek Kadian, Ahmad Al-Dahle, Aiesha Letman, Akhil Mathur, Alan Schelten, Amy Yang, Angela Fan, et al. The llama 3 herd of models. *arXiv e-prints*, pages arXiv–2407, 2024. 6
- [10] Adam Van Etten, Dave Lindenbaum, and Todd M. Bacastow. Spacenet: A remote sensing dataset and challenge series, 2019. 5
- [11] Timnit Gebru, Jamie Morgenstern, Briana Vecchione, Jennifer Wortman Vaughan, Hanna Wallach, Hal Daumé, and Kate Crawford. Excerpt from datasheets for datasets. In *Ethics of Data and Analytics*, pages 148–156. Auerbach Publications, 2022. 21
- [12] Team GLM, Aohan Zeng, Bin Xu, Bowen Wang, Chenhui Zhang, Da Yin, Dan Zhang, Diego Rojas, Guanyu Feng, Hanlin Zhao, et al. Chatglm: A family of large language models from glm-130b to glm-4 all tools. *arXiv preprint arXiv:2406.12793*, 2024. 6
- [13] Ritwik Gupta, Bryce Goodman, Nirav Patel, Ricky Hosfelt, Sandra Sajeev, Eric Heim, Jigar Doshi, Keane Lucas, Howie Choset, and Matthew Gaston. Creating xbd: A dataset for assessing building damage from satellite imagery. In *Proceedings of the IEEE/CVF Conference on Computer Vision and Pattern Recognition (CVPR) Workshops*, 2019. 5
- [14] Darryl Hannan, John Cooper, Dylan White, Timothy Doster, Henry Kvinge, and Yijing Watkins. Foundation models for remote sensing: An analysis of mllms for object localization. In *Proceedings of the Computer Vision and Pattern Recognition Conference*, pages 3028–3037, 2025. 2
- [15] Yuan Hu, Jianlong Yuan, Congcong Wen, Xiaonan Lu, Yu Liu, and Xiang Li. Rsgpt: A remote sensing vision language model and benchmark. *ISPRS Journal of Photogrammetry and Remote Sensing*, 224:272–286, 2025. 1, 2, 3
- [16] Xijie Huang, Xinyuan Wang, Hantao Zhang, Yinghao Zhu, Jiawen Xi, Jingkun An, Hao Wang, Hao Liang, and Chengwei Pan. Medical mllm is vulnerable: Cross-modality jailbreak and mismatched attacks on medical multimodal large language models. In *Proceedings of the AAAI Conference on Artificial Intelligence*, pages 3797–3805, 2025. 2
- [17] Aaron Hurst, Adam Lerer, Adam P Goucher, Adam Perelman, Aditya Ramesh, Aidan Clark, AJ Ostrow, Akila Welihinda, Alan Hayes, Alec Radford, et al. Gpt-4o system card. *arXiv preprint arXiv:2410.21276*, 2024. 6
- [18] Chao Jia, Yinfei Yang, Ye Xia, Yi-Ting Chen, Zarana Parekh, Hieu Pham, Quoc Le, Yun-Hsuan Sung, Zhen Li, and Tom Duerig. Scaling up visual and vision-language representation learning with noisy text supervision. In *International conference on machine learning*, pages 4904–4916. PMLR, 2021. 2
- [19] Nikolaus Kriegeskorte and Pamela K Douglas. Cognitive computational neuroscience. *Nature neuroscience*, 21(9): 1148–1160, 2018. 2
- [20] Kartik Kuckreja, Muhammad Sohail Danish, Muzammal Naseer, Abhijit Das, Salman Khan, and Fahad Shahbaz Khan. Geochat: Grounded large vision-language model for remote sensing. In *Proceedings of the IEEE/CVF Conference on Computer Vision and Pattern Recognition*, pages 27831–27840, 2024. 2, 3
- [21] Bohao Li, Yuying Ge, Yixiao Ge, Guangzhi Wang, Rui Wang, Ruimao Zhang, and Ying Shan. Seed-bench: Benchmarking multimodal large language models. In *Proceedings of the IEEE/CVF Conference on Computer Vision and Pattern Recognition (CVPR)*, pages 13299–13308, 2024. 3
- [22] Ke Li, Gang Wan, Gong Cheng, Lijiu Meng, and Junwei Han. Object detection in optical remote sensing images: A survey and a new benchmark. *ISPRS journal of photogrammetry and remote sensing*, 159:296–307, 2020. 5
- [23] Kun Li, George Vosselman, and Michael Ying Yang. Hrvqa: A visual question answering benchmark for high-resolution aerial images, 2023. 3

- [24] Xiang Li, Jian Ding, and Mohamed Elhoseiny. Vrsbench: A versatile vision-language benchmark dataset for remote sensing image understanding. *Advances in Neural Information Processing Systems*, 37:3229–3242, 2024. 2, 3
- [25] Tsung-Yi Lin, Michael Maire, Serge Belongie, James Hays, Pietro Perona, Deva Ramanan, Piotr Dollár, and C Lawrence Zitnick. Microsoft coco: Common objects in context. In *European conference on computer vision*, pages 740–755. Springer, 2014. 2
- [26] Chenyang Liu, Keyan Chen, Haotian Zhang, Zipeng Qi, Zhengxia Zou, and Zhenwei Shi. Change-agent: Toward interactive comprehensive remote sensing change interpretation and analysis. *IEEE Transactions on Geoscience and Remote Sensing*, 62:1–16, 2024. 3
- [27] Haotian Liu, Chunyuan Li, Qingyang Wu, and Yong Jae Lee. Visual instruction tuning, 2023. 2
- [28] Yuan Liu, Haodong Duan, Yuanhan Zhang, Bo Li, Songyang Zhang, Wangbo Zhao, Yike Yuan, Jiaqi Wang, Conghui He, Ziwei Liu, et al. Mmbench: Is your multi-modal model an all-around player? In *European conference on computer vision*, pages 216–233. Springer, 2024. 3
- [29] Sylvain Lobry, Diego Marcos, Jesse Murray, and Devis Tuia. Rsvqa: Visual question answering for remote sensing data. *IEEE Transactions on Geoscience and Remote Sensing*, 58(12):8555–8566, 2020. 2, 3
- [30] Haoyu Lu, Wen Liu, Bo Zhang, Bingxuan Wang, Kai Dong, Bo Liu, Jingxiang Sun, Tongzheng Ren, Zhuoshu Li, Hao Yang, et al. Deepseek-vl: towards real-world vision-language understanding. *arXiv preprint arXiv:2403.05525*, 2024. 6
- [31] Junwei Luo, Zhen Pang, Yongjun Zhang, Tingzhu Wang, Linlin Wang, Bo Dang, Jiangwei Lao, Jian Wang, Jingdong Chen, Yihua Tan, et al. Skysensegpt: A fine-grained instruction tuning dataset and model for remote sensing vision-language understanding. *arXiv preprint arXiv:2406.10100*, 2024. 1, 3
- [32] Dilxat Muhtar, Zhenshi Li, Feng Gu, Xueliang Zhang, and Pengfeng Xiao. Lhrs-bot: Empowering remote sensing with vgi-enhanced large multimodal language model. In *ECCV (74)*, pages 440–457, 2024. 2, 3
- [33] Dilxat Muhtar, Enzhuo Zhang, Zhenshi Li, Feng Gu, Yanglangxing He, Pengfeng Xiao, and Xueliang Zhang. Quality-driven curation of remote sensing vision-language data via learned scoring models. In *The Thirty-ninth Annual Conference on Neural Information Processing Systems*, 2025. 6
- [34] OpenAI. Introducing gpt-5, 2025. 6
- [35] Chao Pang, Xingxing Weng, Jiang Wu, Jiayu Li, Yi Liu, Jiaxing Sun, Weijia Li, Shuai Wang, Litong Feng, Gui-Song Xia, et al. Vhm: Versatile and honest vision language model for remote sensing image analysis. In *Proceedings of the AAAI Conference on Artificial Intelligence*, pages 6381–6388, 2025. 3
- [36] Alec Radford, Jong Wook Kim, Chris Hallacy, Aditya Ramesh, Gabriel Goh, Sandhini Agarwal, Girish Sastry, Amanda Askell, Pamela Mishkin, Jack Clark, et al. Learning transferable visual models from natural language supervision. In *International conference on machine learning*, pages 8748–8763. PMLR, 2021. 2
- [37] Nils Reimers and Iryna Gurevych. Sentence-bert: Sentence embeddings using siamese bert-networks. *arXiv preprint arXiv:1908.10084*, 2019. 6
- [38] Franz Rottensteiner, Gunho Sohn, Jaewook Jung, Markus Gerke, Caroline Baillard, Sebastien Benitez, and Uwe Breitkopf. The isprs benchmark on urban object classification and 3d building reconstruction. *Göttingen: Copernicus GmbH*, 2012. 5
- [39] Akashah Shabbir, Mohammed Zumri, Mohammed Ben-namoun, Fahad Shahbaz Khan, and Salman Khan. Geopixel: Pixel grounding large multimodal model in remote sensing. In *Forty-second International Conference on Machine Learning*, 2025. 3
- [40] Sagar Soni, Akshay Dudhane, Hiyam Debary, Mustansar Fiaz, Muhammad Akhtar Munir, Muhammad Sohail Danish, Paolo Fraccaro, Campbell D Watson, Levente J Klein, Fahad Shahbaz Khan, et al. Earthdial: Turning multi-sensory earth observations to interactive dialogues. In *Proceedings of the Computer Vision and Pattern Recognition Conference*, pages 14303–14313, 2025. 3
- [41] Xian Sun, Peijin Wang, Zhiyuan Yan, Feng Xu, Ruiping Wang, Wenhui Diao, Jin Chen, Jihao Li, Yingchao Feng, Tao Xu, et al. Fair1m: A benchmark dataset for fine-grained object recognition in high-resolution remote sensing imagery. *ISPRS Journal of Photogrammetry and Remote Sensing*, 184:116–130, 2022. 5
- [42] Christoph Teufel and Paul C Fletcher. Forms of prediction in the nervous system. *Nature Reviews Neuroscience*, 21(4): 231–242, 2020. 2
- [43] Shiqi Tian, Ailong Ma, Zhuo Zheng, and Yanfei Zhong. Hi-ucd: A large-scale dataset for urban semantic change detection in remote sensing imagery, 2020. 5
- [44] Xin-Yi Tong, Gui-Song Xia, Qikai Lu, Huangfeng Shen, Shengyang Li, Shucheng You, and Liangpei Zhang. Land-cover classification with high-resolution remote sensing images using transferable deep models. *Remote Sensing of Environment*, doi: 10.1016/j.rse.2019.111322, 2020. 5
- [45] Di Wang, Qiming Zhang, Yufei Xu, Jing Zhang, Bo Du, Dacheng Tao, and Liangpei Zhang. Advancing plain vision transformer toward remote sensing foundation model. *IEEE Transactions on Geoscience and Remote Sensing*, 61:1–15, 2022. 2
- [46] Di Wang, Jing Zhang, Bo Du, Minqiang Xu, Lin Liu, Dacheng Tao, and Liangpei Zhang. Samrs: Scaling-up remote sensing segmentation dataset with segment anything model. *Advances in Neural Information Processing Systems*, 36:8815–8827, 2023. 5
- [47] Fengxiang Wang, Mingshuo Chen, Yueying Li, Di Wang, Haotian Wang, Zonghao Guo, Zefan Wang, Boqi Shan, Long Lan, Yulin Wang, et al. Geollava-8k: Scaling remote-sensing multimodal large language models to 8k resolution. *arXiv preprint arXiv:2505.21375*, 2025. 1, 3
- [48] Fengxiang Wang, Hongzhen Wang, Zonghao Guo, Di Wang, Yulin Wang, Mingshuo Chen, Qiang Ma, Long Lan, Wenjing Yang, Jing Zhang, et al. Xlrs-bench: Could your multimodal

- llms understand extremely large ultra-high-resolution remote sensing imagery? In *Proceedings of the Computer Vision and Pattern Recognition Conference*, pages 14325–14336, 2025. 2, 3
- [49] Junjue Wang, Zhuo Zheng, Xiaoyan Lu, Yanfei Zhong, et al. Loveda: A remote sensing land-cover dataset for domain adaptive semantic segmentation. In *Thirty-fifth Conference on Neural Information Processing Systems Datasets and Benchmarks Track (Round 2)*. 5
- [50] Junjue Wang, Zhuo Zheng, Zihang Chen, Ailong Ma, and Yanfei Zhong. Earthvqa: Towards queryable earth via relational reasoning-based remote sensing visual question answering. In *Proceedings of the AAAI conference on artificial intelligence*, pages 5481–5489, 2024. 2, 3
- [51] Tong Wu, Guandao Yang, Zhibing Li, Kai Zhang, Ziwei Liu, Leonidas Guibas, Dahua Lin, and Gordon Wetzstein. Gpt-4v (ision) is a human-aligned evaluator for text-to-3d generation. In *Proceedings of the IEEE/CVF conference on computer vision and pattern recognition*, pages 22227–22238, 2024. 2
- [52] xAI. Grok-2 vision (grok-1212), 2024. Accessed: 2025-07-14. 6
- [53] Gui-Song Xia, Xiang Bai, Jian Ding, Zhen Zhu, Serge Beongie, Jiebo Luo, Mihai Datcu, Marcello Pelillo, and Liangpei Zhang. Dota: A large-scale dataset for object detection in aerial images. In *Proceedings of the IEEE conference on computer vision and pattern recognition*, pages 3974–3983, 2018. 5
- [54] An Yang, Anfeng Li, Baosong Yang, Beichen Zhang, Binyuan Hui, Bo Zheng, Bowen Yu, Chang Gao, Chengan Huang, Chenxu Lv, et al. Qwen3 technical report. *arXiv preprint arXiv:2505.09388*, 2025. 6
- [55] Kunping Yang, Gui-Song Xia, Zicheng Liu, Bo Du, Wen Yang, Marcello Pelillo, and Liangpei Zhang. Semantic change detection with asymmetric siamese networks, 2021. 5
- [56] Yang Zhan, Zhitong Xiong, and Yuan Yuan. Rsvg: Exploring data and models for visual grounding on remote sensing data. *IEEE Transactions on Geoscience and Remote Sensing*, 61: 1–13, 2023. 3
- [57] Yang Zhan, Zhitong Xiong, and Yuan Yuan. Rsvg: Exploring data and models for visual grounding on remote sensing data. *IEEE Transactions on Geoscience and Remote Sensing*, 61: 1–13, 2023. 2, 3
- [58] Ruifei Zhang, Wei Zhang, Xiao Tan, Sibei Yang, Xiang Wan, Xiaonan Luo, and Guanbin Li. Vldrive: Vision-augmented lightweight mllms for efficient language-grounded autonomous driving. In *Proceedings of the IEEE/CVF International Conference on Computer Vision*, pages 5923–5933, 2025. 2
- [59] Xing Zi, Jinghao Xiao, Yunxiao Shi, Xian Tao, Jun Li, Ali Braytee, and Mukesh Prasad. Rsvlm-qa: A benchmark dataset for remote sensing vision language model-based question answering. In *Proceedings of the 33rd ACM International Conference on Multimedia*, pages 12905–12911, 2025. 3

1. Overview of the Appendix

This appendix supplements the proposed VLRS-Bench with additional experimental results and details excluded from the main paper due to space constraints. The appendix is organized as follows:

- Sec. 2: More Analysis of L-2 Tasks in VLRS-Bench.
- Sec. 3: More Details of VLRS-Bench.
- Sec. 4: VLRS-Bench Pipeline Details
- Sec. 5: Visualizations of Random Sampling Cases.
- Sec. 6: Datasheets for the VLRS-Bench.
- Sec. 7: Discussion on Limitations and Societal Impact.

2. More Analysis of L-1 and L-2 Dimensions in VLRS-Bench.

To comprehensively evaluate the remote sensing reasoning capabilities of various MLLMs within the VLRS-Bench framework, we extend our analysis to the aggregated L-1 and L-2 dimensions, uncovering macroscopic performance patterns that reveal the fundamental cognitive strengths and limitations of current models in the geospatial domain.

2.1. Results on Cognition Ability

The Cognition dimension serves as the foundational layer of geospatial intelligence, structured into Spatial Cognitive and Spatiotemporal Cognitive tasks. The performance patterns observed here provide compelling evidence for the structural rationality of the VLRS-Bench design. We summarize two key insights:

(1) Differentiation of Static and Dynamic Reasoning.

A significant performance divergence is observed in general MLLMs, which achieve respectable scores on Spatial Cognitive tasks but suffer a sharp decline in Spatiotemporal Cognitive tasks. This phenomenon validates the structural necessity of distinguishing between spatial and spatiotemporal cognition in VLRS-Bench. It demonstrates that static visual perception and dynamic causal reasoning are fundamentally distinct cognitive capabilities. General models, while capable of identifying objects in a single frame, lack the temporal logic required to interpret how geospatial features evolve. By decoupling these dimensions, VLRS-Bench successfully isolates the temporal bottleneck inherent in current multimodal systems, proving that high perceptual accuracy does not automatically translate to an understanding of dynamic geospatial processes.

(2) Hierarchy of Cognitive Depth across Dimensions.

Expanding the analysis to the broader L-1 dimension, the results establish a clear difficulty gradient where Decision dimension generally yield higher scores than Cognition, with Prediction emerging as the most challenging capability. This hierarchy validates the rationality of the L-1 design, confirming that the three dimensions capture distinct levels of cognitive complexity. Decision dimension rep-

resents constraint-based logical execution; Cognition represents the bridging of perception and physical causality; while Prediction represents the extrapolation of unseen states. This distinct stratification proves that VLRS-Bench covers the full spectrum of geospatial intelligence, effectively distinguishing between models that can merely follow rules and those that possess a grounded understanding of the Earth’s physical evolution.

2.1.1. Results on Decision Ability

The Decision dimension examines a model’s ability to select, compare, and evaluate actions under explicit geospatial constraints, and is decomposed into Pre-Decision (Pre-D) and Post-Decision (Post-D) tasks. The results in Table 1 reveal that decision-making in remote sensing is not a monolithic capability, but a staged reasoning process with distinct cognitive demands.

(1) Asymmetric Difficulty between Pre-Decision and Post-Decision Reasoning. Across General MLLMs, performance on Pre-D and Post-D tasks exhibits noticeable asymmetry. While several models maintain comparable scores between the two stages, others show a clear decline in Post-D performance, indicating difficulty in evaluating downstream consequences after a decision has been made. This suggests that Pre-D tasks primarily assess feasibility filtering under spatial constraints, whereas Post-D tasks require counterfactual reasoning and outcome-aware comparison. RS MLLMs demonstrate a more balanced profile across both stages, with *ScoreRS w/ SFT* achieving 0.382 on Pre-D and 0.419 on Post-D, reflecting stronger consistency in multi-stage decision pipelines. This staged decomposition confirms that VLRS-Bench effectively separates early constraint satisfaction from later consequence evaluation.

(2) Domain-grounded Decision Criteria beyond Model Scale. Although larger models generally achieve higher Decision scores, scale alone does not fully account for decision performance. Domain-aligned models consistently outperform or match substantially larger General MLLMs, particularly in tasks requiring adherence to geospatial norms and operational criteria. For example, *ScoreRS w/ SFT* surpasses Qwen2.5-VL-72B in average Decision score despite a significant parameter gap. This indicates that Decision dimension emphasize normative judgment and structured comparison rather than abstract reasoning depth. By embedding domain-specific constraints into both Pre-D and Post-D tasks, VLRS-Bench distinguishes generic logical competence from grounded decision-making ability, highlighting a critical gap between general-purpose reasoning and operationally valid geospatial decisions.

2.1.2. Results on Prediction Ability

The Prediction dimension evaluates a model’s capacity to extrapolate future geospatial states from observed dynam-

Table 1. Performance evaluation of different MLLMs on the L-1 and L-2 dimension of VLRS-Bench. The models are categorized into General Models and Remote Sensing (RS) Models, with average scores provided for each category.

Model	Cognition			Decision			Prediction		
	SC	ST-C	Avg.Score	Pre-D	Post-D	Avg.Score	OP	SP	Avg.Score
General MLLMs									
GPT-5-chat	0.403	0.344	0.374	0.388	0.388	0.388	0.332	0.286	0.309
GPT-4o-2024-11-20	0.390	0.369	0.380	0.286	0.334	0.310	0.384	0.312	0.348
GPT-4o-mini	0.400	0.361	0.381	0.248	0.304	0.276	0.398	0.292	0.345
Gemini-2.5-flash	0.223	0.156	0.190	0.232	0.240	0.236	0.166	0.134	0.150
Claude-3.5-haiku	0.322	0.208	0.265	0.372	0.370	0.371	0.216	0.208	0.212
Grok-2-vision	0.265	0.248	0.256	0.252	0.300	0.276	0.208	0.160	0.184
Deepseek-vl2	0.390	0.177	0.284	0.416	0.446	0.431	0.112	0.072	0.092
GLM-4.5v	0.241	0.113	0.177	0.312	0.340	0.326	0.152	0.146	0.149
LLama-3.2-11B	0.242	X	0.121	0.292	0.286	0.289	X	X	X
LLama-3.2-90B	0.349	0.268	0.308	0.408	0.430	0.419	0.330	0.240	0.285
Qwen2.5-VL-7B	0.247	0.253	0.250	0.198	0.238	0.218	0.304	0.222	0.263
Qwen2.5-VL-32B	0.317	0.259	0.288	0.370	0.308	0.339	0.280	0.196	0.238
Qwen2.5-VL-72B	0.301	0.244	0.272	0.402	0.370	0.386	0.176	0.196	0.186
Qwen3-VL-2B	0.341	0.345	0.343	0.287	0.260	0.273	0.346	0.308	0.327
Qwen3-VL-8B	0.347	0.390	0.369	0.233	0.275	0.254	0.391	0.393	0.392
Qwen3-VL-32B	0.395	0.404	0.400	0.416	0.364	0.390	0.422	0.354	0.388
<i>Gen. MLLMs Avg.</i>	<i>0.323</i>	<i>0.259</i>	<i>0.291</i>	<i>0.320</i>	<i>0.328</i>	<i>0.324</i>	<i>0.264</i>	<i>0.220</i>	<i>0.242</i>
Remote Sensing MLLMs									
GeoChat	0.320	X	0.320	0.352	0.356	0.354	X	X	X
VHM	0.279	X	0.279	0.324	0.332	0.328	X	X	X
ScoreRS w/ SFT	0.384	0.294	0.339	0.382	0.419	0.401	0.331	0.304	0.318
ScoreRS w/ RL	0.332	0.373	0.353	0.409	0.371	0.390	0.326	0.362	0.344
<i>RS MLLMs Avg.</i>	<i>0.329</i>	<i>0.334</i>	<i>0.332</i>	<i>0.367</i>	<i>0.370</i>	<i>0.369</i>	<i>0.329</i>	<i>0.333</i>	<i>0.331</i>

ics, and is decomposed into Object-level Prediction (OP) and Scene-level Prediction (SP) tasks. Unlike Cognition and Decision, Prediction requires models to reason beyond observable evidence and to internalize assumptions about temporal continuity, interaction, and uncertainty.

(1) Distinct Predictive Assumptions at Object and Scene Levels. A consistent performance gap is observed between OP and SP tasks across General MLLMs, with average scores decreasing from 0.264 to 0.220. This gap reflects not merely a difference in spatial scale, but a shift in predictive assumptions. OP tasks primarily rely on localized temporal continuity, where future states can be inferred from object-level inertia and short-term trends. In contrast, SP tasks require models to anticipate coordinated evolution across multiple entities, enforcing global consistency under shared physical and semantic constraints. The pronounced degradation in SP performance indicates that current general models lack an internal mechanism to maintain system-level coherence when extrapolating complex geospatial processes.

(2) Domain-informed Modeling of Temporal Uncer-

tainty. RS MLLMs exhibit more stable performance across OP and SP tasks, with *ScoreRS w/ RL* achieving 0.326 on OP and 0.362 on SP. This relative robustness suggests that domain-aligned models encode stronger priors about plausible geospatial evolution, reducing structurally invalid predictions even under increased uncertainty. While overall Prediction scores remain lower than those of Cognition and Decision, the differentiated behavior across OP and SP confirms that prediction difficulty is closely tied to how uncertainty propagates from local dynamics to global systems. By explicitly separating object-level extrapolation from scene-level evolution, VLRS-Bench exposes a critical limitation of existing MLLMs: the inability to consistently model long-term, system-level geospatial change.

3. More details of VLRS-Bench

This appendix section presents the statistical specifications of VLRS-Bench and provides comprehensive definitions for the fine-grained L-3 reasoning capabilities.

3.1. Configuration and Statistics of VLRS-Bench

Table 2 provides a detailed overview of our proposed VLRS-Bench, the first benchmark specifically designed to evaluate the advanced reasoning capabilities of Multimodal Large Language Models (MLLMs) in the remote sensing domain. The benchmark is meticulously structured into a three-level hierarchy (L-1, L-2, L-3) to comprehensively assess a wide spectrum of MLLMs abilities.

A key feature of VLRS-Bench is its high linguistic complexity, which is directly linked to the reasoning complexity of the tasks. As shown in the “Avg Q”(Average Question Words) column, the average question length consistently exceeds 130 words. This deliberate design choice requires MLLMs to process and understand long, detailed contextual information, thereby testing their capacity for complex reasoning rather than simple pattern matching. For instance, tasks like Counterfactual Reasoning (CFR) and Mechanistic Interaction Reasoning (MIR) present intricate scenarios that demand a deep comprehension of the provided text to arrive at a correct conclusion.

Furthermore, VLRS-Bench is uniquely designed to evaluate spatiotemporal reasoning through its multi-temporal questions. The “Avg Img” and “Max Img” columns highlight this characteristic. While foundational tasks like Causal Reasoning (CR) are based on single images, more advanced tasks, particularly in the Prediction category, leverage multi-temporal data. In our benchmark, this is exemplified by tasks such as Spatiotemporal Morphological Prediction (ST-M-PR) and Spatiotemporal Sequence Prediction (ST-SQ-PR), which require models to process up to 8 images (“Max Img”). This feature compels MLLMs to not only understand individual scenes but also to reason about complex changes, trends, and future states over extended time periods, a critical capability for real-world remote sensing applications.

The table also details the distribution of annotation formats, including Single-Choice (SC), Multi-Choice (MC), Fill in Blank (FB), and True/False (TF). This diversity ensures a multifaceted evaluation, preventing models from overfitting to a single question style. In summary, the combination of high linguistic complexity and multi-temporal data makes VLRS-Bench a robust and comprehensive tool for assessing the advanced reasoning capabilities of MLLMs in the remote sensing domain.

3.2. More Detailed Definitions of L-3 Capabilities

Spatial Cognitive (SC). This L-2 dimension focuses on evaluating the model’s ability to comprehend the formative causes and intrinsic relationships of geospatial patterns at a single point in time.

- **Causal Reasoning (CR).** This capability evaluates the aptitude for etiological inference. It requires the model to transcend surface-level observables to identify the la-

tent drivers, including natural forces or anthropogenic activities, that precipitated a specific spatial phenomenon. The objective is to determine the provenance of the current state by explaining why a phenomenon emerged from underlying environmental conditions.

- **Counterfactual Reasoning (CFR).** This assesses the capacity for abstract simulation via hypothetical intervention. The model must mentally alter specific antecedent variables to deduce divergent spatial trajectories. This tests the understanding of causal dependencies by examining why an outcome is contingent upon specific conditions, thereby exploring the logical consequences of alternative realities.
- **Mechanistic Interaction Reasoning (MIR).** This focuses on the dynamic coupling of geospatial variables. Unlike identifying a single cause, this requires deciphering the invisible physical or logical feedback loops between elements, such as how topography modulates hydrology. It addresses the process-oriented rationale of why the synergistic interplay of these factors physically precipitates the observed risk or phenomenon.
- **Semantic Integration Reasoning (SIR).** This focuses on the holistic synthesis of regional identity. It requires the model to aggregate disparate low-level visual primitives, including land cover distribution and infrastructure density, into a coherent high-level concept. It addresses the structural rationale of why the specific spatial configuration of these elements collectively constitutes the functional character of the region.
- **Spatiotemporal Cognitive (ST-C).** This L-2 dimension focuses on evaluating the model’s ability to understand how and why geospatial patterns evolve over time.
- **Spatiotemporal Causal-Chain Reasoning (ST-CCR).** This capability evaluates the aptitude for constructing diachronic causal chains. It requires the model to elucidate the logical progression of events, explaining why a specific sequence of temporal antecedents inevitably led to the current spatial state. The objective is to decode the causal lineage of a landscape, linking discrete temporal snapshots into a coherent narrative of evolution.
- **Spatiotemporal Counterfactual Reasoning (ST-CFR).** This assesses the capacity for historical simulation via hypothetical intervention. The model must mentally alter a critical past event to derive a divergent evolutionary trajectory. This tests the understanding of temporal dependencies by examining why the present reality is contingent upon specific historical conditions, thereby exploring the logical consequences of alternative developmental paths.
- **Spatiotemporal Evolution Reasoning (ST-ER).** This evaluates the model’s comprehension of long-term functional metamorphosis over time. It requires the model to interpret the latent semantic shift of a region, explaining

Table 2. Characteristics and vision-language formats of VLRS-Bench

L-1 Tasks	L-2 Tasks	L-3 Tasks	Abbr.	Samples	SC	MC	FB	TF	Avg Q	Avg Img	Max Img
Cognition	Spatial Cognitive (SC)	Causal Reasoning	CR	125	31	32	31	31	130.2	1.00	1
		Counterfactual Reasoning	CFR	125	32	31	31	31	137.7	1.00	1
		Semantic Integration Reasoning	SIR	125	31	31	31	32	125.8	1.00	1
		Mechanistic Interaction Reasoning	MIR	125	32	31	31	31	130.8	1.00	1
	Spatiotemporal Cognitive (ST-C)	Spatiotemporal Counterfactual Reasoning	ST-CFR	125	33	29	31	32	133.2	2.00	2
		Spatiotemporal Causal-Chain Reasoning	ST-CCR	125	32	30	30	33	131.1	2.00	2
		Spatiotemporal Evolution Reasoning	ST-ER	125	34	28	32	31	132.9	2.00	2
		Spatiotemporal Consistency Reasoning	ST-CR	125	33	29	31	32	132.2	2.00	2
Decision	Pre-event Decision (Pre-D)	Planning Reasoning	PR	250	69	56	63	62	133.5	1.00	1
	Post-event Decision (Post-D)	Evaluation Reasoning	ER	250	67	58	62	63	133.3	1.00	1
Prediction	Object-level Predictive (OP)	Spatiotemporal Category-State Prediction Reasoning	ST-CS-PR	125	27	35	32	31	146.3	2.34	8
		Spatiotemporal Morphological Prediction Reasoning	ST-M-PR	125	26	37	31	31	149.8	2.31	8
	Scene-level Predictive (SP)	Spatiotemporal Scenario Uncertainty Prediction Reasoning	ST-SU-PR	125	27	36	32	30	146.6	2.42	8
		Spatiotemporal Sequence Prediction Reasoning	ST-SQ-PR	125	26	37	32	30	141.9	2.37	8

SC: Single Choice, MC: Multi Choice, FB: Fill Blank, TF: True/False, Avg Q: Avg Question Words, Avg Img: Avg Image Count, Max Img: Max Image Count

why the accumulation of incremental physical changes constitutes a fundamental transition in land-use identity. For instance, the model must deduce why the emergence of infrastructure transforms a region’s functional definition from agricultural to residential, rather than merely noting the visual difference.

- **Spatiotemporal Consistency Reasoning (ST-CR).** This tests the ability to verify strict temporal coherence through rigorous quantitative logic. Rather than merely identifying change, the model must assess why the observed magnitude or rate of resource evolution aligns or conflicts with expected patterns. This involves validating the logical consistency of the timeline by quantifying key metrics such as loss or gain rates against the inherent physical constraints of the scene.

3.2.1. Decision

The Decision dimension evaluates the capacity for operational spatial problem-solving. It shifts the focus from passive observation to active strategy, requiring the model to determine *how to execute* specific objectives within complex geospatial environments. We categorize this into generative planning and critical evaluation.

Pre-event Decision (PRE-D). This category focuses on the proactive generation of spatial strategies.

- **Planning Reasoning (PR).** This capability tests the aptitude for spatial optimization. The model must formulate an optimal solution to achieve a defined objective, such as site selection or route optimization. This requires synthesizing the visual evidence to propose a plan that satisfies implicit environmental and logistical constraints, effectively answering *how to configure* the space to meet the goal.

Post-event Decision (POST-D). This category focuses on the retrospective assessment of proposed interventions.

- **Evaluation Reasoning (ER).** This capability tests the practical aptitude for rigorous feasibility analysis. The

model must scrutinize a proposed spatial plan against the actual physical reality of the scene to validate its overall robustness. It involves identifying potential risks or latent inefficiencies to determine how viable the plan is given the realistic contextual limitations, ensuring consistent alignment between the proposal and the surrounding environment.

3.2.2. Prediction

The Prediction dimension evaluates the capacity for temporal extrapolation. It requires the model to project historical observations into the unobserved future, forecasting spatiotemporal states at both the discrete object level and the holistic scene level.

Object-level Predictive (OP). This category focuses on forecasting the specific evolutionary trajectories of individual entities.

- **Spatiotemporal Category-State Prediction Reasoning (ST-CS-PR).** This evaluates the aptitude for forecasting semantic transitions. The model must infer the developmental trajectory of an entity to determine its future identity, such as predicting the inevitable conversion of an agricultural plot into commercial infrastructure based on visible urbanization pressures.
- **Spatiotemporal Morphological Prediction Reasoning (ST-M-PR).** This tests a model’s fine-grained capability to extrapolate continuous geometric evolution. It requires modeling physical dynamics to forecast progressive changes in shape or extent. For instance, the model must analyze historical erosion rates to project the future morphology of a receding coastline, deriving the shoreline’s position five years hence.

Scene-level Predictive (SP). This category focuses on reasoning about the macro-scale evolution and stochastic nature of entire landscapes.

- **Spatiotemporal Scenario Uncertainty Prediction Reasoning (ST-SU-PR).** This assesses the capacity for prob-

abilistic forecasting amidst uncertainty. Recognizing that geospatial evolution is non-deterministic, the model must delineate multiple plausible trajectories. For example, it might derive divergent futures for a peri-urban zone, contrasting a low-density sprawl scenario against a high-density mixed-use development based on potential planning policies.

- **Spatiotemporal Sequence Prediction Reasoning (ST-SQ-PR).** This evaluates the understanding of temporal coherence and logical succession. The model must determine the next phase in a multi-step evolutionary process, validating whether a proposed future state represents a causally consistent continuation of the observed historical sequence.

4. VLRS-Bench Pipeline Details

4.1. Data collection

FAIR1M. FAIR1M is designed for fine-grained object recognition in high-resolution remote sensing imagery. It integrates data from the Gaofen satellite series and Google Earth, with a spatial resolution ranging from 0.3 m to 0.8 m. The dataset contains approximately 15,000 images and more than one million annotated instances spanning 5 major categories and 37 subcategories. All objects are labeled using oriented bounding boxes, and metadata such as geographic coordinates and image resolution are provided. Due to its high intra-class variability, wide geographic coverage, large scale changes, and complex backgrounds, FAIR1M is considered substantially more challenging than previous public datasets, offering a realistic and demanding benchmark for remote sensing object detection.

DIOR. DIOR is a large-scale optical remote sensing benchmark for object detection, covering more than 80 countries. It includes 23,463 images and around 192,472 object instances belonging to 20 categories. The dataset explicitly accounts for variations in scale, imaging conditions (weather, season, viewpoint), object morphology, and background complexity, highlighting challenges such as intra-class diversity and semantic ambiguity between similar categories (e.g., “bridge” or “overpass”). Although DIOR mainly provides RGB imagery without infrared or DSM channels, its rich diversity and substantial scale variations make it an important benchmark for evaluating detection algorithms in complex environments.

DOTA. DOTA is one of the most widely used and large-scale datasets for remote sensing object detection. It is constructed from multi-source imagery including Google Earth, GF-2 satellites, and aerial platforms. Original images are extremely large (thousands to tens of thousands of pixels per side) and are typically cropped into 1024×1024 patches for training. Objects are annotated with oriented bounding boxes to accommodate arbitrary orientations, dense lay-

outs, and large scale variations. The latest version DOTA v2.0 contains 11,268 images and approximately 1.79 million annotated instances. Its diversity in scale, rotation, and background complexity has established DOTA as a crucial benchmark for evaluating detection, segmentation, and rotated bounding box algorithms.

LoveDA. LoveDA focuses on semantic segmentation and domain adaptation in high-resolution remote sensing imagery. It consists of images collected from three Chinese cities, covering both urban and rural scenes, with a spatial resolution of approximately 0.3 m. The dataset includes 5,987 images and about 166,768 annotated objects across seven semantic classes: building, road, water, farmland, forest, barren, and background. LoveDA explicitly targets domain discrepancies between urban and rural environments, making it highly suitable for evaluating semantic segmentation and cross-domain learning methods. No infrared or DSM modalities are specified in the released data.

Potsdam. The Potsdam dataset, released as part of the ISPRS “2D Semantic Labeling Contest”, contains high resolution urban imagery with original image sizes of 6000×6000 pixels. It includes RGB, infrared (IR), and DSM (digital surface model) channels, with a typical ground sampling distance of 5 cm. The dataset provides pixel-level annotations for six semantic classes including building, low vegetation, tree, road, car, and clutter. Owing to its extremely high resolution and multi-modal characteristics, Potsdam is widely used for semantic segmentation and urban change detection tasks.

Vaihingen. Vaihingen is another ISPRS benchmark dataset containing high-resolution orthophotos of the Vaihingen region in Germany, accompanied by DSM and infrared imagery. The average image size is approximately 2494×2064 pixels, with a spatial resolution of about 0.5 m. The annotated classes match those in the Potsdam dataset, including building, low vegetation, tree, road, car, and clutter. The dataset is recognized for its challenging scenes characterized by complex backgrounds, occlusions, and strong shadows, making it an important benchmark for advanced semantic segmentation methods.

GID-15. The Gaofen Image Dataset with 15 categories is primarily constructed from GF-2 satellite imagery. It comprises around 150 large-scale images with spatial resolutions ranging from 0.8 m to 2 m, annotated with 15 semantic land-cover categories. GID-15 is widely adopted in land-cover classification, semantic segmentation, and cross-region generalization research, serving as a major resource in the remote sensing community.

miniUCD. miniUCD is a subset of the Hi-UCD series designed for urban semantic change detection. It is based on ultra-high-resolution (0.1 m) aerial orthophotos from Tallinn, Estonia, covering three temporal snapshots (2017, 2018, 2019). Images are cropped into 1024×1024

paired patches, with pixel-level annotations for nine land-cover classes and semantic change types (*e.g.*, building, road, bare soil, vegetation). Emphasizing fine-grained semantics, multi-temporal observations, and detailed change annotations, miniUCD provides a rigorous benchmark for evaluating semantic change detection models in complex urban environments.

SpaceNet7. SpaceNet7, also known as the Multi-Temporal Urban Development (MUDS) dataset, focuses on building footprint detection, tracking, and temporal change analysis using satellite image time series. It contains monthly composite imagery over 24 months, covering more than 100 geographic regions and approximately 40,000 km². The dataset includes over 11 million building annotations, each assigned a unique identifier to facilitate long-term tracking. Tasks supported by SpaceNet7 include building detection, temporal tracking, and construction/demolition change analysis. Its temporal continuity, large geographic coverage, and object-level tracking make it a key dataset for studying urbanization and spatiotemporal remote sensing.

xView2. xView2 focuses on post-disaster building damage assessment, developed from the xView and xBD initiatives. It uses high-resolution satellite imagery (*e.g.*, WorldView-3 with ~ 0.3 m GSD) and provides paired pre-disaster and post-disaster images, multi-level building damage labels (0–3), and polygon-based building annotations. The combination of fine spatial resolution, detailed damage categorization, and diverse disaster scenarios makes xView2 an essential benchmark for change detection and automated disaster response.

SECOND. The Semantic Change Detection Dataset (SECOND) is a large-scale benchmark specifically developed for semantic change detection in high-resolution remote sensing imagery. Released by Wuhan University, it contains approximately 4,662 pairs of multi-temporal aerial/remote sensing images covering urban regions such as Hangzhou, Chengdu, and Shanghai. Each image pair has a size of 512 \times 512 pixels and provides pixel-level semantic change labels covering classes such as water, bare soil, low vegetation, tree, building, and playground. SECOND targets not only binary change detection but also “from-to” semantic transitions, enabling fine-grained modeling of land-cover evolution. Its clear category design, detailed annotations, and complex urban scenes make it a strong benchmark for advancing semantic change detection research.

4.2. Prior Images

A critical stage in the VLRS-Bench generation pipeline is the integration of Prior Images. This step is designed to systematically elevate the complexity of the generated tasks beyond standard visual perception. By treating these priors

as privileged information, our pipeline constructs a comprehensive multimodal instruction that provides the MLLMs with the necessary multi-dimensional context to address the advanced reasoning tasks defined in our benchmark.

The pipeline purposefully integrates three distinct categories of prior images, each serving as a mechanism to generate questions targeting specific cognitive, decision-making, and predictive abilities:

- 1. Multi-source Remote Sensing Priors.** The pipeline automatically ingests multi-source data such as Digital Surface Models (DSM) and Near-Infrared (NIR) imagery from datasets like Potsdam and Vaihingen (see Table 3). This integration is a deliberate step to generate questions for **Spatial Cognitive (SC)** tasks. For instance, by providing a DSM, the pipeline can formulate a Causal Reasoning (CR) question that requires the model to infer a building’s collapse was caused by its location on a steep slope. Similarly, this data allows the pipeline to construct **Decision** tasks like Planning Reasoning (PR), where a question might ask the model to identify suitable locations for new infrastructure based on ground elevation.
- 2. Expert Pixel-Level Priors.** A unique procedure within our pipeline is the strategic use of expert-annotated masks as input conditions rather than as prediction targets. This procedural choice is specifically designed to generate high-level **Decision** tasks. For example, the pipeline can generate a Planning Reasoning (PR) task by providing a risk-zone mask and asking the model to chart an evacuation route that avoids these areas. It can also construct an Evaluation Reasoning (ER) question by supplying a “protected zone” mask and prompting the model to verify post-event policy compliance. This step in the pipeline transforms the nature of the generated task from simple recognition to constrained, goal-oriented problem-solving.
- 3. Multi-temporal Reference Priors.** For spatio-temporal analysis, the pipeline incorporates reference images from different time points (denoted as temp-img) from datasets like xView2 and SpaceNet7. These priors function as “causal anchors” within the generated instruction. **Crucially, for each temporal image, the pipeline embeds a precise timestamp (accurate to the month) into the instruction.** This grounds the reasoning tasks in physical reality, compelling the model to move beyond simple sequential ordering. It must now consider plausible rates of change—for example, distinguishing between rapid post-disaster reconstruction and slow-paced urban growth over several years. This ensures that the generated **Spatiotemporal Cognitive (ST-C)** and **Prediction** tasks adhere to plausible real-world dynamics. This pipeline step is the explicit mechanism for generating all such tasks, from Spatiotemporal Causal-Chain

Table 3. Distribution of reasoning tasks across different datasets in VLRS-Bench.

Dataset	Prior	Multi-temporal	Cognition						Decision		Prediction				Total		
			CR	CFR	SIR	MIR	ST-CFR	ST-CCR	ST-ER	ST-CR	PR	ER	ST-CS-PR	ST-M-PR	ST-SU-PR	ST-SQ-PR	
FAIR1M	Box2Mask	1	D 26	8	33	14	0	0	0	0	41	23	0	0	0	0	145
DIOR	Box2Mask	1	14	18	35	27	0	0	0	0	74	66	0	0	0	0	234
DOTA	Box2Mask	1	3	4	0	5	0	0	0	0	2	4	0	0	0	0	18
LoveDA	Mask	2	18	19	20	14	0	0	0	0	29	28	0	0	0	0	128
Potsdam	Mask, DSM	1	17	15	14	28	0	0	0	0	40	58	0	0	0	0	172
Vaihingen	NIR, MASK, DSM	1	11	10	1	9	0	0	0	0	8	11	0	0	0	0	50
GID-15	Mask	1	17	20	22	27	0	0	0	0	57	60	0	0	0	0	203
xView2	Mask, temp-img	2	11	19	0	0	12	37	36	34	0	0	0	0	0	0	149
SECOND	Mask, temp-img	2	8	12	0	0	9	42	46	25	0	0	0	0	0	0	142
miniUCD	Mask, temp-img	3	0	0	0	0	0	0	0	0	0	0	23	0	0	0	23
SpaceNet7	Mask, temp-img	9	0	0	0	0	104	46	43	66	0	0	102	125	125	125	736
Total	-	-	125	250	250	125	125	125	125	2000							

Reasoning (ST-CCR) to Spatiotemporal Sequence Prediction Reasoning (ST-SQ-PR).

By orchestrating the integration of these three prior types, our pipeline systematically constructs a sophisticated evaluation landscape. This methodological step ensures that VLRS-Bench moves beyond assessing simple pattern recognition to evaluating a model’s capacity for true cognitive synthesis: analyzing multi-source geospatial data, making decisions under expert constraints, and comprehending complex spatio-temporal dynamics that are grounded in the physical laws of the real world.

4.3. Observed Images

The Observed Image serves as the primary visual anchor for every task within the VLRS-Bench pipeline. It is the original RGB image that provides the foundational visual information upon which all subsequent reasoning is built. To ensure our benchmark is comprehensive and robust, we have curated a highly diverse collection of observed images from a wide array of public remote sensing datasets, as summarized in Table 4.

This collection is characterized by its multi-scale nature and semantic richness. The ground resolution spans from very-high-resolution (VHR) imagery, such as mini-UCD (0.1 m) and Potsdam (0.125 m), which allows for the identification of fine-grained details like individual cars, to medium-resolution data like DIOR (up to 30 m), suitable for analyzing large-scale land-use patterns. This vast range in scale ensures that VLRS-Bench can evaluate a model’s reasoning capabilities across different levels of abstraction.

Furthermore, the semantic diversity is extensive, drawing from both object detection and semantic segmentation datasets. Datasets like FAIR1M and DOTA provide a rich vocabulary of specific object categories (e.g., “Airplane,” “Storage tank”), enabling tasks that require fine-grained recognition and spatial relationship analysis. In contrast, datasets such as LoveDA and GID-15 offer broad land-cover categories (e.g., “Forests,” “Industrial land,” “Paddy field”), facilitating reasoning about complex

scenes, ecological systems, and urban functionality. The scenes themselves are equally varied, encompassing dense urban centers (Potsdam), rural and agricultural landscapes (LoveDA), and specialized infrastructure like airports and harbors (DIOR).

By constructing this varied and challenging visual foundation, we ensure that the Observed Images provide a robust starting point for the generation of complex, multi-faceted reasoning problems across all dimensions of VLRS-Bench.

4.4. Mask Info

A fundamental challenge in applying Multimodal Large Language Models (MLLMs) to specialized domains like remote sensing is their inability to comprehend the intrinsic meaning of expert annotations. A segmentation mask, to an MLLMs, is merely a collection of colored pixels. To address this, as illustrated in Figure 1, our pipeline incorporates a novel Mask Info stage, which acts as a powerful semantic bridge, transforming inert pixel data into a rich, interpretable layer of domain knowledge. This step is a cornerstone of our methodology and represents a significant departure from previous approaches.

The figure depicts how this stage deconstructs a raw segmentation mask and reassembles it as a structured, multi-part semantic dictionary. The design of this dictionary, shown in the central part of Figure 1, is our key innovation:

- 1. Semantic Bridge.** The process first establishes a direct link between a class label (e.g., “Industrial land”) and its precise visual representation using a standardized hexadeciml color code (e.g., “#C80000”). This provides a consistent, machine-readable anchor to the image pixels.
- 2. Category Semantic Mapping.** This is a crucial design element. The pipeline does not stop at generating simple category labels; instead, it further appends concise explanations of the functional significance of each category as well as its typical practical implications in real-world scenarios. This descriptive content is crafted to provide the model with a context-aware, expert-level cognitive perspective.

Table 4. Summary of datasets comprising the visual foundation of VLRS-Bench. This table details the source, image size, class diversity, and ground resolution of the observed images used in our benchmark.

Dataset	Source Type	Image Size	Classes	Ground Resolution
FAIR1M		600 × 600	12 (e.g., Airplane, Baseball field, Bridge, ...)	0.3 m to 0.8 m
DIOR	Object Detection	800 × 800	19 (e.g., airplane, airport, harbor, ...)	0.5 m to 30 m
DOTA		1024 × 1024	18 (e.g., airport, bridge, ship, ...)	—
LoveDA		1024 × 1024	8 (e.g., Buildings, Roads, Water bodies, ...)	0.3 m
Potsdam	Semantic Segmentation	1024 × 1024	6 (e.g., Impervious surfaces, Buildings, Trees, ...)	0.125 m
Vaihingen		1024 × 1024	9 (e.g., Building roofs, Low vegetation, Cars, ...)	0.15 m
GID-15		1024 × 1024	15 (e.g., Industrial land, Paddy field, River, ...)	1.0 m
xView2		1024 × 1024	4 (e.g., No damage, Minor damage, Destroyed, ...)	≤ 0.8 m
SECOND	Change Detection	512 × 512	7 (e.g., Non-change, Low vegetation, Building, ...)	—
miniUCD		1024 × 1024	10 (e.g., Water, Grass, Building, ...)	0.1 m
SpaceNet7		1024 × 1024	1 (Building Footprints)	4.0 m

The innovation, visually captured in the figure, lies in shifting the paradigm from simple labeling to in-context knowledge injection. Prior work typically uses masks as ground truth for segmentation tasks or employs simplistic prompts like “the red area is a building.” Such methods only test the model’s ability to associate a shape with a name. Our approach, by contrast, compels the model to understand the implications of a category. It teaches the model not just what something is, but what it means in a broader context.

Figure 1 provides a concrete example using the GID-15 dataset. The color Red (Hex: “#C80000”) is not merely labeled “Industrial land”; the pipeline enriches it with the functional context: “Industrial land... usually marks industrial areas and generally signals manufacturing or facility clusters.” This enrichment, central to the process shown in the figure, equips the MLLMs to answer complex causal reasoning questions, such as: “Given the proximity of the industrial land (red) to the river (blue), what is a potential environmental risk that should be monitored?”

This is a level of reasoning that is impossible without the functional semantic context provided by our Mask Info stage. By systematically converting abstract color codes into a rich, interpretable knowledge base, this step transforms expert priors from passive constraints into active components of a complex reasoning problem. It is this mechanism that fundamentally enables VLRS-Bench to evaluate the deep, domain-specific cognitive abilities that are essential for real-world remote sensing applications.

4.5. Dataset Info

To provide essential context for the visual data, our pipeline incorporates a Dataset Info component. An MLLMs typically processes an image in isolation, unaware of its real-world origin or technical specifications information that is fundamental to any professional analysis. The Dataset Info stage is designed to inject this crucial metadata directly into

the instruction, thereby simulating a more realistic analytical scenario.

As illustrated in Figure 2, the pipeline appends a concise, descriptive summary for each source dataset. This summary provides the MLLMs with a multi-layered contextual scaffold. For instance, the example for the LoveDA dataset shown in the figure informs the model about the image’s “30 cm resolution,” its geographic origin in “Nanjing, Changzhou, and Wuhan,” and the typical land covers it contains. This information allows the MLLMs to make more plausible, context-aware inferences by setting its expectations regarding scale, regional characteristics, and semantic content.

By providing this high-level metadata, the Dataset Info component prevents the model from making ungrounded or generic assumptions. It ensures that the reasoning tasks are not performed in a vacuum but are instead anchored in a specific geographic and technical context, enabling a more realistic and challenging evaluation of the MLLMs geospatial reasoning capabilities.

4.6. Task Special Prompt

Having established the specific composition of data and priors for each reasoning task in Table 5, the final step in our instruction assembly is to translate this structural template into an executable directive for the MLLMs. This is the role of the Task Special Prompt. Therefore, for each subtask in VLRS-Bench, we engineer a highly-constrained prompt that meticulously guides the model’s generation process. This prompt is multi-faceted, imposing several layers of constraints to ensure the output aligns perfectly with our evaluation objectives, focusing on the desired format, question type, and target capability, as detailed in the following subsections.

```

GID_palette = {
# Format: Key: Value( Class_name — hexadecimal_value A short phrase used to describe this
category )
"Industrial land": "***Industrial land** — **Red (Hex: #C80000)** usually marks industrial areas and
generally signals manufacturing or facility clusters.",
"Urban residential": "***Urban residential** — **Pink (Hex: #FA0096)** usually marks dense
residential zones and generally indicates urban housing patterns.",
"Rural residential": "***Rural residential** — **Light red (Hex: #C89696)** usually marks scattered
residences and generally denotes low-density settlement.",
"Traffic land": "***Traffic land** — **Pale red (Hex: #FA9696)** usually marks transport-related
surfaces and generally indicates road or traffic infrastructure.",
"Paddy field": "***Paddy field** — **Green (Hex: #00C800)** usually marks rice paddies and
generally signals wet-agricultural activity and seasonality.",
"Irrigated land": "***Irrigated land** — **Yellow-green (Hex: #96FA00)** usually marks irrigated
fields and generally denotes managed agriculture and water use.",
"Dry cropland": "***Dry cropland** — **Light green (Hex: #96C896)** usually marks dry farmland
and generally indicates non-irrigated crop areas.",
"Garden plot": "***Garden plot** — **Purple (Hex: #C800C8)** usually marks small cultivated plots
and generally signals intensive horticulture or orchards.",
"Arbor woodland": "***Arbor woodland** — **Deep purple (Hex: #9600FA)** usually marks tree-
dominated woodland and generally indicates forested/agroforestry areas.",
"Shrub land": "***Shrub land** — **Light purple (Hex: #9696FA)** usually marks shrub-dominated
areas and generally denotes transitional vegetation cover.",
"Natural grassland": "***Natural grassland** — **Golden yellow (Hex: #FAC800)** usually marks
natural grasslands and generally signals open grassy ecosystems.",
"Artificial grassland": "***Artificial grassland** — **Yellow (Hex: #C8C800)** usually marks man-
made grass plots and generally denotes landscaped or reclaimed green space.",
"River": "***River** — **Blue (Hex: #0000C8)** usually marks rivers and generally indicates flowing
water corridors and drainage.",
"Lake": "***Lake** — **Cyan-blue (Hex: #0096C8)** usually marks lakes and generally denotes
standing water bodies and reservoirs.",
"Pond": "***Pond** — **Light cyan (Hex: #00C8FA)** usually marks small ponds and generally signals
localized water features or aquaculture." }

```

Figure 1. An illustration of the Mask_Info stage using the GID-15 dataset's mask palette as an example. This process acts as a “semantic bridge,” transforming a raw segmentation mask into a structured, semantically rich instruction. For each class in the GID-15 palette, the pipeline maps the pixel color to a standardized hexadecimal code and appends a functional description, bridging the semantic gap and enabling expert-level reasoning about land use.

Table 5. Specification of data and prior requirements for reasoning tasks in VLRS-Bench. This table outlines the specific temporal structure and the combination of priors required for each task. It details the use of our designed **image reference prior** (denoted as extquotedblleft Hidden extquotedblright), which serves as a causal anchor, alongside other expert pixel-level (“Box2Mask”, “MASK”) and auxiliary remote sensing priors (“DSM”, “NIR”) that enrich the task’s context.

Category	Reasoning Task	Abbr.	Temporal Structure Required			Other Priors				Applicable Dataset Category
			Single (1 img)	Dual (2 imgs)	Tri/Multi (≥ 3 imgs)	Box2Mask	MASK	DSM	NIR	
Cognition	Causal Reasoning	CR	✓	✓(Hidden: im_1)	✗	✓	✓	✓	✓	Single: All; Dual: All
	Counterfactual Reasoning	CFR	✓	✓(Hidden: im_1)	✗	✓	✓	✓	✓	Single: All; Dual: All
	Semantic Integration Reasoning	SIR	✓	✗	✗	✓	✓	✓	✓	Single: All
	Mechanistic Interaction Reasoning	MIR	✓	✗	✗	✓	✓	✓	✓	Single: All
Decision	Spatiotemporal Causal-Chain Reasoning	ST-CCR	✗	✗	✓(Hidden: im_2)	✗	✓	✗	✗	All multi-temporal datasets
	Spatiotemporal Counterfactual Reasoning	ST-CFR	✗	✗	✓(Hidden: im_2)	✗	✓	✗	✗	All multi-temporal datasets
	Spatiotemporal Evolution Reasoning	ST-ER	✗	✗	✓(Hidden: im_2)	✗	✓	✗	✗	All multi-temporal datasets
	Spatiotemporal Consistency Reasoning	ST-CR	✗	✗	✓(Hidden: im_2)	✗	✓	✗	✗	All multi-temporal datasets
Prediction	Planning Reasoning	PR	✓	✗	✗	✓	✓	✓	✓	Single: All
	Evaluation Reasoning	ER	✓	✗	✗	✓	✓	✓	✓	Single: All
	Spatiotemporal Category–State Prediction	ST-CS-PR	✗	✗	✓(Hidden: im_{-1})	✗	✓	✗	✗	All multi-temporal datasets
	Spatiotemporal Morphological Prediction	ST-M-PR	✗	✗	✓(Hidden: im_{-1})	✗	✓	✗	✗	All multi-temporal datasets
	Spatiotemporal Scenario Uncertainty Prediction	ST-SU-PR	✗	✗	✓(Hidden: im_{-1})	✗	✓	✗	✗	All multi-temporal datasets
	Spatiotemporal Sequence Prediction	ST-SQ-PR	✗	✗	✓(Hidden: im_{-1})	✗	✓	✗	✗	All multi-temporal datasets

LoveDA_dataset_info = "This dataset provides 30 cm resolution urban and rural scenes from Nanjing, Changzhou, and Wuhan, covering diverse land covers such as roads, buildings, water, forests, and farmland."

Figure 2. An example of the Dataset Info component for the LoveDA dataset. This text provides the MLLMs with high-level contextual information, including geographic origin, ground resolution, and typical scene types. This meta-level knowledge is crucial for enabling more plausible and context-aware reasoning.

4.6.1. Format Constrained Prompt

The first and most fundamental layer of constraint imposed by the Task Special Prompt is the Format-Constrained Prompt. Its primary function is to enforce a rigid output structure, ensuring that every generated item is standardized, machine-readable, and contains all necessary metadata for evaluation and analysis. As detailed in the template shown in Figure 3, this is achieved through a comprehensive JSON schema that specifies all required fields, from the question text to the internal design rationale.

Crucially, the schema enforces a strict separation of concerns. It mandates fields like “design ideas” and “thinking” to capture the generative model’s reasoning process, while explicitly prohibiting this internal logic from appearing in the user-facing “question” and “options”. This prevents the model from creating “shortcut” questions that are easily solved by pattern matching. Furthermore, the hard constraints explicitly forbid the leakage of privileged information into the final question by blacklisting tokens such

as “mask”, “DSM”, or “im1”. The prompt also governs the qualitative aspects of the multiple-choice options, mandating that all distractors be plausible and semantically related to the topic.

By imposing this rigorous format, the Format-Constrained Prompt acts as the foundational quality gate in our pipeline. It guarantees that the output is not only structurally sound but also that the generated questions are self-contained and fairly test the MLLMs reasoning abilities without providing unintended clues.

4.6.2. Reasoning Overarching Constraints Prompt

Beyond the structural integrity enforced by the Format Constrained Prompt, we introduce a more sophisticated layer of control: the Reasoning Overarching Constraints. This prompt layer is not about the output schema, but about the intrinsic quality and cognitive complexity of the reasoning task itself. As exemplified by the multi-select prompt for DSM-enabled datasets shown in Figure 4, its primary purpose is to guide the generative model to produce questions that are deep, challenging, and test specific reasoning pathways. The core of this prompt is dedicated to designing for reasoning depth. It mandates that every option be a complex declarative statement requiring multi-step verification. This is achieved by enforcing the use of “Descriptive Spatial Anchors” (e.g., “the cleared patch adjacent to the main structure”) to ground the reasoning in specific image regions, and “Deterministic Language” to eliminate ambiguity, making each option definitively true or false. For datasets with auxiliary data, the prompt even forces the logical integration of concepts from privileged information (such as height from a DSM) into an RGB-solvable question, compelling the model to translate abstract data into visual cues (e.g., shadows, perspective) and thus increasing the reasoning complexity.

Furthermore, a critical function of these constraints is to ensure the robustness of the evaluation by actively mit-

```

Format_Constrain_TEMPLATE = """
Schema (fields required):
{{

  "id": "<string - sample id or filename>",

  "design_ideas": "<string - detailed step-by-step design rationale including: 1) image analysis from coarse to
fine scale, 2) key features/patterns identified, 3) reasoning chain construction, 4) question formulation
strategy, 5) option design logic>",

  "question": "<string - human-facing question using probabilistic language like 'most likely', 'most probable',
'best indicates', 'primarily suggests'; MUST NOT contain forbidden tokens>",

  "qa_type": "single_choice",

  "options": {"A": "...", "B": "...", "C": "...", "D": "...", "E": "..."},

  "correct_letters": ["A"],

  "declared_answer_text": "<original answer text - short>",

  "thinking": "<string - summary -> breakdown -> summary>",

  "meta": [{"dataset": "{dataset}", "visibility_stage": "{visibility_stage}"},

    "images_used": {visible_images_path}, "masks_used": {hidden_images_path} ]}

}}

```

Hard constraints:

- qa_type is fixed as 'single_choice'
- options must include keys 'A'..'E' exactly (five options for single choice)
- correct_letters must be a JSON array with exactly one uppercase letter A..E
- question must NOT contain forbidden tokens (mask/DSM/im1/im2/im3/segmentation)
- do NOT include extra top-level keys outside schema (if you must indicate error, return: [{"error": "<reason>"}])
- The thinking processes in the "thinking" and "design_ideas" fields, as well as the thinking and logic behind the question design process, must be prohibited from appearing in the "question" and "options" fields.

All five options must be:

- Plausible and semantically related to the question topic
- Differentiated by probability/likelihood rather than absolute correctness
- Based on reasonable interpretations of visual evidence
- Avoid options that are obviously wrong or irrelevant

Figure 3. The template for the Format-Constrained Prompt. This template enforces a strict JSON schema and a set of validation rules, ensuring that all generated evaluation items are structurally consistent, machine-readable, and adhere to predefined quality standards.

igating known MLLMs biases. We observed that models often exhibit positional preference, favoring earlier options (e.g., A, B, C) when selecting from a large set. To counteract this, the prompt enforces a strict “Answer Randomization Protocol”: a predefined number of correct and incorrect statements are generated internally and then shuffled before being assigned letters. This procedure ensures that the cor-

rect answers are distributed randomly, preventing models from succeeding based on lazy heuristics rather than genuine reasoning. Furthermore, the prompt’s “Deception and High Challenge Requirement” ensures that all options are plausible and difficult, forcing a thorough analysis for both true and false statements. In essence, the Reasoning Overarching Constraints act as a cognitive blueprint, compelling

```

def get_num_correct_options():
    """
    Randomly determines the number of correct options (out of 8 total)
    based on the specified distribution:
    """
    .....
    return num_correct_options

def Universal_Overarching_Constraints_dsm(name="", num_correct_options=None):
    """
    Generates a multi-select question prompt tailored for visual reasoning,
    incorporating DSM and MASK data, with a specified number of correct options.
    """
    if num_correct_options is None:
        num_correct_options = get_num_correct_options()
    num_incorrect_options = 8 - num_correct_options
    return f"""

When generating questions, the model will simultaneously 'observe' two auxiliary images and one original image:
1) MASK segmentation map (for model reference in question generation only; humans solving the question **do not see it**)
2) DSM elevation map (for model reference in question generation only; humans solving the question **do not see it**)
3) Original remote sensing image (visible to humans during solving; used solely during question generation to verify the accuracy of question information).

Requirements for the generated output:
- Produce a question stem (e.g., "Which of the following statements are true?") and **exactly eight answer options (A-H)**.
- The question stem and all eight options must align with the original remote sensing image, avoiding any semantic details inconsistent with it.
- **Strictly adhere to dataset categories**: Each color in the MASK image represents a specific land feature category; do not speculate or fabricate categories not present, strictly adhering to the provided color-to-category mappings.
- **DSM Elevation Interpretation**: In the DSM elevation map, darker colors indicate higher relative elevations of features, while lighter colors indicate lower relative elevations.
- Prior to question generation, first summarize the image information by providing an overview from coarse to fine scales, **then cross-verify with the original remote sensing image for corrections**, and subsequently design the question in accordance with the '{name}' logic.
- Ensure that the question and all options are semantically and logically correct, avoiding scenarios inconsistent with the image information, as well as obvious semantic errors or logical contradictions.
- **No internal terms**: The question and options must not include terms such as 'Mask', 'DSM'. They should only feature natural scene elements and reasoning clues, without revealing details from the MASK or DSM maps.

**Crucial: Answer Randomization Protocol**
# To avoid positional bias (e.g., always having correct answers among the first few options), you MUST follow this procedure:
1. **Internal Generation**: First, internally generate exactly **{num_correct_options} correct (True) statements** and **{num_incorrect_options} plausible but incorrect (False) statements**. Do not label them A-H at this stage.
2. **Randomization**: Next, **randomly shuffle the order** of these eight generated statements.
3. **Identify Answers**: In the '<Answer>' tag, provide a **comma-separated list** of the letters (e.g., 'A, C, G') that correspond to the original correct statements' new positions. This is a mandatory step to ensure the final answers are not concentrated or predictable.

- **Mandatory Multi-Step Reasoning**: Each of the eight option statements must incorporate at least 2-3 combined elements (e.g., quantifiers + descriptive spatial anchors + relational claims) to require verifiable multi-step visual reasoning. Internally, build a chain of 4-6 steps to finalize each claim (e.g., Step 1: Identify key regions with descriptive anchors like 'the empty area in the lower-left corner of the image'; Step 2: Apply quantifiers to visible features within those regions; Step 3: Establish relations or comparisons (e.g., 'adjacent to'); Step 4: Infer functional aspects based on patterns; Step 5: Cross-verify cues for ambiguity; Step 6: Ensure the claim is testable and grounded in visible details).
- **Prohibit Trivial Outputs**: Strictly avoid simple pixel-level or descriptive statements without reasoning layers; instead, design claims that appear straightforward but demand step-by-step analysis to judge.
- **Descriptive Spatial Anchor Requirement**: Each option statement must include precise, descriptive spatial anchors** that combine location with visible features (e.g., 'the empty area in the lower-left corner of the image', 'the cleared patch adjacent to the main structure', 'the dense cluster north of the large building') in the claim to anchor the reasoning to specific, observable areas. Avoid abstract terms like 'lower-left quadrant' without descriptive integration.
- **Claim Length and Richness Requirement**: To ensure each option is informationally complete and abundant in details, **the question sentence must be at least 40-60 words long**, **each of the eight option statements must be at least 20-40 words long**, achieved by logically incorporating nested descriptions, quantifiers, relations, and inferences (e.g., using clauses to elaborate visible cues). Avoid short, incomplete sentences: prioritize richness that supports multi-step verification without redundancy.
- **Deterministic Language Requirement**: Each option statement must use definitive, certain language** to form a clear declarative statement that can be judged strictly as True or False. Avoid any words or phrases implying uncertainty, such as 'seems', 'appears', 'suggests', 'possibly', 'might', or equivalents in other languages. Instead, use direct, assertive terms like 'consists of', 'contains', 'demonstrates', 'is used as', 'shows', or 'indicates' only if it conveys certainty based on visible evidence.
- **Deception and High Challenge Requirement**: To create a high-quality challenge, all options (both correct and incorrect) must be deceptive and difficult to ascertain.
- **The {num_correct_options} Correct (True) Options**: Each must contain subtle information that might initially suggest it is False, or its correctness is hard to verify without careful, multi-step logical reasoning using only RGB evidence. **Do not provide obvious truths or directly output internal reasoning steps; instead, craft claims that require non-trivial analysis to confirm.**
- **The {num_incorrect_options} Incorrect (False) Options**: Each must be highly plausible. Their surface cues should lean strongly toward being True, but they must be definitively provable as False upon closer inspection and multi-step analysis of the RGB image. They should serve as strong, well-crafted distractors.
- **Difficulty Assurance**: Validate that the question is highly challenging (e.g., surface-level ambiguity resolvable only through detailed RGB evidence and careful multi-step reasoning), aligning with high-quality reasoning standards without relying on dataset-specific internals.
- **Force Logical Height Integration**: For datasets with DSM elevation data (used internally for verification), **every option statement must logically incorporate height-related information** grounded in visible RGB cues (e.g., 'elevated ridge', 'sloped terrain higher than adjacent areas', 'raised platforms indicating height variations'). Ensure this is naturally integrated into the reasoning (e.g., combined with spatial anchors or functional inferences) to enhance verifiability, without mentioning DSM or other internals.

Use the following color→category mapping for internal verification:"""

```

Figure 4. An example of the Reasoning Overarching Constraints, specifically the template for a multi-select question utilizing DSM as a prior. This prompt layer governs the substantive quality of the generated content by enforcing rules for reasoning depth, mitigating MLLMs biases through a mandatory randomization protocol, and ensuring a high degree of challenge.

the generative model to function less like a data labeler and more like an expert question designer. This ensures the high difficulty and validity of the VLRS-Bench evaluation items by simultaneously demanding deep reasoning and neutralizing predictable model behaviors.

4.6.3. Temporal Prior Prompt

To operationalize the diverse temporal data structures defined in Table 5, our pipeline employs a dynamic Temporal Prior Prompt. This component translates the abstract concept of an image reference prior (*e.g.*, “Hidden: im_2 ”) into a concrete, linguistically framed reasoning problem. As shown in Figure 5, this is not a single static prompt, but a rule-based system that constructs a specific temporal narrative tailored to the target reasoning task.

The system uses two primary phrasing strategies to control the MLLMs temporal perspective. For tasks like Spatiotemporal Prediction (“ST-CS-PR”, “ST-M-PR”, *etc.*), it uses a “relative-to-now”framing (“im123_phrase”). This establishes the middle image as the present viewpoint (“now”) and describes the past and future with precise, human-readable offsets (*e.g.*, “the scene nine months before now”). This structure forces the model to reason forward or backward from a known anchor point.

In contrast, for tasks requiring reasoning about a hidden intermediate state, such as Spatiotemporal Causal-Chain Reasoning (“ST-CCR”), the prompt uses an “earliest-latest”framing (‘im1_im3_only_phrase’). This strategy deliberately omits any mention of the middle image, forcing the model to reason about the causal gap between the first and last visible images across a total elapsed interval. This directly implements the “Hidden: im_2 ”logic from our task design, compelling the model to infer the unobserved process rather than simply describe a sequence.

By dynamically selecting and applying these strict phrasing rules, the Temporal Prior Prompt ensures that each question is precisely aligned with the intended cognitive challenge. It grounds the reasoning in physical time and forces the MLLMs to adopt the exact temporal perspective required by the specific reasoning skill being evaluated.

4.6.4. Capability Constrained Prompt

The Capability-Constrained Prompt represents the most specialized layer of our instruction design, acting as the cognitive core that defines the essence of each L-3 reasoning subtask. While other prompts manage structure and general quality, this component provides the specific “intellectual blueprint”for a single capability. Its purpose is to guide the MLLMs to construct a question that not only aligns with a task’s name but embodies its fundamental reasoning challenge. The prompt for Spatiotemporal Category-State Prediction Reasoning (ST-CS-PR), shown in Figure 6, serves as a powerful example of this design philosophy.

The primary significance of this prompt layer is its ability to enforce deep, task-specific logic. As seen in the ST-CS-PR example, the prompt does not simply ask for a prediction. Instead, it mandates a specific reasoning pathway: the MLLMs must generate a question where the solution requires extrapolating trends derived from hidden temporal masks, trends that are deliberately ambiguous in the visible RGB images. This principle is generalized across all our L-3 tasks. For a causal reasoning task, the prompt would similarly force the generation of a question where the cause is non-obvious and requires integrating multi-source priors. This ensures that each question is a valid and targeted test of its intended capability.

Furthermore, this prompt layer is engineered to create a high-challenge, high-fidelity evaluation. The ST-CS-PR example illustrates this by demanding “hyper-complex prediction chains”and “quintuple-nested twists,”forcing the MLLMs to design a problem with multiple layers of deception. It also requires “high structural similarity”among options, a strategy we employ to create strong, plausible distractors that test for fine-grained understanding rather than coarse pattern matching. This design principle, which involves creating non-trivial, deceptive, and deeply layered problems, is a universal feature of our Capability-Constrained Prompts.

In essence, the Capability-Constrained Prompt is where we translate an abstract reasoning skill into a concrete, solvable, yet extremely challenging problem. By providing a detailed, task-specific “recipe”for thought, we compel the MLLMs to move beyond superficial generation and act as an expert designer of cognitive puzzles. This ensures that VLRS-Bench does not merely ask questions, but presents complex reasoning scenarios that rigorously probe the advanced capabilities of MLLMs in the geospatial domain.

4.6.5. Instruction for VLRS-Bench

The culmination of our instruction design methodology is the final instruction assembly, orchestrated by the master template shown in Figure 7. This template serves as the final directive that synthesizes all the independent informational components and logical constraints into a single, coherent package for the MLLMs.

As shown in the figure, this master directive systematically integrates the task’s contextual information, which includes Dataset info, Mask palette that serves as a semantic bridge, and the file paths for Prior images and Observed images, with the task-specific generative logic contained in the task prompt.

The purpose of this final synthesis is to provide the MLLMs with a complete and unambiguous problem definition. It clearly separates the available contextual information from the specific generative task it must perform, which is triggered by the final command to “Generate exactly one JSON object.”This structured synthesis ensures that every

```

im123_phrase = (
    f"\n **Temporal phrasing rules (use exactly these styles):**\n"
    f" - The middle image is the current viewpoint and should be described as \"now\" (the solver's primary view).\n"
    f" - Describe the earlier image as: \"the scene {interval_1to2} before now\" (i.e., now - {interval_1to2}).\n"
    f" - Describe the later image as: \"the scene {interval_2to3} after now\" (i.e., now + {interval_2to3}).\n"
    f" - If the later image is not visible, phrase tasks as predictions: e.g., \"predict the scene {interval_2to3} after now.\n"
    f" - If the earlier image is not visible, phrase tasks as reconstructions: e.g., \"infer the scene {interval_1to2} before now.\n"
    f" - Do NOT use vague time words such as 'earlier'/'later' or ordinal words 'first/second/third' in the question text.\n"
    f" - Use numeric, human-readable offsets (examples: 'nine months', 'four months', 'one year') when stating times.\n"
)

# phrasing for jobs that must NOT reference the middle image and instead use interval_total between earliest and latest images
im1_im3_only_phrase = (
    f"\n **Temporal constraint for earliest-vs-latest tasks:**\n"
    f" - The question must explicitly state the elapsed interval `interval_total` describing the time between the earlier image and the later
image.\n"
    f" - For example: \"The interval between the earlier image and the later image is {interval_total}.\"\n"
    f" - In such tasks, do NOT mention or describe the middle/current image at all. Frame all temporal language solely around the
earlier/later pair\n"
    f" (e.g., \"the earlier scene {interval_total} before the later scene\").\n"
)
if job == "ST_CCR":
    prior += im1_im3_only_phrase
    return build_spatiotemporal_causal_chain_prompt(datasets=datasets,
                                                    interval_1to2=interval_1to2, interval_2to3=interval_2to3, interval_total=interval_total)
elif job == "ST_CFR":
    prior += im1_im3_only_phrase
    return build_spatiotemporal_counterfactual_prompt(datasets=datasets,
                                                    interval_1to2=interval_1to2, interval_2to3=interval_2to3, interval_total=interval_total)
elif job == "ST-ER":
    # this task uses only the earlier (im1) and later (im3) images in the question stem
    prior += im1_im3_only_phrase
    return build_multitemporal_evolution_prompt(datasets=datasets, interval_1to2=interval_1to2, interval_2to3=interval_2to3,
                                                interval_total=interval_total)
elif job == "ST_CS":
    prior += im1_im3_only_phrase
    return build_multitemporal_consistency_prompt(datasets=datasets, interval_1to2=interval_1to2, interval_2to3=interval_2to3,
                                                interval_total=interval_total)
elif job == "ST_CS_PR":
    prior += im123_phrase
    return build_multitemporal_class_state_prediction_prompt(datasets=datasets,
                                                    interval_1to2=interval_1to2, interval_2to3=interval_2to3)
elif job == "ST_M_PR":
    prior += im123_phrase
    return build_multitemporal_shape_prediction_prompt(datasets=datasets,
                                                    interval_1to2=interval_1to2, interval_2to3=interval_2to3)
elif job == "ST_SU_PR":
    prior += im123_phrase
    return build_multitemporal_uncertainty_prediction_prompt(datasets=datasets,
                                                    interval_1to2=interval_1to2, interval_2to3=interval_2to3)
elif job == "ST_SQ_PR":
    prior += im123_phrase
    return build_multitemporal_sequence_prediction_prompt(datasets=datasets,
                                                    interval_1to2=interval_1to2, interval_2to3=interval_2to3)
else:
    # undefined job: preserve original fallback behavior
    return f"[DEFAULT PROMPT for {job} on {datasets}]"

```

Figure 5. An example of the Temporal Prior Prompt, demonstrating how three-phase temporal data is used to construct diverse reasoning tasks. The code illustrates how different images are strategically employed as hidden reference priors. By dynamically selecting phrasing rules, this mechanism significantly enhances the logical realism and reasoning depth of the generated questions.

```

def build_multitemporal_class_state_prediction_prompt_of_ability():
    name="Multi-Temporal Class State Prediction Reasoning",   # Task name defining the reasoning type, used to enforce task-specific logic alignment
    intervals=["one year", "one year"],                         # List of time interval strings representing sequential phase intervals; determines n_phases calculation
    interval_total="two years"                                  # Total aggregated time span description for examples when intervals have multiple entries
):
    n_phases = len(intervals) + 1
    last_interval = intervals[-1]
    prior_intervals_str = " ; ".join([f"im{i}" to im[i+1] over {intervals[-1]} for i in range(1, n_phases)])
    past_intervals = ", ".join(intervals[-1])
    # Used to describe the chain of past intervals
    specific_constraints = f"""

    **Important Temporal Assumption**: You must assume the last visible image (im{n_phases-1}) is the current time point (now), and the task is to predict the state in the hidden future image (im{n_phases}) (last_interval) after now. Do not use image labels like im{n_phases-1} or im{n_phases} in the generated question text; use natural phrasing such as "predict ... (last_interval) after now".

    - Adhere strictly to '{name}' — the task is about predicting the **future category state** of a given object {last_interval} after now, using multi-temporal hidden evidence to uncover trends in remote sensing contexts.
    - To elevate difficulty via maximal utilization of hidden masks (mask1 to mask{n_phases}) across all phases, leverage temporal mask differences for precise trend extrapolations (e.g., category transition rates over {past_intervals}, density change thresholds, implicit evolution graphs across phases) that visible images from {past_intervals} ago to now cannot resolve alone, ensuring correct prediction only via these hidden mask details.
    - To build hyper-complex prediction chains, construct at least 9 steps with quintuple-nested twists, where each step builds on multi-mask derived metrics (e.g., temporal fragmentation index from mask1 to mask2 over {intervals[0]}), projected density shifts for {last_interval}, creating logical interdependencies that collapse distractors stepwise.
    - Design for high similarity in answers: All options must share 80-90% structural similarity (e.g., all predict 'urban transition' but differ in subtle multi-mask validated states like specific class persistence rates), causing non-multi-mask models to misjudge due to inability to discern fine temporal distinctions.
    - **Force time interval integration in options**: Every generated option must explicitly reference the time intervals (e.g., "(prior_intervals_str), the state was X: predict Y (last_interval) after now"), ensuring solvers reason with temporal context.
    - Follow this advanced multi-step process for brain-teaser elevation:
        1. **Identify ultra-ambiguous** multi-mask dependent trend**: Trajectory where visible images to now suggest multiple similar states, but hidden masks pivot the extrapolation {last_interval} after now.
        2. **Layer hyper-deep prediction chains**: 9+ steps with sub-layers and temporal twists (e.g., Step 1: Visible ambiguity; Step 2-4: Initial trends from mask1-2 over {intervals[0]}; Step 5: First twist via transition rates; Step 6: Second via density shifts; Step 7: Third via evolution graphs; Step 8: Fourth paradoxical inversion; Step 9: Multi-mask exclusive future state for {last_interval}).
        3. **Incorporate quintuple-nested twists**: Multi-level deceptions with high similarity (e.g., twists progressively refine similar predictions, only multi-mask precision breaks the tie).
        4. **Design hyper-similar deceptive distractors**: Options mirror correct state in wording/structure but falter on multi-mask specifics (e.g., 'persistent farmland' vs. 'converted farmland—masks alone confirm').
        5. **Validate extreme difficulty and multi-mask centrality**: Ensure without hidden masks, similarity leads to random/misjudged choices; with them, chain logically coheres via remote sensing authenticity like temporal change detection.
    {change_scope}
    - **Focus**: predict the **future category state** of a given object {last_interval} after now (the current visible image).
    - Solver sees images from {past_intervals} ago to now (past to current visible images).
    - **Hidden**: the future image (im{n_phases}): {last_interval} after now and all masks (mask1 to mask{n_phases}), used internally to ground transitions and validate predictions.

    - **Constraints for Question and Options Generation**:
        - Generate a lengthy question that describes complex past observations in natural language, integrating time intervals naturally without using image labels or exposing reasoning chains.
        - Generated options should be lengthy and descriptive, focusing solely on the predicted future state {last_interval} after now, with high structural similarity and subtle differences validated only by multi-mask details.
        - Do NOT include reasoning steps, historical changes, detailed timelines, or process descriptions in options—reserve all logic and explanations for the solving rationale. Naturally integrate time references (e.g., "{last_interval} after now, the state will be...") without repeating past events.

    - The reasoning chain must be **multi-step and context-sensitive**:
        1. Detect how the object changed across visible images from {past_intervals} ago to now, using hidden masks for precise trends.
        2. Examine surrounding regions (e.g., proximity to roads, rivers, urban edges).
        3. Combine trajectory + context → predict category {last_interval} after now.
        4. Ensure distractor categories are plausible but contradicted by spatial or semantic context revealed by masks.

    - **Example twists**:
        - Farmland visible shrinking from {past_intervals} ago to now, surrounded by residential expansion, is unlikely to remain farmland → predicted state becomes residential or industrial {last_interval} after now.
        - Forest visible thinning from {past_intervals} ago to now, adjacent to new infrastructure, is unlikely to stay forest → predicted state becomes bare land or farmland {last_interval} after now.
        - Wetland visible shrinking from {past_intervals} ago to now, adjacent to urbanization, is unlikely to recover → predicted state becomes urban {last_interval} after now.
    .....

    # Proofreading: Dynamically generate examples to avoid ungrammatical sentences.
    if len(intervals) == 2:
        past_description = f"{intervals[0]} ago to now"
    else:
        past_description = f"the past {interval_total} to now"
    examples = f"""
         From {past_description}, the central zone changed from intact farmland to scattered houses. Now predict what the category will be {last_interval} after now. </Q>
         From {past_description}, the upper-left forest thinned. Now predict what the category will be {last_interval} after now. </Q>
    """
    return f"""
        You are a professional expert in multi-temporal class state prediction reasoning for remote sensing images, specializing in hyper-challenging brain-teasers where high-similarity options mislead non-multi-mask models, resolved by hidden temporal details in remote sensing style.
        {auto_start_prompt(datasets, name)}
        {specific_constraints}
        {examples}
    """
    Based on the above requirements, generate one extremely complex, multi-mask critical question that aligns with '{name}' for remote sensing image challenges, and provide a complete step-by-step solving rationale highlighting hidden masks' pivotal roles in predicting the future state {last_interval} after now. """strip()

```

Figure 6. The template for the Capability-Constrained Prompt, shown for the Spatiotemporal Category–State Prediction Reasoning (ST-CS-PR) task. This prompt injects the specific reasoning logic for this capability, compelling the MLLMs to generate a hyper-challenging question that is solvable only by leveraging hidden temporal mask information to extrapolate future states.

piece of information and every constraint is correctly passed to the model, forming a complete and well-defined reason-

ing problem ready for generation.

```

Instruction_for_vlrs = """
You are given (generation-only):
- Dataset_name: {dataset_name}
- Mask_palette: {mask_palette} # semantic bridge for MASK to MLLMs
- Prior_images: {prior} # list of filenames, such as DSM, Mask, NIR
- Observed_images: {observed_images} # list of filenames humans will
see
- Dataset_info: {Dataset_info}

Also you are provided with a task_prompt that defines the reasoning
goal:
{task_prompt} # prompts specifically designed for the reasoning
characteristics of each sub-ability

Task:
Generate exactly one JSON object matching the schema below. The
JSON will be consumed automatically; DO NOT output ANY extra fields
or free text outside the object.

"""

```

Figure 7. The master template for the final instruction assembly. This code orchestrates the synthesis of all previously defined components, which include dataset info, the mask info, and the specific task prompt, into a single, comprehensive instruction fed to the MLLMs.

4.7. Cross Verification By Models

4.7.1. Model-Based Analysis Generation

The first stage of our verification process is an automated, model-driven analysis designed to deconstruct the reasoning logic of each generated QA item. To mitigate the risk of a single model’s inherent biases or logical blind spots, we do not simply ask another model to “agree” or “disagree” with the answer. Instead, we compel a “proposer” model to generate a detailed, evidence-based justification for its own interpretation of the question. This generated analysis then becomes the object of scrutiny in the subsequent cross-verification stage.

To achieve this, we employ a highly structured prompt, as detailed in Figure 8. This prompt instructs the proposer model to act as a “REMOTE SENSING INFERENCE QA” expert. It is tasked with performing a rigorous analysis of the provided question and, critically, every single option. For each option, the model must follow a strict procedure: restate the claim, cite specific visual evidence from all available modalities (e.g., “optical: dark elongated shadow at center-right,” “DSM: +3.2 m rooftop at upper-left”), determine its correctness, and provide a concise justification.

The prompt explicitly requires the model to think in terms of remote sensing principles, such as cross-modal corroboration and the implications of ground sample distance (GSD). It also mandates the creation of a final “chain_of_reasoning” that summarizes the logical steps leading to its conclusion. The output is constrained to a rigid JSON schema, ensuring that the analysis is structured, consistent, and machine-readable.

This initial step is crucial because it forces the under-

lying logic of the QA item to be made explicit. The resulting “option_analysis” and “chain_of_reasoning” serve as a transparent “statement of logic” that can be systematically evaluated for factual accuracy and logical consistency by other models in the next stage of our verification pipeline.

4.7.2. Cross-Verification by an Evaluator Model

Following the generation of a detailed analysis by the “proposer” model, the QA item and its accompanying analysis enter the cross-verification stage. The goal of this stage is to subject the initial analysis to a rigorous, multi-faceted critique by a separate and independent “evaluator” model. This process is designed to detect logical fallacies, factual inaccuracies, or biases that the original model may have overlooked.

To orchestrate this evaluation, we employ a specialized prompt, as detailed in Figure 9. This prompt guides the evaluator model through a structured, two-part assessment process.

To ensure an unbiased initial assessment, the evaluator model is first instructed to answer the question independently, without any access to the proposer’s reasoning. This step is critical as it provides a baseline answer derived from a different “perspective,” helping to identify cases where the original question might be ambiguous or where the proposer’s logic was flawed from the outset.

After forming its own opinion, the evaluator model then proceeds to critically assess the proposer’s JSON analysis. The evaluation is broken down into five key dimensions: ‘Evidence Alignment’ (are the cited visual cues real?), ‘Reasoning Quality’ (is the geospatial logic valid?), ‘Option Decision Correctness’ (is the true/false judgment correct?), ‘Remote Sensing Expertise’ (is the domain knowledge accurate?), and ‘Question Design Quality’ (is the question itself well-posed?). Each dimension is scored on a scale, forcing a granular and quantitative assessment.

Finally, the evaluator model provides a “final_score” and a concise “verdict” on whether the QA item is of sufficient quality to be retained. This multi-stage, multi-dimensional verification process, performed by a panel of distinct models, acts as a robust automated filter.

The effectiveness of this cross-verification pipeline is demonstrated by its rigorous filtering capability. **From an initial pool of over 6,500 generated QA items, this automated process systematically identified and discarded those with logical inconsistencies, factual errors, or poor design. Ultimately, only 2,694 items met our stringent quality criteria** and were passed on to the final stage of human expert review, highlighting the crucial role of this automated verification in ensuring the benchmark’s integrity.

4.8. Sampling Inspection by RS Experts

While the automated cross-verification pipeline provides a robust filter against logical and factual errors, the nuance

```
Generate_Analysis = ""
```

You are an expert in **REMOTE-SENSING INFERENCE QA**.

Given a single QA item about a remote-sensing image, perform a **rigorous, evidence-based, logic-driven analysis** of the question and **EVERY option**, using available image modalities (optical, DSM, mask, NIR, etc.). Focus on how to combine modalities in reasoning (**cross-modal corroboration**), cite approximate image regions (e.g., "upper-left", "center-right"), and clearly state any missing modalities. Return **ONLY a single JSON object** (no extra text).

INPUT (you will receive this JSON-like object; images/channels may be attached separately):

```
{  
  "id": "...",  
  "dataset": "...",  
  "job": "...",  
  "qa_type": "single_choice" or "multi_choice",  
  "image": ["path/to/image.png", ...],  
  "question_text": "Full question text with options inline or separately",  
  "options": { "A": "text", "B": "text", ... },  
  "reference_answer": "A,B" // optional  
}
```

ANALYSIS REQUIREMENTS (behavioral & logical):

Treat the task as **REMOTE-SENSING INFERENCE QA**: reasoning must **cite and combine** remote-sensing evidence (e.g., DSM height delta, shadow length/direction, spectral/color cues in optical or NIR, mask/building footprint alignment, spatial layout and known object geometry, GSD implications).

For **Each option** (A, B, ...), produce the following stepwise fields:

- a) **claim**: one-line restatement of the option.
- b) **visual_evidence**: a list of short items like "optical: dark elongated shadow at center-right", "DSM: +3.2 m rooftop at upper-left", "mask: building polygon aligns with feature" — or ["No visual evidence"] if none. If a modality is missing, include "**Missing modality: DSM**".
- c) **is_correct**: boolean (true/false) based strictly on available evidence.
- d) **final_justification**: concise 1-2 sentence justification tying evidence to is_correct.

After per-option analyses, provide:

- final_answer**: list of chosen option letters (single or multiple).
- chain_of_reasoning**: 3-6 concise factual steps (bullet-like) that lead to the final_answer; reference modalities and approximate regions.

Strict OUTPUT JSON schema (no other fields allowed). Use the schema below and no extra commentary. Values must be strings, booleans, lists, or nested objects as appropriate.

OUTPUT JSON schema:

```
{  
  "id": "...",  
  "dataset": "...",  
  "image": ["path/to/image.png", ...],  
  "job": "...",  
  "qa_type": "single_choice" or "multi_choice",  
  "question_text": "...",  
  "options": { "A": "text", "B": "text", ... },  
  "option_analysis": {  
    "A": {  
      "claim": "short restatement",  
      "visual_evidence": ["optical: ... at upper-left", "DSM: ..."] OR ["No visual evidence" or "Missing modality: DSM"],  
      "is_correct": true/false,  
      "final_justification": "1-2 sentence justification",  
      "additional_support": ["cross-modal corroboration 1", ...] OR []  
    },  
    "B": { ... }, ...  
  },  
  "final_answer": ["A", "D"],  
  "chain_of_reasoning": ["step 1", "step 2", ...]  
}
```

ADDITIONAL CONSTRAINTS:

- **Emphasize REMOTE-SENSING inference** throughout. Every evidence item should **tag the modality used**.
- Keep language concise and technical.
- If a modality from input is false or missing, include that fact in **visual_evidence** for each relevant option as "**Missing modality: <name>**".
- **Output strict JSON only**. Nothing else.

•••••

Figure 8. The prompt template for the Model-Based Analysis Generation stage. This structured directive compels a model to act as a remote sensing expert, performing a rigorous, evidence-based analysis of a given QA item. It requires the model to deconstruct each option, cite multi-modal visual evidence, and produce a detailed justification, which serves as the basis for the subsequent cross-verification step.

Eval_Prompt = "":

You are a senior **evaluator** of remote sensing reasoning **QA**. You will receive a **JSON** produced by a reasoning model. Your task is to independently verify this output and evaluate the **QA** item from multiple dimensions.

Part 1 – Independent Answering

1. Without looking at the model's analyses, first answer the question yourself based on the available modalities (optical, DSM, mask).

2. Produce a short reasoning explaining your own answer.

{input_json}

Part 2 – Evaluation of the Model's JSON

Using the option analyses and chain-of-reasoning in the **JSON**, evaluate:

- ****Evidence Alignment**:**

Whether the per-option "visual_evidence" references real, plausible remote sensing cues.

- ****Reasoning Quality**:**

Whether "final_justification" and chain-of-reasoning follow valid geospatial logic (e.g., land-use consistency, geometry, spatial adjacency, object morphology).

- ****Option Decision Correctness**:**

Whether the claimed correctness (is_correct) aligns with actual evidence.

- ****Remote Sensing Expertise**:**

Accuracy in interpreting remote sensing concepts (industrial structures, DSM elevation cues, land-cover types, etc.).

- ****Question Design Quality**:**

Whether the question is logically sound, solvable from imagery, and truly requires reasoning rather than simple detection.

Each dimension should be scored from ****1-5**** (5 = excellent).

Part 3 – Final Verdict

Provide:

- A 1-2 sentence summary of whether the **QA** item is worth keeping.

- A ****final_score**** (1-100) based on the weighted combination of all criteria.

Output Format (Strict JSON)

Return **ONLY** a **JSON** object with the following fields:

```
{  
  "independent_answer": ["A", "D"],  
  "independent_reasoning": "your reasoning here",  
  "scores": {  
    "evidence_alignment": 1-20,  
    "reasoning_quality": 1-20,  
    "option_correctness": 1-20,  
    "remote_sensing_expertise": 1-20,  
    "question_design": 1-20  
  },  
  "final_score": 0-100,  
  "verdict": "short statement"  
}
```

Figure 9. The prompt template for the Cross-Verification stage. This directive instructs an “evaluator” model to perform a two-part assessment. It first answers the question independently to avoid bias, then critically evaluates the “proposer” model’s analysis across multiple dimensions, culminating in a final score that determines the **QA** item’s quality.

Table 6. Statistics of the expert review process. A panel of nine Ph.D. experts evaluated 2,694 candidate items, rejecting 694 based on four rigorous quality criteria to select the final 2,000 items for VLRS-Bench.

Evaluation Criterion	Description of Defect	Rejected Items	Rejection Rate
Ambiguity & Clarity	Question/Options are vague or allow multiple interpretations	241	34.7%
Visual Evidence Mismatch	Ground truth is not strictly supported by visible image cues	186	26.8%
Triviality	Reasoning is too simple (e.g., pure detection) or lacks depth	154	22.2%
Professional Relevance	Terminology is non-standard or scenario is unrealistic	113	16.3%
Total	-	694	100%

and professional validity of remote sensing reasoning require human judgment. To ensure the highest standard of quality for VLRS-Bench, we implemented a final, rigorous stage of human expert review.

We invited a panel of nine domain experts in remote sensing, all holding Ph.D. degrees, to conduct a systematic inspection of the 2,694 candidate items that survived the automated filtering. These experts evaluated each item against four strict criteria: clarity, evidence alignment, reasoning depth, and professional relevance. As detailed in Table 6, this process was highly selective, resulting in the rejection of 694 items.

To illustrate the rigor of this process, we highlight two typical rejection cases encountered during the review:

- **Over-Interpretation (Ambiguity):** One rejected item asked, “*Which processes most likely contribute to the observed configuration...?*” with options including “*Taxiway congestion management*” and “*Emergency response operations*.” Experts rejected this because such dynamic operational procedures cannot be definitively inferred from a static snapshot of parked aircraft without temporal context, making the question speculative rather than reasoning-based.
- **Visual Evidence Mismatch:** Another item regarding recreational fields asked about factors contributing to “*patchy and compacted ground surfaces*,” offering options like “*Pest infestation*” or “*Irrigation system malfunction*.” This was rejected because, at the given resolution, distinguishing between pest damage, irrigation issues, or simple foot traffic wear is impossible based solely on RGB visual cues, rendering the “correct” answer arbitrary.

This expert review served as the ultimate quality gate. **Consequently, a final set of 2,000 high-quality, expert-validated reasoning tasks was selected to constitute the official VLRS-Bench.** This multi-tiered verification process—combining automated logic checks with human expert scrutiny—ensures that VLRS-Bench represents a reliable, challenging, and professionally rigorous benchmark for the remote sensing community.

5. Visualizations of Random Sampling Cases.

We present additional example of our VLRS-Bench in Figure 10-23. It can be seen that our VLRS-Bench poses great challenges to existing MLLMs.

5.1. Visualization Examples of Spatial Cognition (SC)

As shown in Fig 10-13, SC tasks evaluate whether a model can transform a static remote sensing image into a coherent, multi-step spatial reasoning process, rather than relying on isolated visual cues. The intended reasoning procedure begins with spatial anchoring and semantic partitioning of the scene, followed by the formulation of candidate causal or functional hypotheses based on geometric configuration, relative elevation cues, material appearance, and neighborhood relationships. These hypotheses must then be validated or rejected by checking intermediate spatial consistency, such as connectivity, directional alignment, or mutual exclusivity between scene elements.

A representative example is CR in Figure 10. The correct solution does not emerge from recognizing a single salient region, but from constructing a causal chain: identifying potential source elements, inferring how effects propagate spatially, and verifying whether the final observable outcome is consistent with this propagation path. The primary difficulty lies in the fact that decisive evidence is weak and distributed—for instance, subtle gradients, adjacency patterns, or indirect structural hints—while multiple distractors preserve strong local visual similarity. As a result, reasoning based solely on appearance similarity (e.g., dark regions or linear structures) is insufficient.

VLRS-Bench deliberately amplifies this difficulty by incorporating remote sensing-specific priors during question construction, such as fine-grained semantic distributions, region-level relationships, and scene-dependent functional constraints. These priors are not exposed to the solver but are used to generate distractors that are locally plausible yet globally inconsistent. Empirically, this design yields a clear behavioral pattern: most general-purpose MLLMs achieve reasonable performance on single-choice spatial questions but fail sharply when tasks require eliminating multiple confounders or validating a full causal chain, whereas models with remote sensing exposure exhibit measurable but still limited robustness. This divergence demonstrates that SC tasks in VLRS-Bench effectively isolate the gap between visual recognition and genuine spatial-causal reasoning, validating their role as a diagnostic benchmark rather than a perceptual test.

5.2. Visualization Examples of Spatiotemporal Cognitive (ST-C)

As illustrated in Fig. 15-17, ST-C tasks extend spatial reasoning into the temporal domain, requiring models to en-

force consistency across multiple observations and reason about change as a structured process rather than a collection of independent frames. The expected reasoning strategy involves extracting early-stage signals, hypothesizing plausible evolution mechanisms, and continuously verifying these hypotheses against later observations to ensure temporal coherence. Crucially, reasoning must account for rate, directionality, and persistence of change, rather than treating all variations as equally informative.

This is exemplified by Spatiotemporal Causal-Chain Reasoning (ST-CCR) in Figure 14. A valid solution requires detecting subtle early indicators (e.g., nascent disturbances or emerging structures), inferring how these indicators propagate through time, and confirming that later-stage patterns align with the hypothesized causal trajectory. The key challenge arises from the existence of multiple short-term explanations that appear valid when considering only adjacent frames, yet only one explanation remains consistent across the entire sequence.

In VLRS-Bench, this ambiguity is intentionally preserved. Temporal priors and multi-phase reference information are used to construct sequences in which misleading local trends coexist with a globally coherent evolution. Consequently, models must maintain intermediate hypotheses across time and reject explanations that fail sequence-level validation. Experimental results reveal a consistent trend: while general MLLMs can often recognize changes frame-by-frame, they struggle to preserve causal hypotheses over longer temporal spans, leading to severe performance degradation in multi-choice and sequence-based formats. Domain-exposed baselines perform better but remain far from saturation, indicating that ST-C tasks reflect real-world spatiotemporal reasoning difficulty and provide a sensitive measure of temporal inference capability.

5.3. Visualization Examples of Pre-event Decision (Pre-D)

As depicted in Fig. 18, Pre-D tasks evaluate whether a model can translate perceptual and inferred spatial knowledge into actionable planning decisions under multiple constraints. The appropriate reasoning process starts with feasibility screening based on hard constraints (accessibility, exclusion zones, physical viability), followed by multi-criteria evaluation that balances operational efficiency, long-term stability, and environmental compatibility. A correct decision must satisfy all constraint layers simultaneously.

The Planning Reasoning (PR) example in Figure 18 illustrates this requirement. Superficially optimal candidates may excel under a single criterion—such as area size or proximity—but fail when secondary constraints are considered. The difficulty therefore lies not in identifying good-looking options, but in recognizing and rejecting pseudo-optimal solutions that violate less visible but critical constraints.

strains.

VLRS-Bench embeds remote sensing-specific contextual priors into the generation of planning options, ensuring that distractors reflect realistic planning trade-offs encountered in practice. These distractors are designed to exploit known weaknesses of general MLLMs, which tend to prioritize salient visual features over constraint integration. Empirical evaluation confirms this: general-purpose models frequently select visually attractive but operationally invalid options, while remote sensing-trained baselines demonstrate greater awareness of latent constraints. This clear separation supports the benchmark’s claim that Pre-D tasks measure applied decision reasoning rather than visual preference, reinforcing their operational realism.

5.4. Visualization Examples of Post-event Decision (Post-D)

As presented in Fig. 19, Post-D tasks assess the ability to evaluate outcomes against structured criteria, such as compliance, damage severity, or effectiveness of prior actions. The reasoning process requires aligning observable evidence with predefined evaluation standards, resolving conflicts between multiple indicators, and applying hierarchical rules to reach a final judgment. Importantly, visually salient changes do not necessarily correspond to evaluative significance.

In Evaluation Reasoning (ER) (Figure 19), the challenge lies in distinguishing superficial appearance changes from substantive violations or impacts. VLRS-Bench addresses this by constructing evaluation scenarios where misleading evidence is intentionally present, requiring careful cross-checking of multiple indicators. Remote sensing priors are used to ensure that correct evaluations align with expert judgment rather than intuitive visual assessment.

Model behavior reveals that general MLLMs often produce plausible but weakly grounded evaluations, whereas domain-exposed baselines achieve better alignment with evaluation criteria but still struggle with fine-grained rule application. This confirms that ER tasks capture a critical but underexplored aspect of remote sensing intelligence: evidence-based judgment under structured norms.

5.5. Visualization Examples of Object-level Predictive (OP)

Fig. 20–21 demonstrates that OP tasks focus on forecasting category or morphological changes of individual objects or localized regions. The correct reasoning process involves detecting early functional signals, distinguishing persistent trends from transient noise, and extrapolating future states under spatial and contextual constraints. Prediction must therefore be constrained and explainable, not merely extrapolative.

In Spatiotemporal Morphological Prediction (ST-M-PR)

(Figure 20), functional transformation often precedes visible morphological change, creating a temporal gap that challenges appearance-driven prediction. VLRS-Bench leverages long-term temporal priors and object-level transition patterns to generate predictions that cannot be solved by short-horizon trend fitting alone.

Empirically, generative prediction formats expose a pronounced gap: while many models can select plausible future states when options are provided, they fail to generate accurate predictions independently. Domain-exposed baselines show partial improvement, indicating that OP tasks successfully assess early-signal interpretation and constrained extrapolation—core competencies for reliable object-level forecasting.

5.6. Visualization Examples of Scene-level Predictive (SP)

It can be seen from Fig. 22–23 that SP tasks evaluate reasoning at a macro scale, requiring aggregation of distributed evidence, comparison of competing future trajectories, and reasoning under uncertainty. The intended approach involves synthesizing signals across regions, assessing interaction and propagation effects, and ranking or probabilistically weighting possible futures.

The Spatiotemporal Sequence Prediction (ST-SQ-PR) example in Figure 23 demonstrates this challenge. Multiple future sequences are designed to appear locally consistent, differing only in global ordering or causal plausibility. Solving the task requires evaluating collective evidence rather than focusing on any single region.

VLRS-Bench constructs such scenarios using remote sensing temporal priors and structured uncertainty modeling, ensuring that the distinction between correct and incorrect sequences is subtle yet principled. Experimental results show near-universal difficulty for general MLLMs and only moderate gains for domain-exposed models, confirming that SP tasks capture the inherent uncertainty and complexity of real-world scene-level forecasting.

6. Datasheets

In this section, we document essential details about the proposed datasets and benchmarks following the CVPR Dataset and Benchmark guidelines and the template provided by [11].

6.1. Motivation

The questions in this section are primarily intended to encourage dataset creators to clearly articulate their reasons for creating the dataset and to promote transparency about funding interests. The latter may be particularly relevant for datasets created for research purposes.

1. “*For what purpose was the dataset created?*”

A: Existing remote sensing (RS) benchmarks are predominantly perception-oriented, focusing on simple detection or classification, which fails to evaluate the higher-order thinking required for real-world applications. To address these limitations, we introduce **VLRS-Bench**, a comprehensive benchmark designed to assess the complex reasoning capabilities of MLLMs across three core cognitive dimensions: Cognition, Decision, and Prediction.

2. “*Who created the dataset (e.g., which team, research group) and on behalf of which entity?*”

A: The dataset was created by the following authors:

- Zhiming Luo,
- Di Wang,
- Haonan Guo,
- Jing Zhang,
- Bo Do

All of authors from School of Computer Science, Wuhan University and Zhongguancun Academy.

3. “*Who funded the creation of the dataset?*”

A: The dataset creation was funded by the affiliations of the authors involved in this work.

6.2. Composition

Most of the questions in this section are intended to provide dataset consumers with the information they need to make informed decisions about using the dataset for their chosen tasks. Some of the questions are designed to elicit information about compliance with the EU’s General Data Protection Regulation (GDPR) or comparable regulations in other jurisdictions. Questions that apply only to datasets that relate to people are grouped together at the end of the section. We recommend taking a broad interpretation of whether a dataset relates to people. For example, any dataset containing text that was written by people relates to people.

1. “*What do the instances that comprise our datasets represent (e.g., documents, photos, people, countries)?*”

A: The dataset primarily consists of multi-source remote sensing images (including RGB, Near-Infrared, and DSM) sourced from 11 diverse public datasets, along with their corresponding complex reasoning textual annotations. All datasets utilized in VLRS-Bench are publicly accessible and nonprofit.

2. “*How many instances are there in total (of each type, if appropriate)?*”

A: VLRS-Bench is structured around a hierarchy of 3 dimensions, 6 specific abilities, and 14 fine-grained tasks. It contains thousands of high-quality reasoning instances featuring high linguistic complexity, with an average question-answer length of 70.96 words.

3. “*Does the dataset contain all possible instances or is it a sample (not necessarily random) of instances from a larger set?*”

- A:** The images in VLRS-Bench are curated from 11 existing high-quality datasets (e.g., DOTA, FAIR1M, LoveDA, SpaceNet), and all reasoning-focused textual annotations were independently generated via our automated pipeline.
4. *“Is there a label or target associated with each instance?”*
A: Yes, for each instance, we provide a detailed instruction enriched with expert priors (e.g., masks, DSM values) and a ground-truth reasoning answer.
 5. *“Is any information missing from individual instances?”*
A: No, each individual instance is complete.
 6. *“Are relationships between individual instances made explicit (e.g., users’ movie ratings, social network links)?”*
A: Yes, the relationship is explicit as instances are categorized into Cognition, Decision, and Prediction dimensions.
 7. *“Are there recommended data splits (e.g., training, development/validation, testing)?”*
A: The dataset is designed to evaluate the reasoning boundaries of MLLMs, so we recommend using it in its entirety as a test set.
 8. *“Is the dataset self-contained, or does it link to or otherwise rely on external resources (e.g., websites, tweets, other datasets)?”*
A: VLRS-Bench is self-contained and will be open-sourced on platforms like Hugging Face, integrated into standard evaluation pipelines.
 9. *“Does the dataset contain data that might be considered confidential (e.g., data that is protected by legal privilege or by doctor–patient confidentiality, data that includes the content of individuals’ non-public communications)?”*
A: No, all data are derived from public sources and are clearly licensed.
 10. *“Does the dataset contain data that, if viewed directly, might be offensive, insulting, threatening, or might otherwise cause anxiety?”*
A: No, VLRS-Bench does not contain any data with negative information.

6.3. Collection Process

In addition to the goals outlined in the previous section, the questions in this section are designed to elicit information that may help researchers and practitioners create alternative datasets with similar characteristics. Again, questions that apply only to datasets that relate to people are grouped together at the end of the section.

1. *“How was the data associated with each instance acquired?”*
A: The images are sourced from 11 established remote sensing datasets. We enrich these images

with reasoning-oriented annotations generated through a pipeline that combines RS expert priors (like semantic masks and elevation data) with large model capabilities.

2. *“What mechanisms or procedures were used to collect the data (e.g., hardware apparatuses or sensors, manual human curation, software programs, software APIs)?”*
A: We employed an automated generation pipeline verified by human experts. The process involves extracting pixel-level priors, prompting advanced MLLMs (e.g., GPT-5.1) with these priors to generate reasoning chains, and a final rigorous manual review to ensure logical correctness.
3. *“If the dataset is a sample from a larger set, what was the sampling strategy (e.g., deterministic, probabilistic with specific sampling probabilities)?”*
A: We utilized a stratified sampling strategy to ensure coverage of diverse semantic categories and geographic locations from the source datasets.

6.4. Preprocessing, Cleaning, and Labeling

The questions in this section are intended to provide dataset consumers with the information they need to determine whether the “raw” data has been processed in ways that are compatible with their chosen tasks. For example, text that has been converted into a bag-of-words” is not suitable for tasks involving word order.

1. *“Was any preprocessing/cleaning/labeling of the data done (e.g., discretization or bucketing, tokenization, part-of-speech tagging, SIFT feature extraction, removal of instances, processing of missing values)?”*
A: Yes. We standardized the annotation formats from different source datasets using the SAMRS framework. For the reasoning tasks, we processed expert priors (e.g., converting bounding boxes to masks, normalizing DSM values) to create structured prompts that facilitate precise logic generation.
2. *“Was the ‘raw’ data saved in addition to the preprocessed/cleaned/labeled data (e.g., to support unanticipated future uses)?”*
A: Yes, raw data from the original datasets is accessible.
3. *“Is the software that was used to preprocess/clean/label the data available?”*
A: Yes, the necessary software and the generation pipeline scripts used to create the benchmark are publicly available.

6.5. Uses

The questions in this section are intended to encourage dataset creators to reflect on tasks for which the dataset should and should not be used. By explicitly highlighting these tasks, dataset creators can help dataset consumers make informed decisions, thereby avoiding potential risks or harms.

1. “Has the dataset been used for any tasks already?”
A: No.
2. “Is there a repository that links to any or all papers or systems that use the dataset?”
A: Yes, we will provide such links in the GitHub and the Huggingface repository.
3. “What (other) tasks could the dataset be used for?”
A: VLRS-Bench provides extensive annotations for complex reasoning tasks. In addition to evaluating general-purpose MLLMs, it can be used to train specialized RS MLLMs for tasks requiring domain knowledge, logical deduction, and future state prediction.
4. “Is there anything about the composition of the dataset or the way it was collected and preprocessed/cleaned/labeled that might impact future uses?”
A: No.
5. “Are there tasks for which the dataset should not be used?”
A: N/A.

6.6. Distribution

Dataset creators should provide answers to these questions prior to distributing the dataset either internally within the entity on behalf of which the dataset was created or externally to third parties.

1. “Will the dataset be distributed to third parties outside of the entity (e.g., company, institution, organization) on behalf of which the dataset was created?” **A:** No. The datasets will be made publicly accessible to the research community.
2. “How will the dataset be distributed (e.g., tarball on website, API, GitHub)?”
A: We will provide VLRS-Bench in the GitHub and the Huggingface repository.
3. “When will the dataset be distributed?”
A: We will create a repository to release the data once the paper is officially published, ensuring compliance with the anonymity principle.
4. “Will the dataset be distributed under a copyright or other intellectual property (IP) license, and/or under applicable terms of use (ToU)?”
A: Yes, the dataset will be released under the Creative Commons Attribution-NonCommercial-ShareAlike 4.0 International License.
5. “Have any third parties imposed IP-based or other restrictions on the data associated with the instances?”
A: No.
6. “Do any export controls or other regulatory restrictions apply to the dataset or to individual instances?”
A: No.

6.7. Maintenance

As with the questions in the previous section, dataset creators should provide answers to these questions prior to distributing the dataset. The questions in this section are intended to encourage dataset creators to plan for dataset maintenance and communicate this plan to dataset consumers.

1. “Who will be supporting/hosting/maintaining the dataset?”
A: The authors of this work serve to support, host, and maintain the datasets.
2. “How can the owner/curator/manager of the dataset be contacted (e.g., email address)?”
A: The curators can be contacted via the email addresses listed on our paper or webpage.
3. “Is there an erratum?”
A: There is no explicit erratum; updates and known errors will be specified in future versions.
4. “Will the dataset be updated (e.g., to correct labeling errors, add new instances, delete instances)?”
A: Future updates (if any) will be posted on the dataset website.
5. “Will older versions of the dataset continue to be supported/hosted/maintained?”
A: Yes. This initial release will be updated in the future, with older versions replaced as new updates are posted.
6. “If others want to extend/augment/build on/contribute to the dataset, is there a mechanism for them to do so?”
A: Yes, we will provide detailed instructions for future extensions.

7. Limitation and Potential Societal Impact

In this section, we discuss the limitations and potential societal impact of this work.

7.1. Potential Limitations

While **VLRS-Bench** provides a comprehensive benchmark for evaluating the reasoning capabilities of MLLMs in remote sensing, there are several limitations to consider:

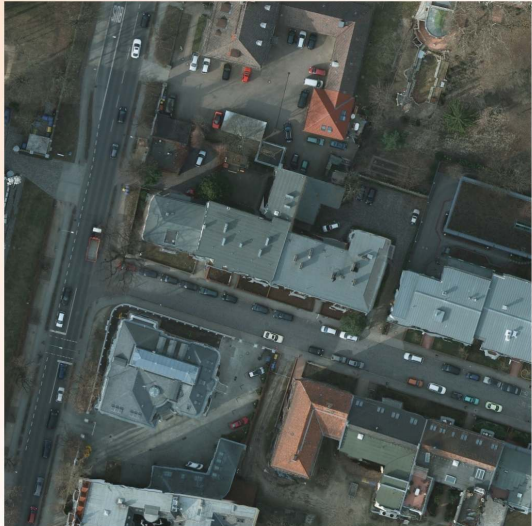
- **Scope of Sensors:** Although our benchmark integrates RGB, Near-Infrared (NIR), and DSM data from 11 sources, it may not cover all specialized sensor types such as Synthetic Aperture Radar (SAR) or Hyperspectral imaging, potentially limiting generalizability in extreme conditions.
- **Model and Dataset Diversity:** In this paper, we extensively evaluated over 15 general-purpose and RS-specific MLLMs (e.g., GPT-4o, InternVL). As new models emerge, their evaluation results will be added to our leaderboard. Additionally, VLRS-Bench will be expanded to include more fine-grained reasoning tasks in future iterations.

- **Multilingual Support:** VLRS-Bench currently supports English, which is the dominant language in current MLLM research. In the future, we aim to extend support to other languages to serve a broader global research community.

7.2. Potential Negative Societal Impact

- **Safety Risks:** VLRS-Bench is designed to evaluate complex reasoning, including prediction and decision-making in scenarios like disaster relief. However, excessive reliance on model outputs without human oversight could lead to risks in high-stakes environments. It is crucial to implement human-in-the-loop supervision when deploying these MLLMs for real-world decision support.
- **Environmental Impact:** Training MLLMs and conducting extensive evaluations on VLRS-Bench requires significant computational resources. To mitigate this, we provide a public leaderboard and detailed model analysis, reducing the need for researchers to perform redundant evaluations.
- **Bias and Fairness:** VLRS-Bench relies on 11 public datasets which may have inherent geographic or selection biases (e.g., favoring urban areas over rural ones). While we strove for diversity, models trained or evaluated solely on this benchmark might exhibit performance disparities across different regions. We aim to continuously expand the dataset diversity to minimize such biases.

Causal Reasoning (CR)



In the upper-right area of the image, a small cluster of vegetation appears denser and greener than surrounding patches. Which of the following explanations most likely accounts for this localized vegetation density pattern? (Select one option. Format example: B)

- A. The vegetation density in the upper-right area is a consequence of seasonal leaf fall from nearby trees, which temporarily enriches the soil surface and supports short-term vegetation growth.
- B. The vegetation density in the upper-right area originates from construction debris accumulation that altered soil composition, unintentionally promoting plant colonization in nutrient-rich rubble pockets.
- C. The vegetation density in the upper-right area results from consistent shading by nearby tall buildings, which reduces evaporation and allows plants to thrive under cooler conditions throughout the day.
- D. The vegetation density in the upper-right area is primarily due to water runoff from adjacent higher building roof, which channels moisture toward the lower courtyard, enhancing plant growth in that confined zone.
- E. The vegetation density in the upper-right area is caused by deliberate landscaping associated with a residential garden, where irrigation systems maintain uniform moisture independent of surrounding structures.

Answer: D

"Thinking": " The methodological framework for this question centers on inferring the causal mechanism of localized vegetation density in a dense urban block through multi-source data fusion—integrating optical imagery analysis, DSM (Digital Surface Model) elevation extraction, and semantic mask interpretation—with a focus on coupling spatial layout characteristics (building density, elevation gradient) and environmental processes (surface impermeability, runoff accumulation). First, a systematic scene analysis is conducted on the Potsdam urban block: multi-story buildings line narrow streets, with flat gray roofs dominating the central and lower regions and scattered red-tiled roofs in the upper-right/lower-right corners; streets are lined with parked cars, and sparse vegetation is concentrated in the upper-right small courtyard. Key features identified include continuous impervious surfaces (dominant in the central block, limiting water infiltration), a clear elevation gradient (DSM confirms higher central buildings and a gentle slope toward the upper-right courtyard), and a localized vegetation cluster in the lower-elevation upper-right courtyard. The reasoning chain synthesizes these cues: the urban block's high impervious surface coverage reduces rainfall infiltration; the DSM-verified elevation gradient drives runoff from higher central roofs toward the lower-elevation upper-right courtyard; the accumulated runoff creates a moisture-retentive microenvironment, which supports denser vegetation growth—forming a causal chain of "elevation difference → runoff convergence → moisture retention → vegetation clustering."

The valid inference, corroborated by multi-source data (optical imagery, DSM, semantic mask), is the localized vegetation density in the upper-right courtyard is primarily caused by runoff accumulation from adjacent higher buildings: the elevation gradient confirmed by DSM provides the hydrological driving force for runoff, while the widespread impervious surfaces (verified by masks) reduce lateral infiltration and redirect water flow to the low-elevation courtyard, creating sustained moisture conditions that facilitate vegetation growth. This conclusion integrates spatial topology, elevation dynamics, and urban hydrological processes, fully aligning with the hidden data and visible environmental cues.

In contrast, the distractor options (attributing vegetation density to shading, construction debris, or artificial irrigation) exhibit fundamental inconsistencies with multi-source evidence: the shading hypothesis ignores the DSM-verified elevation gradient and runoff mechanism, as the upper-right courtyard's vegetation density is more strongly correlated with moisture than light conditions; the construction debris proposal lacks spatial or semantic mask support—no debris accumulation signals are observed in the target area; the irrigation claim contradicts the urban block's dense built-up layout and lack of visible irrigation infrastructure, while failing to reconcile with the elevation-driven runoff pattern documented by DSM. Though these distractors carry superficial visual plausibility (e.g., shading from adjacent buildings), they ultimately decouple the vegetation distribution from core controlling factors (elevation gradient, impermeability, runoff), conflicting with the integrated causal logic derived from multi-source remote sensing data and urban environmental processes."

Model	Res.	Model	Res.	Model	Res.	Model	Res.	Model	Res.	Model	Res.
Claude-3.5-Haiku	✗	Deepseek-VL2	✗	GLM-4.5v	✓	GPT-4o (11-20)	✗	GPT-4o-mini	✗	GPT-5-chat	✗
Gemini-2.5-Flash	✗	Grok-2-Vision	✗	Llama-3.2-11B	✗	Llama-3.2-90B	✗	Qwen2.5-VL-32B	✓	Qwen2.5-VL-72B	✗
Qwen2.5-VL-7B	✗	Qwen3-VL-2B	✗	Qwen3-VL-32B	✓	ScoreRS w/ RL	✓	ScoreRS w/ SFT	✓	VLRS-Base	✓

Figure 10. Example of Causal Reasoning

Counterfactual Reasoning (CFR)



If the central floodplain area visible near the meandering river had remained covered with natural vegetation instead of being converted into farmland, which of the following outcomes would most likely have occurred according to spatial and hydrological reasoning? (Select all that apply)

- A. If vegetation had persisted, the main transportation route crossing the floodplain would have been rendered unusable due to continuous canopy obstruction and lack of stable ground.
- B. The vegetated floodplain would have enhanced water retention capacity, reducing downstream flood peaks and stabilizing seasonal flow patterns across the lower-right settlements.
- C. If vegetation had remained, the agricultural productivity of the surrounding upland fields would have sharply declined due to reduced irrigation water availability from the main river channel.
- D. The persistence of vegetation would have limited the expansion of built-up areas along the eastern corridor by maintaining natural flood barriers and discouraging construction in low-lying zones.
- E. The vegetated floodplain would have increased evapotranspiration rates, slightly moderating local microclimates and reducing heat accumulation in the adjacent urban clusters.
- F. The natural vegetation cover would have supported biodiversity corridors connecting the western forest patches with the eastern riparian zones, enhancing ecological resilience.
- G. Retaining vegetation would have caused severe waterlogging in the southern lowlands, leading to widespread abandonment of nearby settlements and infrastructure collapse.
- H. Maintaining vegetation in the central floodplain would have decreased sediment deposition along the inner river bends, leading to clearer water channels and improved aquatic habitat continuity."

Answer: B, D, E, F, H

"Thinking": " The methodological framework for addressing this question is rooted in inferring the multi-dimensional consequences of a counterfactual land-cover change—specifically, the retention of vegetation in the central floodplain instead of its conversion to agricultural land—through integrated scene analysis, key feature extraction, and cross-disciplinary reasoning (hydrological, ecological, and anthropogenic). First, a systematic analysis is conducted on the imagery depicting a large meandering river system, encompassing adjacent floodplains, agricultural fields, scattered built-up areas, a bright greenish water body (likely a reservoir or estuary) in the upper-right region, rectangular agricultural plots dominating the lower-left and central zones, and denser human settlements in the right-central area. Subsequently, salient landscape features are identified, including sinuous river channels, levee-like embankments, rectangular aquaculture ponds, road networks linking settlements, and scattered vegetation patches (with darker tones indicating forested or shrub-covered areas). The reasoning chain then explores how the counterfactual vegetation retention would alter hydrological connectivity, flood retention capacity, soil stability, and human settlement distribution, anchoring in the intrinsic linkages between land cover, ecological processes, and anthropogenic activities.

The valid conclusions, corroborated by hidden spatial structure and realistic environmental processes, are five mutually consistent outcomes reflecting hydrological stability, ecological resilience, and moderated human impact: a vegetated central floodplain enhances water retention capacity and mitigates flood peaks by acting as a natural buffer; vegetation cover stabilizes soil aggregates, reduces sedimentation into the river system, and thereby improves water clarity; natural flood-regulating barriers formed by floodplain vegetation discourage unconstrained urban expansion in high-risk areas; increased evapotranspiration from the vegetated surface moderates local microclimates by regulating temperature; and the continuity of vegetation patches facilitates the formation of biodiversity corridors, supporting ecological connectivity. These correct inferences integrate hydrological, ecological, and anthropogenic mechanisms, aligning with the inherent logic of land cover-ecosystem service interactions.

In contrast, the invalid options exhibit fundamental inconsistencies with environmental processes or misinterpret the magnitude/direction of counterfactual effects: the claim that vegetation retention would reduce irrigation water availability is hydrologically implausible, as floodplain vegetation does not substantially alter upstream water flow regimes that sustain irrigation; the assertion of severe waterlogging leading to settlement abandonment exaggerates the ecological consequences of vegetation retention—natural floodplain vegetation regulates water dynamics rather than inducing catastrophic waterlogging; and the proposition that vegetation canopy would obstruct road use is ecologically and practically implausible, as floodplain vegetation typically maintains compatibility with transportation infrastructure and does not form impenetrable barriers to road accessibility. All invalid options, despite superficial plausibility, either misstate the functional relationships between vegetation and environmental/anthropogenic systems or overstate the intensity of potential consequences, conflicting with the principles of hydrological regulation, ecological resilience, and human-land interaction."

Model	Res.	Model	Res.	Model	Res.	Model	Res.	Model	Res.	Model	Res.
Claude-3.5-Haiku	X	Deepseek-VL2	X	GLM-4.5v	X	GPT-4o (11-20)	0.5	GPT-4o-mini	X	GPT-5-chat	X
Gemini-2.5-Flash	X	Grok-2-Vision	X	Llama-3.2-11B	X	Llama-3.2-90B	X	Qwen2.5-VL-32B	X	Qwen2.5-VL-72B	X
Qwen2.5-VL-7B	X	Qwen3-VL-2B	X	Qwen3-VL-32B	X	ScoreRS w/ RL	X	ScoreRS w/ SFT	X	VLRS-Base	X

Figure 11. Example of Counterfactual Reasoning

Semantic Integration Reasoning (SIR)



Considering the large open area dominating the left half of the image and its spatial relationship to the residential buildings along the right edge, which interpretation most likely represents the functional character of this zone? (Select one option. Format example: B)

- A. The open area on the left, with its geometric layout and adjacent paved road, is most likely a parking or vehicle staging area associated with the residential buildings to the east.
- B. The open space on the left, with its visible linear divisions and sparse vegetation, primarily serves as an industrial storage yard supporting nearby residential logistics.
- C. The large open tract on the left, bordered by roads and buildings, is most likely an undeveloped construction site awaiting future urban expansion and infrastructure development.
- D. The open area on the left, characterized by its flatness and faint grid-like texture, primarily functions as an agricultural field used for seasonal crop cultivation adjacent to the residential zone.
- E. The broad open field on the left, with its intersecting linear paths and proximity to residential buildings, most likely represents a managed urban green space or parkland maintained for community recreation and aesthetic continuity.

Answer: E

"Thinking": The methodological framework for addressing this question hinges on integrating spatial pattern analysis, key feature extraction, functional inference, and elevation cue verification to determine the primary function of the target area. First, a systematic scene analysis is conducted on the rectangular urban block depicted in the imagery: the left half is dominated by a large open green area, bounded by a vertical paved road and detached residential buildings with pitched roofs and driveways on the right; the green area exhibits a uniform texture with faint linear patterns, and a small cultivated or bare soil patch is present near the bottom, while the DSM (Digital Surface Model) confirms low elevation variation across the open field and relatively higher elevations for the built-up structures. Subsequently, core spatial features are identified, including a large, flat grassy field with geometric paths, a minor cultivated/bare soil patch, a road with parked vehicles, and residential buildings surrounded by vegetation. The reasoning chain then synthesizes these cues: the open field's uniform texture, low elevation consistency, and presence of structured paths indicate a managed green space rather than agricultural land (the small cultivated patch is too negligible to define the area's primary function); its adjacency to residential buildings further supports a functional role serving nearby housing, ruling out industrial or undeveloped land uses.

The valid inference, corroborated by spatial relationships, structural characteristics, and elevation data, is a managed urban green space adjacent to residential housing, which aligns with the area's uniform grassy texture, structured paths, adjacency to residential buildings, and flat terrain (consistent with recreational or communal green space).

In contrast, the distractor options—proposing agricultural, industrial, or undeveloped land uses—are each contradicted by empirical spatial or structural evidence: the interpretation of agricultural land conflicts with the open field's uniform texture, presence of structured paths, and primary association with residential areas (the small cultivated patch is incidental rather than defining); the industrial land proposition lacks supporting evidence such as industrial infrastructure, storage facilities, or characteristic spatial patterns; and the undeveloped land claim is inconsistent with the area's managed features (e.g., maintained grassy texture, intersecting paths) and adjacency to developed residential blocks, which indicate intentional management rather than a natural or unmanaged state. All distractors, while superficially plausible, fail to align with the integrated spatial, structural, and functional cues that define the area's true nature."

Model	Res.	Model	Res.	Model	Res.	Model	Res.	Model	Res.	Model	Res.
Claude-3.5-Haiku	X	Deepseek-VL2	X	GLM-4.5v	X	GPT-4o (11-20)	✓	GPT-4o-mini	✓	GPT-5-chat	✓
Gemini-2.5-Flash	X	Grok-2-Vision	X	Llama-3.2-11B	X	Llama-3.2-90B	X	Qwen2.5-VL-32B	X	Qwen2.5-VL-72B	X
Qwen2.5-VL-7B	X	Qwen3-VL-2B	✓	Qwen3-VL-32B	X	ScoreRS w/ RL	✓	ScoreRS w/ SFT	✓	VLRS-Base	✓

Figure 12. Example of Semantic Integration Reasoning

Mechanistic Interaction Reasoning (MIR)



Assuming a new elevated roadway was constructed across the central lake area connecting the southwest industrial zone to the northeastern settlement, which of the following statements most likely describes the current landscape configuration observable in the image?

- A. Forest patches west of the lake maintain uniformly dense canopy coverage across all edges adjacent to the new roadway with no observable decrease in vegetative vigor or tonal variation along the shoreline.
- B. Vegetation bordering the new roadway exhibits reduced canopy coverage compared to distant forest patches, while the lake surface near the bridge shows dispersed pale-green sediment indicating moderate disturbance of aquatic areas.
- C. Agricultural plots immediately adjacent to the new roadway reveal unchanged crop texture and water retention characteristics, with unaltered moisture gradients visible across the entire valley zone.
- D. Lake water color remains consistently deep blue across the entire basin, demonstrating stable optical properties without any indication of increased sediment or suspended material near transportation infrastructure.
- E. Urban expansion directly covers the majority of the lake's northern shoreline, generating homogeneous light-colored surfaces consistent with extensive industrial paving across previously natural lake margins.

Answer: E

"Thinking": " The core of the problem-solving approach is deducing post-construction landscape changes through image analysis, key feature identification, and spatial logical reasoning: first, conduct an overall scan of the image's mixed urban-peri-urban landscapes, central lake, surrounding vegetation, agricultural lands, and transportation corridors to identify core visual elements such as the central water body, dense vegetation patches, southwest industrial zone, soil disturbance areas, and expanded road networks; then, establish a reasoning chain centered on the disturbance effects of the new cross-lake roadway, linking construction activities to vegetation stress and aquatic sediment changes, which are verified by tonal differences and pattern boundaries in the image; finally, synthesize multiple visual facts including vegetation density gradients, sediment distribution, and development layout to rule out implausible outcomes inconsistent with pixel-level category transitions, leading to the most accurate conclusion—vegetation bordering the new roadway exhibits reduced canopy coverage compared to distant forest patches, while the lake surface near the bridge shows dispersed pale-green sediment indicating moderate disturbance of aquatic areas—a result validated by the mask's mixed-category boundary patterns that reflect ecological responses to roadway construction. As for other options, each has distinct flaws: the option claiming uniform dense canopy coverage and no tonal changes of vegetation adjacent to the road is unreasonable as it overlooks construction-induced vegetation disturbance, contradicting the visual signals of vegetation stress in the image; the option asserting unchanged crop texture, water retention, and moisture gradients of farmland near the road makes an unrealistic stable assumption, violating the objective logic that roadway construction may affect the surrounding agricultural ecosystem and conflicting with implied details like soil disturbance in the image; the option denying potential impacts of construction on water quality and claiming no increased sediment near transportation infrastructure is an idealized conclusion, ignoring possible sediment inflow into the lake from construction and conflicting with the light-toned sediment patterns in the river area of the image that suggest water movement and sedimentation; the option presenting unrestricted urban expansion covering most of the lake's northern shoreline with homogeneous light-colored surfaces is an extreme scenario that exaggerates the scope and intensity of urban growth, inconsistent with the image's features of persistent vegetation patches and complex shoreline morphology and violating spatial logical landscape balance rules. All these incorrect options either oversimplify facts, make implausible assumptions, or contradict the image's fine-scale details and spatial logical relationships."

Model	Res.	Model	Res.	Model	Res.	Model	Res.	Model	Res.	Res.	
Claude-3.5-Haiku	✗	Deepseek-VL2	✗	GLM-4.5v	✗	GPT-4o (11-20)	✓	GPT-4o-mini	✗	GPT-5-chat	✗
Gemini-2.5-Flash	✗	Grok-2-Vision	✗	Llama-3.2-11B	✗	Llama-3.2-90B	✓	Qwen2.5-VL-32B	✓	Qwen2.5-VL-72B	✓
Qwen2.5-VL-7B	✗	Qwen3-VL-2B	✗	Qwen3-VL-32B	✓	ScoreRS w/ RL	✗	ScoreRS w/ SFT	✗	VLRS-Base	✗

Figure 13. Example of Mechanistic Interaction Reasoning

Spatiotemporal Causal-Chain Reasoning (ST-CCR)



Based on the changes visible between the earlier and later images, which statement most likely explains the transformation observed in the large vegetated tract occupying the right-central portion of the scene adjacent to the industrial complex in the lower-left quadrant? (Select one option. Format example: B)

- A. The right-central vegetated tract that was previously dense with mixed greenery has been reforested with denser canopy cover, showing a process of ecological restoration and vegetation recovery adjacent to the industrial area.
- B. The right-central vegetated tract that was previously dense with mixed greenery has been converted into cultivated farmland with visible plowing patterns, indicating a shift from natural vegetation to agricultural use.
- C. The right-central vegetated tract that was previously dense with mixed greenery has been replaced by bare soil and sparse vegetation due to seasonal drying, implying a temporary reduction in vegetation cover rather than land-use change.
- D. The right-central vegetated tract that was previously dense with mixed greenery has been converted into a large water body connected to the rectangular pond in the upper-left, suggesting a deliberate expansion of aquaculture facilities.
- E. The right-central vegetated tract that was previously dense with mixed greenery has been converted into impervious surfaces and new industrial buildings extending from the lower-left complex, indicating a process of industrial expansion replacing vegetation.

Answer: E

"Thinking": " The methodological framework for this question revolves around detecting subtle land-cover transitions through multi-temporal image analysis and inferring the most probable causal process (anthropogenic urban/industrial expansion) rather than natural changes. First, a systematic scene analysis is conducted on the semi-rural area depicted in the imagery: the earlier image features a large vegetated field dominating the right-central region, a rectangular pond with tree rows in the upper left, and industrial buildings in the lower left; the later image reveals that the vegetated field has been replaced by impervious surfaces and new constructions, while the pond area has undergone partial filling or conversion. Key features identified include the upper-left rectangular pond, the right-central large vegetated tract, and the lower-left industrial complex, with the most prominent change being the conversion of vegetation to built-up surfaces—an indicator of urban/industrial expansion. The reasoning chain progresses through six core steps: identifying vegetation loss in the right-central region; detecting the increase in impervious surfaces and building density; noting the adjacency of the changed area to the existing industrial zone; inferring that industrial expansion is the most likely driver of vegetation loss; verifying the stability of water bodies to rule out natural disturbances like flooding; and concluding that the causal mechanism is industrial expansion leading to vegetation conversion.

The valid inference, corroborated by spatial adjacency relationships, land-cover transition characteristics, and elimination of alternative causes, is industrial expansion as the primary driver of land-cover change: the right-central large vegetated tract was replaced by impervious surfaces and new buildings, while the upper-left rectangular pond was partially filled or converted, with this transition directly linked to the adjacency of the existing lower-left industrial complex and supported by the absence of evidence for natural changes or other anthropogenic processes.

In contrast, the distractor options exhibit fundamental inconsistencies with empirical evidence and causal logic: interpretations attributing the change to agricultural conversion lack supporting spatial cues (e.g., no emergence of agricultural plot patterns, uniform vegetated area converted to built-up surfaces rather than cultivated land); claims of flooding are contradicted by the stability of water bodies observed in both temporal images, which show no signs of inundation affecting the vegetated region; and propositions of vegetation recovery are directly incompatible with the temporal transition—from a vegetated state to built-up surfaces—reversing the alleged "recovery" trend. While these distractors anchor to similar spatial regions as the correct inference to enhance plausibility, they fail to align with the core land-cover transition features (vegetation → impervious surfaces/buildings), spatial adjacency to industrial zones, and elimination of alternative causal processes, ultimately conflicting with the integrated evidence for industrial expansion-driven land conversion."

Model	Res.	Model	Res.	Model	Res.	Model	Res.	Model	Res.	Model	Res.
Claude-3.5-Haiku	✗	Deepseek-VL2	✗	GLM-4.5v	✗	GPT-4o (11-20)	✗	GPT-4o-mini	✓	GPT-5-chat	✓
Gemini-2.5-Flash	✗	Grok-2-Vision	✗	Llama-3.2-11B	✗	Llama-3.2-90B	✗	Qwen2.5-VL-32B	✗	Qwen2.5-VL-72B	✗
Qwen2.5-VL-7B	✓	Qwen3-VL-2B	✗	Qwen3-VL-32B	✓	ScoreRS w/ RL	✗	ScoreRS w/ SFT	✓	VLRS-Base	✓

Figure 14. Example of Spatiotemporal Causal-Chain Reasoning

Spatiotemporal Counterfactual Reasoning (ST-CFR)



Between the earlier and later images, the central valley shows a marked transformation. Considering the spatial continuity of the darkened channel and adjacent slopes, which scenario most likely explains the observed change if the flow event had not occurred?

- A. The central channel would have been converted into a paved access road connecting the upper-left ridge to the lower-right settlement, resulting in the same linear dark feature seen in the later image.
- B. The central channel would have been reforested through natural succession, producing a denser canopy and darker tone similar to the later image's debris-covered surface.
- C. The central channel would have remained a stable, lightly vegetated drainage corridor with continuous green cover along its banks, maintaining slope integrity and preventing the deposition of dark volcanic debris now visible in the later image.
- D. The central channel would have expanded naturally due to seasonal flooding, leading to the same darkened deposits and slope scouring observed in the later image even without a volcanic flow event.
- E. The central channel would have been filled by agricultural terraces extending from the lower-left field, creating a patchwork of cultivated plots matching the darkened texture in the later image.

Answer: C

"Thinking": " The methodological framework for this question centers on detecting subtle geomorphic and vegetation changes through multi-temporal image analysis, integrating spatial-temporal reasoning, and conducting counterfactual inference about the implications of a volcanic debris flow (lahar) event. First, a systematic scene analysis is performed on the mountainous terrain featuring a north-south trending narrow valley, a small settlement in the lower-right corner, and a winding central channel: the earlier image depicts a dry, sparsely vegetated channel, while the later image shows darker, freshly exposed material consistent with a lahar, alongside reduced vegetation near the channel. Key features identified include the central geomorphic channel, vegetated valley slopes, the lower-right building cluster, and the critical spectral-textural change (from light brown to dark gray) along the channel—attributed to fresh volcanic debris deposition. The reasoning chain progresses through identifying the central channel as a core geomorphic anchor, documenting the spectral change, inferring volcanic debris deposition, observing vegetation loss, concluding a lahar event occurred between the two timepoints, and extending to counterfactual reasoning: the absence of the lahar would preserve vegetation continuity and slope stability in the central channel.

The valid inference, corroborated by geomorphic, spectral, and vegetation evidence, is the counterfactual scenario where the lahar had not occurred, the central channel would maintain its original vegetated state and slope stability, without the deposition of dark volcanic debris or reduction in adjacent vegetation.

In contrast, the distractor options are inherently inconsistent with the empirical evidence and geomorphic processes: those misattributing the dark channel material to flooding, road construction, reforestation, or agricultural activities fail to align with the spectral characteristics of volcanic debris and the lack of supporting spatial cues (e.g., no road expansion traces, no agricultural plot patterns, or ecological implausibility of rapid reforestation in the context); others erroneously propose vegetation regrowth, urban encroachment, or unrelated geomorphic changes, which contradict the observed vegetation loss and the exclusive geomorphic signal of a lahar event. All distractors leverage specific spatial cues to enhance plausibility but ultimately misinterpret the core spectral-textural and geomorphic changes, conflicting with the integrated evidence of volcanic debris flow-induced deposition and vegetation disturbance."

Model	Res.	Model	Res.	Model	Res.	Model	Res.	Model	Res.	Model	Res.
Claude-3.5-Haiku	✗	Deepseek-VL2	✗	GLM-4.5v	✗	GPT-4o (11-20)	✗	GPT-4o-mini	✗	GPT-5-chat	✓
Gemini-2.5-Flash	✗	Grok-2-Vision	✗	Llama-3.2-11B	✗	Llama-3.2-90B	✗	Qwen2.5-VL-32B	✗	Qwen2.5-VL-72B	✗
Qwen2.5-VL-7B	✗	Qwen3-VL-2B	✗	Qwen3-VL-32B	✗	ScoreRS w/ RL	✓	ScoreRS w/ SFT	✓	VLRS-Base	✓

Figure 15. Example of Spatiotemporal Counterfactual Reasoning

Spatiotemporal Evolution Reasoning (ST-ER)



In the area east of the north-south road, the rectangular plot that was predominantly [BLANK1] in the earlier image has by the later image transitioned into a more uniform brown surface, indicating a shift toward [BLANK2] as part of the seasonal agricultural cycle. (Answer format: BLANK1: <answer>; BLANK2: <answer>)

Answer: "Blank1": "cultivated farmland", "Blank2": "fallow field"

"Thinking": The methodological framework for these fill-in-the-blank questions centers on detecting temporal land cover and functional transitions through multi-temporal remote sensing image analysis, integrating spectral-textural feature comparison, agricultural and rural landscape characteristic identification, and logical reasoning about land use dynamics. First, systematic scene analysis is conducted for each case: the first scenario (hurricane-affected semi-rural area) features earlier imagery of a predominantly agricultural landscape with rectangular crop fields, a central building cluster, elongated sheds, and distinct plowed textures, while later imagery reveals darker, more uniform field surfaces and partial water body conversion—signals of moisture accumulation; the second scenario (rural agricultural area) presents earlier imagery of a central rectangular field east of a north-south road, characterized by patchy green-brown vegetation consistent with active crop growth, and later imagery showing a uniform brown tone with reduced vegetation and soil exposure, reflecting agricultural cycle shifts. Key features identified across both scenarios include core agricultural fields (spatial anchors), spectral-textural changes (tonal uniformity, vegetation vigor shifts), and stable auxiliary structures (buildings, roads) that rule out structural disturbance. The reasoning chain follows a consistent multi-step process: isolating key evolving zones, comparing temporal spectral-textural characteristics, linking changes to ecological or agricultural processes (hurricane-induced flooding, crop harvest cycles), and cross-validating with adjacent landscape stability to eliminate alternative explanations.

The valid inferences, corroborated by empirical visual evidence and landscape dynamics logic, are two sets of temporally linked functional transitions: for the first scenario, the rectangular fields north of the central building changed from agricultural land to flood-affected zone—derived from earlier distinct plowed patterns and rectangular field boundaries confirming active agricultural use, and later darker, less-textured surfaces indicating water saturation associated with hurricane impacts; for the second scenario, the central rectangular field east of the main road transitioned from cultivated farmland to fallow field—supported by earlier green, textured surfaces with visible crop rows (evidence of active cultivation) and later uniform brown tones with soil exposure (consistent with post-harvest or resting agricultural phases). These inferences align with the inherent dynamics of agricultural systems and environmental disturbance processes, while the reasoning process ensures that each blank answer is grounded in quantifiable spectral-textural cues and spatial-temporal logical consistency, avoiding arbitrary interpretations unrelated to observed landscape changes."

Model	Res.	Model	Res.	Model	Res.	Model	Res.	Model	Res.	Model	Res.
Claude-3.5-Haiku	X	Deepseek-VL2	X	GLM-4.5v	X	GPT-4o (11-20)	X	GPT-4o-mini	X	GPT-5-chat	X
Gemini-2.5-Flash	X	Grok-2-Vision	X	Llama-3.2-11B	X	Llama-3.2-90B	X	Qwen2.5-VL-32B	X	Qwen2.5-VL-72B	X
Qwen2.5-VL-7B	X	Qwen3-VL-2B	X	Qwen3-VL-32B	X	ScoreRS w/ RL	X	ScoreRS w/ SFT	X	VLRS-Base	X

Figure 16. Example of Spatiotemporal Evolution Reasoning



Spatiotemporal Consistency Reasoning (ST-CR)

Between the earlier and later images of this residential area, extensive flooding has altered the landscape. Which of the following statements about the consistency of these changes with natural flood progression are most likely correct? (Select all that apply)

- A. The long rectangular buildings in the central-lower section appear brighter in the later image, indicating that they were unaffected by flooding and remained dry, consistent with their position on elevated terrain above the surrounding streets.
- B. The tennis court in the lower-right area shows no visible water coverage in the later image, implying that the floodwaters receded from this zone earlier than from surrounding areas, consistent with rapid drainage through nearby channels.
- C. The small pools scattered throughout the residential complexes remain visible but with altered coloration, indicating partial submersion by floodwater mixing, which is consistent with shallow inundation rather than complete coverage.
- D. The narrow road running vertically through the center of the image exhibits consistent submersion along its entire length, suggesting that the floodwaters followed the natural topographic depression connecting the northern and southern sections.
- E. The cluster of apartment buildings in the lower-right quadrant shows water accumulation primarily along internal driveways and parking areas, which aligns with expected drainage patterns where impermeable surfaces channel runoff toward lower elevations.
- F. The expansion of water from the central pond into adjacent residential streets in the upper-central area is consistent with natural overflow behavior during heavy rainfall, as the pond's perimeter shows a continuous connection to newly inundated zones.
- G. The detached houses with orange roofs in the upper-left corner remain completely dry in the later image, indicating that the floodwaters did not reach this higher ground, consistent with their elevated position relative to the pond.
- H. The wooded area surrounding the pond in the upper-right region shows a reduction in visible canopy density, suggesting that floodwaters caused vegetation loss, which is consistent with prolonged submersion effects on riparian vegetation.

Answer: C, D, E, F, H

"Thinking": " The methodological framework for this question lies in detecting spatially coherent flood patterns and evaluating the consistency of observed landscape evolution with natural hydrological behavior, through multi-temporal image comparison, key spatial feature extraction, and hydrological logic reasoning. First, a systematic scene analysis is conducted on the suburban residential neighborhood depicted in the imagery: the area comprises multiple apartment complexes, detached houses, swimming pools, and a central pond, with the earlier image showing dry conditions and the later image revealing extensive flooding—water covers roads, lawns, and parts of buildings. Key features identified include the upper-center large pond (a core hydrological source), lower-half rectangular apartment blocks, upper-left detached houses with orange roofs, and flood inundation traces such as water encroachment into streets and courtyards. The reasoning chain focuses on three core dimensions: identifying areas with consistent flood spread, verifying the integrity of structures post-flooding, and detecting paradoxical changes (e.g., water accumulation in theoretically higher zones) that would contradict hydrological principles.

The valid inferences, corroborated by spatial relationships, elevation logic, and hydrological consistency, are five mutually coherent flood-related changes reflecting natural hydrological behavior: the central pond overflows into nearby streets (consistent with the hydrological mechanism of flood propagation from water bodies); water pools along driveways and parking lots (matching expected runoff accumulation in low-lying, impervious surfaces); the central vertical road is fully submerged (aligning with its role as a low-lying drainage corridor); swimming pools exhibit color changes and partial submersion (consistent with shallow flood inundation); and vegetation near the pond shows reduced canopy visibility (reflecting stress induced by prolonged flood submersion). These conclusions integrate spatial connectivity, elevation gradients, and hydrological flow rules, fully aligning with the observed flood evolution patterns.

In contrast, the invalid options exhibit fundamental inconsistencies with hydrological logic and empirical image evidence: the claim that orange-roofed houses remain dry contradicts the later image showing these structures surrounded by floodwater; the assertion that the tennis court experienced early drainage is incompatible with visible flood retention on the court surface; and the proposition that central-lower rectangular buildings are protected by elevation and remain dry conflicts with the observed water surrounding these structures. While these distractors leverage plausible hydrological or spatial assumptions (e.g., elevation-based flood avoidance), they ultimately misinterpret flood extent, ignore visible inundation evidence, or reverse hydrological flow logic—failing to reconcile with the integrated spatial, elevation, and hydrological cues that define the true flood scenario."

Model	Res.	Model	Res.	Model	Res.	Model	Res.	Model	Res.	Model	Res.
Claude-3.5-Haiku	X	Deepseek-VL2	X	GLM-4.5v	X	GPT-4o (11-20)	X	GPT-4o-mini	X	GPT-5-chat	X
Gemini-2.5-Flash	X	Grok-2-Vision	0.5	Llama-3.2-11B	X	Llama-3.2-90B	X	Qwen2.5-VL-32B	X	Qwen2.5-VL-72B	0.5
Qwen2.5-VL-7B	X	Qwen3-VL-2B	X	Qwen3-VL-32B	X	ScoreRS w/ RL	0.5	ScoreRS w/ SFT	X	VLRS-Base	X

Figure 17. Example of Spatiotemporal Consistency Reasoning

Planing Reasoning (PR)



The lower-left residential block, characterized by larger open lawns and fewer trees, predominantly contains more visible parked vehicles than the upper-right block that is more shaded by dense vegetation and tree canopies. (Answer format: True or False)

Answer: False

"Thinking": " The methodological framework for this question lies in verifying the truth value of a spatial comparison claim through integrated suburban scene comprehensive analysis, key feature refined extraction, and multi-step logical reasoning—with the core focus on comparing parked vehicle density between two spatially distinct residential blocks, while critically distinguishing between visual occlusion caused by vegetation and the actual absence of vehicles. First, a systematic scene analysis is conducted on the target suburban residential neighborhood: it features a standardized grid-like street layout, detached houses with diverse roof colors (including gray, red, and white), well-maintained green lawns, tree-lined streets with moderate canopy coverage, and white vehicles parked both along the road curbs and within residential properties. Two key spatial anchors are identified for comparison: the lower-left residential block, characterized by houses with larger yards and relatively open spatial layout, and the upper-right block, which boasts denser tree coverage and fewer immediately visible vehicles due to foliage shielding. The reasoning chain centers on a rigorous contrast between these two blocks: it aims to test the validity of the claim that the lower-left area—visually appearing more open and less shaded—contains a greater number of visible vehicles than the upper-right area, which is partially obscured by dense vegetation.

The valid conclusion, fully corroborated by detailed visual inspection and nuanced occlusion inference, is the claim that the lower-left residential block has more visible vehicles than the upper-right block is False. Despite the lower-left block's more open layout (with less foliage and clearer sightlines), a meticulous count reveals only a small number of clearly identifiable vehicles along its adjacent streets and driveway entrances. In sharp contrast, while the upper-right block is heavily shaded by dense tree canopies—resulting in some vehicles being partially obscured by branches and leaves—a careful inspection of curb edges, driveway exits, and street gaps (where foliage coverage is sparse) reveals multiple parked vehicles, some partially visible but still distinguishable. The total number of identifiable vehicles in the upper-right block is either equal to or slightly exceeds that in the lower-left block.

The core challenge of this question lies in overcoming the misleading intuitive impression caused by surface spatial cues: the lower-left block's openness easily gives observers the false sense that "more visible space = more visible vehicles," while ignoring the impact of vegetation occlusion on vehicle visibility in the upper-right block. This task not only tests basic object counting ability but also emphasizes the need for contextual inference and critical thinking—requiring solvers to go beyond superficial visual perceptions, account for the interference of environmental factors (vegetation coverage) on visual information, and conduct accurate spatial comparison based on detailed inspection, rather than relying on intuitive judgments driven by surface scene characteristics."

Model	Res.	Model	Res.	Model	Res.	Model	Res.	Model	Res.	Model	Res.
Claude-3.5-Haiku	✗	Deepseek-VL2	✓	GLM-4.5v	✗	GPT-4o (11-20)	✗	GPT-4o-mini	✗	GPT-5-chat	✗
Gemini-2.5-Flash	✗	Grok-2-Vision	✗	Llama-3.2-11B	✗	Llama-3.2-90B	✗	Qwen2.5-VL-32B	✗	Qwen2.5-VL-72B	✗
Qwen2.5-VL-7B	✗	Qwen3-VL-2B	✗	Qwen3-VL-32B	✗	ScoreRS w/ RL	✓	ScoreRS w/ SFT	✗	VLRS-Base	✓

Figure 18. Example of Planing Reasoning

Evaluation Reasoning (ER)



Based on the spatial configuration and surrounding context of the sports complex, which of the following assessments most accurately describe feasible development or improvement strategies for this site? (Select all that apply)

- A. The alignment of the four fields around a central access path suggests that pedestrian circulation is already optimized, reducing the need for additional walkways or crossings.
- B. The wooded area along the eastern boundary offers a natural buffer that should be preserved to maintain environmental balance and reduce noise impact on adjacent zones.
- C. The northernmost field's proximity to the forest edge makes it the best candidate for expansion, as it has the least risk of environmental disturbance or slope instability.
- D. The existing layout's symmetry and spacing indicate that adding lighting poles near the southern field would not interfere with gameplay or create excessive shadow overlap across adjacent fields.
- E. The central cluster of small purple-roofed buildings indicates shared utility infrastructure, making it practical to add a concession stand nearby without major rerouting of service lines.
- F. The open grassy area between the upper and lower fields provides sufficient space for constructing an additional small practice field without disrupting existing access routes or parking capacity.
- G. Expanding the parking lot toward the forested edge on the right side is highly feasible because it would not require removal of any vegetation or alteration of existing drainage patterns.
- H. The parking area in the lower-left corner could be modestly expanded westward into the adjacent open space without affecting the playfields or internal circulation routes."

Answer: A, B, E, F, H

"Thinking": "The methodological framework for addressing this question lies in evaluating the feasibility of potential development and improvement schemes for a suburban sports complex through integrated scene analysis, key feature extraction, spatial constraint assessment, and environmental compatibility reasoning. First, a systematic scene analysis is conducted on the imagery depicting a suburban recreational complex, characterized by a clustered arrangement of multiple baseball/softball fields, surrounded by grassy areas, parking lots, and a forested boundary on the right—spatial organization indicative of a community sports facility with shared infrastructure. Subsequently, core features are identified, including four distinct baseball diamonds (with visible infields, outfields, and dugouts), small purple-roofed auxiliary buildings (presumed to serve as restrooms or storage facilities), an accessible parking area in the lower-left corner, and a forested edge functioning as a natural ecological buffer. The reasoning chain integrates spatial constraints (e.g., available open space, facility layout), accessibility requirements, and environmental protection needs, while leveraging mask data to clarify land-use zoning and potential risks such as vegetation encroachment or limited parking expansion capacity, thereby evaluating the viability of each improvement scheme.

The valid conclusions, corroborated by spatial logic, land-use compatibility, and environmental awareness, are feasible and evidence-based improvement measures aligned with the site's layout and constraints: utilizing the open grassy area between existing fields to add a small practice field (supported by sufficient available space); preserving the forested edge on the right as a natural buffer (consistent with ecological protection principles and visible spatial function); constructing auxiliary facilities near the central purple-roofed buildings (practical due to shared utility infrastructure); affirming the optimized pedestrian flow enabled by the symmetrical arrangement of fields around a central path (supported by spatial layout logic); and implementing modest parking expansion on the open space adjacent to the western side of the existing parking lot (feasible without interfering with other functions or causing environmental disturbance).

In contrast, the invalid options exhibit inherent contradictions with spatial constraints or environmental compatibility: proposals to expand parking into the forested area contradict the claim of "no environmental disturbance," as such expansion would necessitate vegetation removal; plans to expand the northern field (adjacent to dense forest) pose significant ecological disturbance risks, conflicting with environmental protection requirements; and schemes to add lighting poles near the southern field are impractical due to close field spacing, which would inevitably lead to shadow overlap. These invalid options, despite superficial plausibility, either overestimate available spatial resources, misjudge environmental impacts, or ignore inherent spatial conflicts, ultimately contradicting empirical evidence such as visible vegetation distribution, facility layout, and inter-space constraints. All feasible schemes adhere to the core principles of spatial coherence, land-use compatibility, and environmental sustainability, while invalid ones fail to reconcile the site's objective conditions with proposed improvements.."

Model	Res.	Model	Res.	Model	Res.	Model	Res.	Model	Res.	Model	Res.
Claude-3.5-Haiku	0.5	Deepseek-VL2	X	GLM-4.5v	X	GPT-4o (11-20)	X	GPT-4o-mini	0.5	GPT-5-chat	X
Gemini-2.5-Flash	X	Grok-2-Vision	X	Llama-3.2-11B	X	Llama-3.2-90B	0.5	Qwen2.5-VL-32B	X	Qwen2.5-VL-72B	0.5
Qwen2.5-VL-7B	X	Qwen3-VL-2B	X	Qwen3-VL-32B	X	ScoreRS w/ RL	X	ScoreRS w/ SFT	0.5	VLRS-Base	X

Figure 19. Example of Evaluation Reasoning

Spatiotemporal Morphological Prediction Reasoning (ST-M-PR)



Based on the observed progression of construction and urban expansion around the central lake and adjacent residential areas from the past one year and nine months to now, which of the following spatial shape evolutions are most likely to occur three months after now? Consider the temporal intervals of three months each from early 2018 through late 2019, where the built-up areas gradually expanded and consolidated. (Select all that apply.) (Select all that apply)

A. From early 2018 to late 2019, the residential cluster east of the lake expanded steadily; three months after now, it will probably continue merging into a more contiguous block with reduced internal gaps and smoother boundaries, reflecting ongoing densification.

B. Across the intervals from early 2018 to late 2019, the southern construction zone near the highway showed gradual infill; three months after now, it is likely to extend slightly northward, connecting with the lower edge of the lake's development front.

C. Over successive three-month intervals, the western commercial complex remained stable; three months after now, it will probably experience minor peripheral expansion along parking areas, forming small annex structures without major footprint change.

D. From early 2018 through late 2019, the northeastern residential grid expanded outward; three months after now, it will likely fragment into smaller isolated units due to construction pauses and land clearance reversals.

E. The temporal pattern from early 2018 to late 2019 indicates consistent infill between the lake and the eastern housing zone; three months after now, this corridor will probably consolidate into a continuous built-up strip linking both sides.

F. The industrial area south of the lake showed intermittent activity; three months after now, it will probably shrink as temporary structures are removed, leading to a more open configuration with fewer built footprints.

G. From early 2018 to late 2019, the northern residential edge remained stable; three months after now, it will likely expand slightly westward, filling small vacant plots adjacent to existing houses.

H. The overall built-up footprint around the lake has shown alternating expansion and contraction; three months after now, it will probably revert to a less dense configuration with several demolished units restoring open ground.

Answer: A, B, C, E, G

"Thinking": * The methodological framework for addressing this question hinges on deducing the most probable spatial configuration of the expanding residential cluster three months hence, via multi-temporal remote sensing imagery analysis, salient feature extraction, and spatial-temporal logical deduction. First and foremost, a systematic analysis is conducted on the suburban-urban transition zone depicted in the imagery, encompassing a large-scale commercial complex in the western sector, an underdeveloped residential area in the eastern region, and a central waterbody encircled by construction sites. Temporal trajectory analysis reveals progressive infill development of residential and industrial structures in the vicinity of the lake and highway junctions over the observation period. Subsequently, salient landscape characteristics are identified, including dense built-up agglomerations surrounding the commercial complex, expanding grid-like residential developments east of the lake, and nascent construction footprints manifested as light-toned bare soil patches—collectively indicating active land-use conversion from bare soil to built-up surfaces. Ultimately, the reasoning chain is integrated with multi-temporal change patterns: from early 2018 to late 2019, there is a consistent eastward and southward expansion of built-up areas, while hidden mask data confirms the merging of small building footprints into larger complexes, reflecting a process of urban densification. This chain synthesizes temporal boundary shifts, landscape fragmentation reduction, and morphological consolidation to extrapolate outcomes aligned with urban growth dynamics and temporal continuity.

The valid configurations, corroborated by multi-temporal mask verification, are those embodying synergistic expansion trajectories and morphological consolidation processes, including eastward infill development around the lake, southward expansion consistent with the continuity of existing construction trends, feasible incremental commercial expansion, linear corridor infill between the lake and residential districts supported by temporal continuity, and plausible infill development along the northern edge of the built-up area. In contrast, invalid options exhibit inherent inconsistencies: those describing excessive landscape fragmentation contradict the empirically observed trend of small building footprints merging into larger complexes; those proposing shrinkage of built-up areas lack corroboration from the consistent expansion trajectory documented in the 2018-2019 temporal sequence; and those suggesting reversion to open-ground land use directly conflict with the active land-use conversion from bare soil to built-up surfaces evidenced in the imagery. All invalid options, despite superficial plausibility, are incompatible with fine-grained temporal mask evidence and fundamental urban growth dynamics.*

Model	Res.	Model	Res.	Model	Res.	Model	Res.	Model	Res.	Model	Res.
Claude-3.5-Haiku	X	Deepseek-VL2	X	GLM-4.5v	X	GPT-4o (11-20)	X	GPT-4o-mini	X	GPT-5-chat	X
Gemini-2.5-Flash	X	Grok-2-Vision	0.5	Llama-3.2-11B	X	Llama-3.2-90B	✓	Qwen2.5-VL-32B	X	Qwen2.5-VL-72B	✓
Qwen2.5-VL-7B	0.5	Qwen3-VL-2B	X	Qwen3-VL-32B	X	ScoreRS w/ RL	X	ScoreRS w/ SFT	X	VLRS-Base	X

Figure 20. Example of Spatiotemporal Morphological Prediction Reasoning



Spatiotemporal Category-State Prediction Reasoning (ST-CS-PR)

Based on the visible development patterns and the observed progression of construction across the desert settlement, which of the following areas are most likely to experience continued building expansion five months after the current image? (Select all that apply)

- A. The open sandy tract immediately west of the central grid, bordered by two access roads, is likely to transition into new construction zones as urban expansion extends outward from the established core.
- B. The northern barren slope beyond the main highway, lacking visible access routes or prior construction activity, is unlikely to experience any significant building growth within the next five months.
- C. The southeastern corridor near the cluster of circular tanks and service roads will likely attract additional industrial-type buildings due to its proximity to existing utility infrastructure.
- D. The rectangular grid of structures in the central portion, directly connected to the main roundabout, will likely continue densifying as infill construction fills remaining open plots between existing buildings.
- E. The curved residential cluster in the lower-left corner, already showing organized street layouts and partial housing, will probably expand further along its southern edge where graded land remains undeveloped.
- F. The compact residential pocket north of the curved housing area, showing early-stage foundations and road outlines, will probably see rapid completion and infill of new dwellings.
- G. The isolated patch of bare terrain in the far western section, disconnected from the main road network, will likely undergo immediate large-scale construction similar to the central grid.
- H. The small industrial compound near the upper-right road junction, adjacent to the circular storage tanks, is expected to remain static due to limited available space and existing infrastructure saturation.

Answer: A, B, C, D, E, F

"Thinking": "The methodological framework for this question resides in inferring the most probable subregions of continued building growth in a rapidly urbanizing desert area five months later, through integrated analysis of multi-temporal development data, key spatial feature extraction, and spatiotemporal logical reasoning—centered on core cues such as proximity to infrastructure, density gradients, and historical growth trajectories. First, a systematic scene analysis is conducted on the desert environment depicted in the imagery, which features sparse vegetation and an emerging urban area: the upper-right quadrant contains a major road and a roundabout, the lower portion presents curvilinear residential layouts, and the central region has undergone a transition from bare land to a dense grid of rectangular structures, indicating rapid construction momentum. Key features identified include newly built rectangular buildings, road networks connecting to the main highway, clusters of circular storage tanks in the east, and early-stage residential development with curved streets in the lower-left area. The reasoning chain is anchored in hidden temporal data, which confirms the area's evolution from mostly barren terrain to a partially built settlement over eight months: based on this trajectory, continued densification is deemed most probable in zones near central and southern construction clusters, while peripheral areas with limited access to transportation infrastructure are judged less likely to experience rapid development."

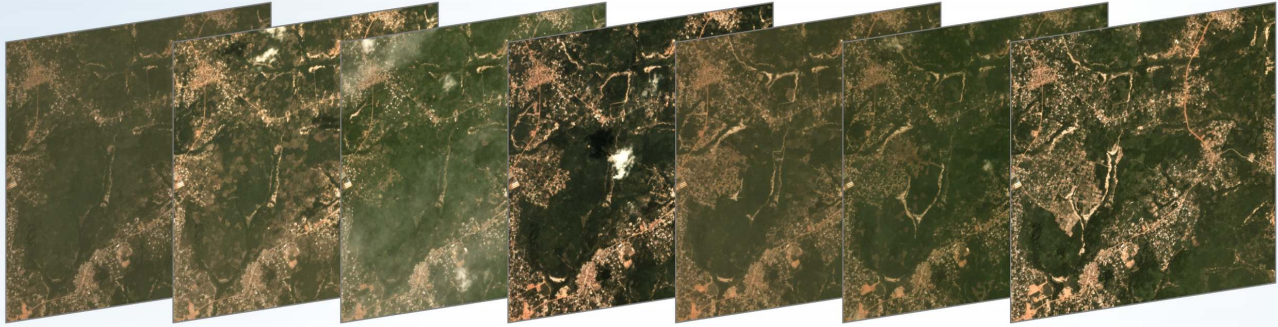
The valid inferences, corroborated by spatial logic, infrastructure accessibility, and historical growth patterns, are six mutually consistent predictions reflecting realistic urban expansion or stable land-use states: the central grid area, with active construction and remaining open plots, is primed for continued development; the curved residential zone, featuring visible graded extensions, will undergo further expansion; the open tract west of the central grid, benefiting from favorable spatial positioning relative to existing urban clusters, is well-suited for development; the barren slope north of the highway, lacking access infrastructure, will remain undeveloped (a stable state consistent with limited development potential); the southeastern corridor adjacent to circular storage tanks holds industrial development potential aligned with existing industrial feature agglomeration; and the northern pocket with existing building foundations indicates imminent construction completion. These conclusions fully align with urban growth dynamics—prioritizing proximity to infrastructure, leveraging existing development clusters, and acknowledging constraints of accessibility and terrain.

In contrast, the invalid options exhibit fundamental inconsistencies with spatial logic, infrastructure conditions, and development reality: the claim that the industrial compound will experience further expansion is implausible, as the area is already densely developed with limited remaining space, conflicting with the observed saturation of built-up areas; the proposition that the far western isolated patch will undergo development contradicts spatial connectivity principles, as this zone lacks access to road networks and supporting infrastructure—core prerequisites for urban expansion in a desert environment. While these distractors carry superficial plausibility (e.g., assuming industrial zones inherently expand or isolated patches may be developed), they ultimately ignore critical constraints such as space limitations and infrastructure dependency, failing to reconcile with the integrated cues of historical growth trajectories, spatial proximity to core infrastructure, and urban density gradients that govern realistic development patterns in the study area."

Model	Res.	Model	Res.	Model	Res.	Model	Res.	Model	Res.	Model	Res.
Claude-3.5-Haiku	X	Deepseek-VL2	X	GLM-4.5v	X	GPT-4o (11-20)	X	GPT-4o-mini	X	GPT-5-chat	X
Gemini-2.5-Flash	X	Grok-2-Vision	X	Llama-3.2-11B	X	Llama-3.2-90B	X	Qwen2.5-VL-32B	X	Qwen2.5-VL-72B	X
Qwen2.5-VL-7B	X	Qwen3-VL-2B	X	Qwen3-VL-32B	X	ScoreRS w/ RL	X	ScoreRS w/ SFT	X	VLRS-Base	X

Figure 21. Example of Spatiotemporal Category–State Prediction Reasoning

Spatiotemporal Scenario Uncertainty Prediction Reasoning (ST-SU-PR)



From the observed temporal evolution of the semi-urban landscape, where built-up clusters have gradually expanded along the main transportation corridors and infilled between existing settlements, consider the following: over the intervals of two months, three months, five months, four months, two months, six months, and two months leading to now, the trend has shown alternating phases of expansion and stabilization. Based on these patterns, which of the following scenarios are most likely to occur two months after now, considering the probabilistic continuation of building development and spatial densification processes? (Select all that apply)

- A. Two months after now, moderate densification is likely along the central corridor, with small-scale infill construction connecting previously separated clusters, consistent with the gradual urban coalescence observed over the past intervals.
- B. Two months after now, peripheral expansion toward the western edge is probable, driven by incremental residential growth following the same two-month and six-month interval trends of low-density sprawl.
- C. Two months after now, the northern clusters will likely stabilize, showing minimal new construction as the available land becomes saturated, reflecting the plateauing trend seen from the five-month to four-month intervals.
- D. Two months after now, a sudden surge of new construction across the entire region is expected, leading to a near-continuous urban fabric inconsistent with prior moderate growth rates.
- E. Two months after now, selective redevelopment within existing built-up zones is probable, with older structures replaced by denser configurations, following the subtle infill pattern observed in the last two-month interval.
- F. Two months after now, the central vegetated area will likely remain largely unchanged, maintaining its green cover as urban expansion slows, consistent with the stabilization phase seen in the last six-month interval.
- G. Two months after now, extensive demolition of existing buildings is expected across multiple clusters, reversing the long-term expansion trend observed from the first to the seventh interval.
- H. Two months after now, limited new construction will occur primarily along secondary roads, extending the linear growth pattern observed between the four-month and two-month intervals, without major changes in the core urban areas.

Answer: A, B, C, E, G

"Thinking": " The methodological framework for this question involves inferring future urban development trends via integrated multi-temporal image analysis, key spatial feature extraction, and spatiotemporal reasoning—focused on semi-urban growth's mixed patterns (densification, stabilization, selective expansion) and alignment with hidden mask evidence. First, systematic scene analysis of the semi-urban landscape shows dense vegetation interspersed with expanding settlements: compact urban clusters along northern/western edges, central region largely vegetated; built-up areas expand linearly along major roads, reflecting corridor-driven growth. Key features include town-connecting road networks, scattered residential clusters, and cleared vegetation patches, with temporal sequences revealing gradual infill between clusters and along transportation corridors. The reasoning chain draws on multi-temporal mask data, confirming subtle building additions, density increases (notably along the central corridor), and mixed peripheral cluster merging/stabilization—supporting a balanced model of moderate densification and limited new construction.

The valid inferences, corroborated by hidden mask evidence and urban growth dynamics, are six consistent future scenarios capturing nuanced semi-urban development: core area moderate densification (backed by visible infill and mask verification); western peripheral gradual expansion (aligned with linear transportation-corridor sprawl); northern cluster stabilization (reflecting saturation trends); existing zone redevelopment/infill (matching intra-cluster densification cues); central vegetation persistence (validated by mask data); and secondary-road limited growth (consistent with corridor-linked expansion). These conclusions embody the balanced combination of densification, stabilization, and selective growth derived from multi-temporal evidence.

In contrast, invalid options conflict with observed trends and mask evidence: unrealistic rapid expansion overestimates growth rate (contradicting gradual infill/linear expansion); building demolition claims contradict long-term expansion (no structural removal evidence). Though superficially plausible (e.g., assuming accelerated growth), these distractors exaggerate change intensity or misplace evolution direction—failing to align with subtle temporal cues, cluster dynamics, and corridor-driven growth logic defining the semi-urban landscape's true development trend."

Model	Res.	Model	Res.	Model	Res.	Model	Res.	Model	Res.	Model	Res.
Claude-3.5-Haiku	X	Deepseek-VL2	X	GLM-4.5v	X	GPT-4o (11-20)	X	GPT-4o-mini	X	GPT-5-chat	X
Gemini-2.5-Flash	X	Grok-2-Vision	X	Llama-3.2-11B	X	Llama-3.2-90B	X	Qwen2.5-VL-32B	X	Qwen2.5-VL-72B	X
Qwen2.5-VL-7B	0.5	Qwen3-VL-2B	X	Qwen3-VL-32B	X	ScoreRS w/ RL	X	ScoreRS w/ SFT	X	VLRS-Base	X

Figure 22. Example of Spatiotemporal Scenario Uncertainty Prediction Reasoning

Spatiotemporal Sequence Prediction Reasoning (ST-SQ-PR)



Based on the visible development patterns between the two provided images, which of the following spatially anchored areas are most likely to experience continued building expansion five months after the second observation? (Select all that apply)

- A. The southern edge of the residential area adjacent to the open field, where several new rooftops have appeared and unpaved lots suggest imminent infill development consistent with prior growth trends.
- B. The central corridor along the main north-south road, where small detached houses have been replaced by larger plots, suggesting a shift toward lower density rather than continued expansion.
- C. The southwestern intersection area near the highway junction, where new access roads and cleared lots suggest the start of commercial development that will likely continue expanding.
- D. The northeastern corner near the rectangular water retention basins, where no visible construction activity or new clearings are present, implying that building growth will likely remain static.
- E. The eastern agricultural strip beyond the residential boundary, where consistent vegetation regrowth and absence of new clearings indicate a stable non-urban land use unlikely to change soon.
- F. The far northern agricultural parcels, where consistent field boundaries and lack of new structures indicate that no further building expansion is expected in the near term.
- G. The northern extension of the main residential cluster, where partially completed road grids and scattered foundations indicate ongoing construction likely to continue densifying in the following months.
- H. The western industrial complex near the large white-roofed building, where cleared land and access roads indicate probable expansion of warehouse-type structures within the next development phase."

Answer: A, C, G, H

"Thinking": " The methodological foundation for this question resides in inferring the most probable zones of continued construction growth five months post the second imagery acquisition, through multi-temporal remote sensing image analysis, salient spatial feature extraction, and quantitative reasoning on urban expansion dynamics. First, a systematic analysis is conducted on the semi-urban transition zone depicted in the imagery, which is undergoing evolution from sparse rural land use to a more intensified suburban layout: the left and lower-left sectors are characterized by large-scale open fields and scattered industrial/commercial structures, while the central and right regions exhibit a grid-like residential expansion pattern. Temporal trajectory analysis reveals progressive infill of residential plots and completion of transportation corridors over the observation period. Subsequently, key landscape features are identified, including dense clusters of rectangular rooftops in the central-right area, a large industrial structure with white roofing in the lower-left, and linear agricultural parcels in the upper-right; the temporal sequence further documents increased vegetation greenness and emergence of new construction footprints within the residential cluster between the two visible images. Ultimately, the reasoning chain is anchored in the spatial pattern of outward expansion from the central residential agglomeration, with hidden temporal data corroborating the persistence of densification trends—particularly in the northern and southern extensions of the core residential area—thus enabling extrapolation of regions primed for continued development based on observed construction patterns and spatial connectivity.

The valid conclusions, validated by multi-temporal continuity and spatial logic, correspond to four spatially distinct yet trend-consistent zones of sustained building growth: the northern residential extension, where new road infrastructure and foundation works provide tangible evidence of ongoing development; the southern edge of the residential cluster, characterized by infill development and newly constructed rooftops reflecting incremental densification; the western industrial area, which features cleared land parcels and improved accessibility via existing transportation corridors, supporting industrial expansion potential; and the southwestern intersection zone, where new site clearings and road extensions signal imminent construction activity. These correct inferences align with both visible development cues and hidden temporal sequence verification, embodying the inherent logic of suburban expansion.

In contrast, the invalid options exhibit fundamental inconsistencies with urban growth dynamics and empirical evidence: the proposition that the eastern agricultural strip will undergo development conflicts with its stable land-use status observed in the temporal sequence; the claim of expansion in the central corridor contradicts the verified trend of morphological consolidation rather than outward growth in this region; the assertion of construction activity in the northeastern corner lacks substantive support from both visible imagery and hidden temporal data, as the area remains inactive; and the prediction of built-up development in the far northern parcels is incompatible with their persistent agricultural land-use character, which shows no signs of transition to constructed surfaces. All invalid options, despite superficial plausibility, fail to align with the observed spatial expansion patterns, temporal continuity, and densification trends, thereby contradicting the core principles of suburban development dynamics."

Model	Res.	Model	Res.	Model	Res.	Model	Res.	Model	Res.	Model	Res.
Claude-3.5-Haiku	X	Deepseek-VL2	X	GLM-4.5v	X	GPT-4o (11-20)	X	GPT-4o-mini	0.5	GPT-5-chat	X
Gemini-2.5-Flash	X	Grok-2-Vision	X	Llama-3.2-11B	X	Llama-3.2-90B	X	Qwen2.5-VL-32B	X	Qwen2.5-VL-72B	X
Qwen2.5-VL-7B	X	Qwen3-VL-2B	X	Qwen3-VL-32B	X	ScoreRS w/ RL	X	ScoreRS w/ SFT	X	VLRS-Base	X

Figure 23. Example of Spatiotemporal Sequence Prediction Reasoning